

Copyright Undertaking

This thesis is protected by copyright, with all rights reserved.

By reading and using the thesis, the reader understands and agrees to the following terms:

1. The reader will abide by the rules and legal ordinances governing copyright regarding the use of the thesis.
2. The reader will use the thesis for the purpose of research or private study only and not for distribution or further reproduction or any other purpose.
3. The reader agrees to indemnify and hold the University harmless from and against any loss, damage, cost, liability or expenses arising from copyright infringement or unauthorized usage.

IMPORTANT

If you have reasons to believe that any materials in this thesis are deemed not suitable to be distributed in this form, or a copyright owner having difficulty with the material being included in our database, please contact lbsys@polyu.edu.hk providing details. The Library will look into your claim and consider taking remedial action upon receipt of the written requests.

**Rational Design and Development of Moenomycin
A-Derived Fluorescent Biosensors for Screening of
Peptidoglycan Glycosyltransferase Inhibitors**

YUAN JIAN

Ph.D

The Hong Kong Polytechnic University

2016

The Hong Kong Polytechnic University
Department of Applied Biology and Chemical Technology

**Rational Design and Development of Moenomycin A-Derived
Fluorescent Biosensors for Screening of Peptidoglycan
Glycosyltransferase Inhibitors**

YUAN JIAN

**A Thesis Submitted in Partial Fulfillment of the Requirements for
the Degree of Doctor of Philosophy**

January, 2016

Certificate of Originality

I hereby declare that this thesis is my own work and that, to the best of my knowledge and belief, it reproduces no material previously published or written, nor material that has been accepted for the award of any other degree or diploma, except where due acknowledgement has been made in the text.

YUAN JIAN

January, 2016

Abstract

Antibacterial resistance prevents the effective treatment of an ever-increasing number of pathogenic bacteria infections, which has caused a serious threat to human health across the world. To combat the growing problem of antibiotic resistance, there is an urgent need to develop novel antibiotics with new chemotypes or acting on novel targets. The peptidoglycan glycosyltransferase (PGT), which catalyzes the essential process of lipid II (the single unit of peptidoglycan) polymerization, is a promising target for new antibiotic development as a result of the following two reasons. Firstly, PGT is located at the outside of bacterial cell membrane which makes it easy to access to drugs. The second reason is that PGT is highly conservative in both antibiotic sensitive and resistant strains. PGT as an antibacterial target has been studied for several decades. However, there is no antimicrobial drugs targeting PGT used clinically. Moenomycin A (Moe A), a natural product isolated from several strains of *Streptomyces*, is the only well proven PGT inhibitor by binding to the active sites of PGT. However, Moe A does not show antibacterial activity in human due to its poor bioavailability. Moe A is currently only used as a growth promoter in animal feed. One of the major reasons for the slow progress on development of PGT inhibitors is lack of efficient assays to evaluate potential drug candidates.

In recent years, several crystal structures of complexes of PBPs with Moe A and lipid II unveiled the mysterious process of transglycosylation in peptidoglycan biosynthesis.

This new development has prompted researchers to develop new assays for PGT inhibitor screening to facilitate novel antibiotic discovery. In this project, a fluorescent biosensing system for PGT inhibitor screening was constructed based on photoinduced electron transfer (PET).

In constructing the biosensor, three fluorescent Moe A derivatives (**F-*n*-Moe A**, *n* = **2, 3** and **4**) were synthesized by attaching fluorescein-5-isothiocyanate isomer I (FITC) to Moe A. Furthermore, five amino acid residues near the active site (Q161, H162, D199, Y210 and D241) of the *S. aureus* PBP2 glycosyltransferase domain were muted to tryptophan, a fluorescence quencher of fluorescein. The interaction between Moe A and PGT mutants as analyzed by surface plasmon resonance (SPR) spectroscopy showed that the mutations did not significantly alter the binding affinity. Fluorescent measurement showed that the D199W and D241W mutants can quench the fluorescence of the three probes at different levels. Moreover, addition of free Moe A can subsequently restore the fluorescence intensity of the quenched probes. When the fluorescein-labelled Moe A binds to the active site of PGT domain, the nearby tryptophan residue can interact with and quench the fluorophore group of the probes through a PET process if the linkers have appropriate lengths. When free Moe A was added into the system, it competitively binds to the same pocket of the probes and the fluorescent quenching effect was relieved once the probes were displaced by Moe A and the fluorescence intensity of the probes was restored.

Among different combinations of mutants and probes, three probe / mutant pairs, namely **F-3-Moe A** / D241W, **F-4-Moe A** / D199W and **F-4-Moe A** / D241W, showed

the best fluorescence quenching efficiency. While Moe A was added into the system, the fluorescence intensity of probes were restored up to 90 % of the original level, whereas no change in fluorescence signal was observed when the antibiotics ampicillin and kanamycin were added as negative controls. In order to further validate the biosensing system, the change in fluorescence of the **F-4-Moe A** / D199W pair with two small molecule PGT inhibitors **14** and **16** reported in literature were also studied. While compound **16** did not induce any observable fluorescence change for the **F-4-Moe A** / D199W pair, compound **14** was able to restore its fluorescence. Compared to fluorescence polarization based bioassay, the PET-based bioassay has the advantage that the enzyme can be immobilized on a surface during the screening process. The success in the construction of this PET-based biosensor will allow the future development of high-throughput screening of PGT inhibitors using microfluidic chip-based devices.

Acknowledgements

I would like to extend my sincere gratitude to my supervisor, Prof. K. Y. Wong for his generous guidance, unwavering support and encouragement throughout my postgraduate study. Without his consistent and illuminating instruction, the completion of the thesis would not have been possible. I am deeply grateful to him for providing me such a meaningful project and teaching me to think critically about problems.

I would also like to thank Prof. Thomas Y. C. Leung for his valuable comments and suggestions. Dr. Ann L. Y. So is thanked for teaching me the essential techniques and her generous assistance in protein engineering. I would also like to thank Dr. Ning Sun for teaching me the techniques of SPR, Dr. Yong Wang and Mr. W. L. Cheung for pre-HPLC, Mr. Hugo Fung for protein expression, Dr. G. L. Law and Mr. W. S. Lo for their generous assistance in fluorescence lifetime measurement and Dr. P. K. So for his generous assistance in mass spectrometry.

In addition, I would like to express my gratitude to my groupmates, Dr. Lawrence Lee, Dr. K. F. Chan, Dr. Enna Ha, Dr. Rui Hu, Dr. Yajuan Guo, Dr. Carol Tsang, Dr. Fenghua Li, Mr. Steven H. W. Man, Mr. Liangsheng Hu, Mr. Wenbin Jin, Ms. Christy K. Y. Chow for their encouragement and lending their helping hands throughout my research study.

Prof. Kevin Burgess of Texas A & M University is sincerely thanked for giving me the opportunity to attach to his research group in 2015. Prof. Shengbiao Wan of Ocean University of China is gratefully thanked for his encouragement during my study period.

I also sincerely thank my family and friends for their persistent love, unceasing support and patience throughout my postgraduate study.

Last but not the least, I would like to acknowledge the Research Committee of the Hong Kong Polytechnic University for offering me a studentship from the year of 2012 to 2015, and a travelling grant to visit Texas A & M University in 2015.

Table of Contents

Certificate of Originality	ii
Abstract.....	iii
Acknowledgements	vi
Table of Contents	viii
List of Abbreviations.....	xi
Chapter 1 Introduction.....	1
1.1 Antibiotics and bacterial resistance	1
1.2 Bacterial cell wall synthesis and penicillin binding proteins	7
1.2.1 The biosynthesis of peptidoglycan	7
1.2.2 Enzymes involved in the last stages of peptidoglycan synthesis.....	12
1.3 Peptidoglycan glycosyltransferases as antibacterial target	14
1.4 Moenomycin A and its mimics as PGT inhibitors	20
1.4.1 Moenomycin A as a PGT inhibitor.....	20
1.4.2 Synthetic PGT inhibitors based on moenomycin and lipid II	23
1.5 Assays for PGT inhibitors screening and potential PGT inhibitors from HTS	26
1.5.1 Lipid II based peptidoglycan glycosyltransferase inhibition assays	26
1.5.2 Moenomycin A based displacement assays.....	27
1.6 Photoinduced electron transfer (PET) based biosensor	31
1.6.1 Fluorescence quenching and photoinduced electron transfer.....	32
1.6.2 Fluorescence quenching by amino acids	35
1.6.3 Applications of PET based biosensors	37
1.7 Aims and objectives	38
Chapter 2 Synthesis and characterization of fluorescein-labeled moenomycin A	41
2.1 Introduction	41
2.2 Experimental.....	45

2.2.1 Materials	45
2.2.2 Instruments	45
2.2.3 Preparation of moenomycin A.....	46
2.2.4 Synthesis of fluorescein-labeled Moe A.....	47
2.2.5 Fluorescence quantum yield measurement.....	53
2.2.6 Fluorescence lifetime measurement	53
2.3 Results and discussion	55
2.3.1 Spectral properties of fluorescein-labeled Moe A.....	55
2.3.2 Quantum yield and lifetime of the fluorescent probes	60
2.4 Concluding remarks	63
Chapter 3 Rational design, preparation and characterization of PGT mutants..	64
3.1 Introduction	64
3.2 Experimental.....	67
3.2.1 Materials	67
3.2.2 Cloning and expression of PGT mutants.....	70
3.2.3 Sodium dodecyl sulfate-polyacrylamide gel electrophoresis (SDS-PAGE).....	75
3.2.4 Electrospray ionization-mass spectrometry (ESI-MS).....	76
3.2.5 Determination of protein concentration.....	76
3.2.6 SPR assay for determining PGT mutants-Moe A binding affinity.....	77
3.3 Results and discussion	79
3.3.1 Preparation of wild type PGT and mutants	79
3.3.2 Characterization by ESI-MS.....	81
3.3.3 Binding affinity determination of the PGT mutants with Moe A by SPR ..	84
3.4 Concluding remarks	87
Chapter 4 Validation of the PET based biosensor for screening of PGT inhibitors	88
4.1 Introduction	88
4.2 Experimental.....	89
4.2.1 Measurement of steady-state fluorescence intensity	89

4.2.2 Determination of the dissociation constant K_D by fluorescence titration of probes with PGT mutants	89
4.2.3 Displacement assay with PGT inhibitors and K_I determination	90
4.3 Results and discussion	92
4.3.1 The effect of linker lengths and mutation locations on the fluorescence quenching of probes by PGT mutants	92
4.3.2 Specificity of the quenching by PGT mutants	99
4.3.3 PGT proteins titration and determination of K_D values	101
4.3.4 Fluorescence recovery upon the addition of Moe A	106
4.3.5 Determination of K_I of Moe A from the competitive displacement assay	109
4.3.6 The effect of DMSO on FI of F-4-Moe A in Tris solution (pH 8.0)	112
4.3.7 Further validation of the best performed F-4-Moe A / D199W	114
4.4 Concluding remarks	117
Chapter 5 Conclusions	118
Appendix I	122
Appendix II	144
Appendix III	149
References	161

List of Abbreviations

CH ₃ CN	Acetonitrile
CH ₂ Cl ₂	Dichloromethane
DMF	Dimethylformamide
DMSO	Dimethylsulfoxide
FITC	Fluorescein isothiocyanate
CDI	N,N'-Carbonyldiimidazole
MoeA	Moenomycin A
HPLC	High-performance liquid chromatography
NMR	nuclear magnetic resonance
ESI-MS	Electrospray ionization-mass spectrometry
TLC	Thin layer chromatography
BSA	Bovine serum albumin
<i>E. coli</i>	<i>Escherichia coli</i>
IPTG	Isopropyl β-D-1-thiogalactopyranoside
SPR	Surface plasmon resonance
LB medium	Luria-Bertani medium
rpm	Revolution per minute
PBP	Penicillin-binding protein
PGT	Peptidoglycan glycosyltransferase
PCR	Polymerase chain reaction

SDM	Site-directed mutagenesis
PET	Photo-induced electron transfer
PBS	Phosphate buffered saline
TCSPC	Time-correlated single photon counting
Da	Dalton
K_D	Dissociation constant
K_I	Inhibitory constant
λ	Lambda; wavelength
s	Second(s)
min	Minute(s)
h	Hour(h)
nm	nanometer
HTS	High-throughput screening
TP	transpeptidase
OD _x	Optical density at wavelength of x nm
MeOH	Methanol
HMM	High molecular mass
LMM	Low molecular mass
τ	Tau; lifetime
PDB	Protein data bank

Chapter 1

Introduction

1.1 Antibiotics and bacterial resistance

The first antibiotic penicillin was discovered by Scottish microbiologist Alexander Fleming in the 1930s [1]. In the following 40 years, most classes of antibiotics currently used in clinic were developed, and the period was known as the “golden era” of antibiotic research [2]. The discovery of antibiotics was once recognized as the final victory of the war against bacterial infections, which was wiped out by the widespread of bacterial resistance to common antibiotics. Antibiotic resistance is the resistance of a microorganism towards one or more antibacterial drugs which were originally effective for treating the corresponding infection. The major cause of antibiotic resistance is the misuse and abuse of antibiotics, as excessive uses of antibiotic promote resistant strains to thrive within a population of bacteria. Moreover, bacteria are not only intrinsically resistant to some antibiotics but they can also acquire antibiotic resistance through mutations in genes, alternation in targets and horizontal gene transfer [3]. The major mechanisms of bacterial resistance can be summarized into four major types [3]. The first one is prevention of antibiotics access to target. Some bacteria can decrease the penetration of antibiotics through membrane to inhibit drugs from reaching their target, and some resistant strains can even pump out antibiotics by overexpression

of efflux pumps on the surface of cell membrane so that the endogenous concentration of antibiotics is below the effective concentration. For example, reduced membrane permeability is achieved by *Pseudomonas* and *Acinetobacter* for to resist antibiotics such as carbapenems and cephalosporins [4]. It has been confirmed that the MexXY multidrug efflux system is the major cause of the aminoglycoside resistance in *Pseudomonas aeruginosa* [5]. Furthermore, single site point mutation in the gene encoding an antibiotic target can also confer resistance to the antibiotic. For example, linezolid-resistant *S. pneumoniae* and *S. aureus* were developed through mutation in the 23S rRNA ribosomal subunit [6]. The third effective antibacterial resistance mechanism is by the modification of the antibiotic target. For example, methylation of 16S rRNA and alteration of drug-binding site by erythromycin ribosome methylase (*erm*) prevent the binding of several antibiotics such as macrolides, lincosamines and streptogramins [7]. Last but not the least, bacteria can modify or destroy antibiotics to inactivate their activity. For example, β -lactamases present in bacteria can hydrolyze β -lactam antibiotics, such as penicillins, cephalosporins, monobactams to remove the antibacterial activity [8]. Moreover, some strains can find other ways to obtain antibiotic resistance. For example, methicillin-resistant *S. aureus* (MRSA) is resistant to a series of β -lactam antibiotics by expression of an alternative protein PBP2a which can carry out transpeptidation but with a lower binding affinity towards antibiotics comparing to PBP2 [9, 10].

As bacteria can find ways to develop resistance when antibiotics are introduced (Figure 1.1), the overuse and abuse of antibiotics accelerate the rapid development of

bacterial resistance worldwide [11]. Antibiotic-resistant gonorrhea was first found in Vietnam in 1967, then spread to the Philippines and finally the United States [12, 13]. Another example is the New Delhi Metallo-beta-lactamase-1 (NDM-1), first detected in a *Klebsiella pneumoniae* isolated from a patient of Indian origin in 2008, is now found all over the world [14]. The widespread of antibiotic resistant pathogens combined with a diminished antibiotic pipeline have caused serious threats to people in every country during the past 20 years [15]. Based on the data from Centers for Disease Control and Prevention in 2013, each year in the United States, at least 2 million people suffer from infections of bacteria that are resistant to one or more antibiotics which are designed to kill these pathogens, and more than 23,000 people died directly from antibiotic resistant infections [16]. Europe is also under a serious situation while 400,000 people acquired infections by multidrug-resistant bacteria in 2007, and 25,000 people died of such infections in that year. MRSA is one of the most problematic pathogens. It was recently reported that up to 89% of nosocomial infections are caused by MRSA resulting in 19,000 deaths in the US each year [17-21]. Vancomycin which binds to the bacterial peptidoglycan precursor lipid II was once considered as the last barrier against antibiotic resistant strains and has been used commonly in the treatment of MRSA infections. However, vancomycin-resistant *Enterococcus* strains, which produce D-alanine-D-lactate variation instead of D-alanine-D-alanine in the pentapeptide of lipid II, resulting in the loss of one hydrogen-bonding interaction between vancomycin and the peptapeptide were discovered in 2002 [22].

Antibiotic resistance also increases the cost in medical care, since antibiotic resistant

infections commonly require prolonged and costly treatments. It is estimated that antibiotic resistant infections caused an extra USD 20 billion in healthcare costs and 8 million additional hospital days in the United States, and over €1.6 billion and 2.5 million additional hospital days in the European Union each year [23]. Therefore, antibiotic resistance has been recently listed as one of the greatest threats to human health in the World Economic Forum Global Risks reports [3].

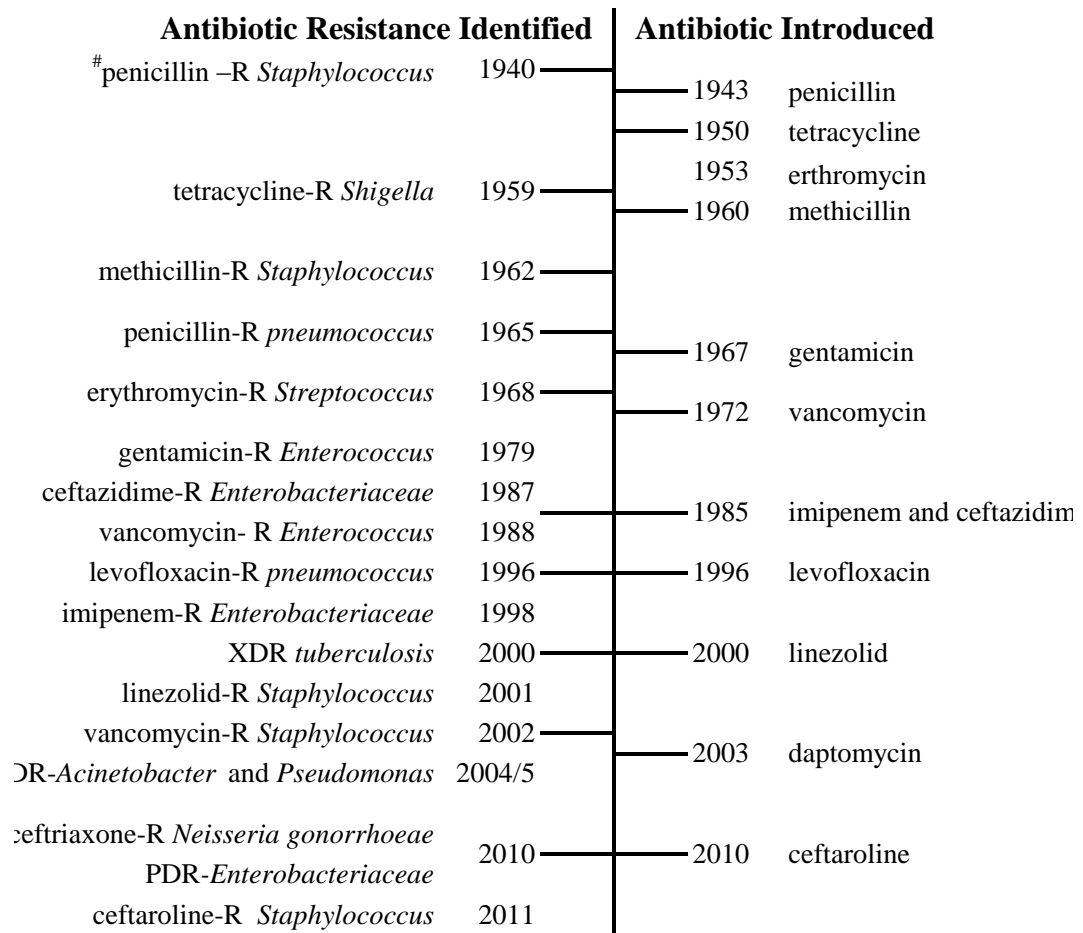


Figure 1.1 Timeline of key antibiotic resistance (adapted from [11]) #It was not until 1943 that penicillin was in widespread popular usage.

According to a report from CDC in 2013, there are mainly four ways to prevent the spreading of antibiotic resistance. Preventing infections is in the first place to reduce the usage of antibiotics, which will reduce the possibility of antibiotic resistance development during the therapy. The second method is to track the antibiotic resistant bacteria, to collect data about their infections and causes of infections. This information will facilitate people to develop specific strategies to prevent antibiotic resistant pathogens from spreading. The third way is by improving antibiotic prescription. Using less antibiotics and choosing the right antibiotics are of high importance to prevent the development and spreading of antibiotic resistant infections. As mentioned above, bacteria can innately be resistant, which is a natural process and cannot be stopped. So, there is a desperate need for novel antibiotics with new skeletons or targets to keep pace with the development of resistant bacteria [24].

1.2 Bacterial cell wall synthesis and penicillin binding proteins

The pathway of bacterial cell wall peptidoglycan (PG) assembly and maintenance has been a well-proven target for antibiotics development. Enzymes involving in the assembly process are acting sites of several important antibiotics including the β -lactam and glycopeptide antibiotics [25]. Furthermore, peptidoglycan biosynthesis is essential and highly conservative in both Gram-positive and Gram-negative strains. So, peptidoglycan biosynthesis is an important target for development of broad-spectrum antibiotics.

1.2.1 The biosynthesis of peptidoglycan

Bacterial peptidoglycan (also known as murein) is the bone structure of the cell wall and provides strength, shape and a scaffold for the other components of the cell wall in both Gram-positive and Gram-negative bacteria [26]. Any interference with the integrity of peptidoglycan will lead to cell lysis due to the low osmotic pressure in its surrounding environment. Peptidoglycan is a polymer consisting of repeating residues of β -(1, 4) linked N-acetylglucosamine (GlcNAc) and N-acetylmuramic acid (MurNAc) disaccharide units (NAG-NAM) that are cross-linked via the flexible peptide chains attached to the MurNAc [27]. Peptidoglycan biosynthesis has been extensively studied during the past 30 years and the entire process can be divided into three stages [28-30]. The first stage, shown in Figure 1.2, occurs in the cytoplasm and results in the synthesis of amino sugar nucleotides UDP-N-acetylmuramyl-pentapeptide (UDP-MurNAc-pentapeptide) and UDP-N-acetylglucosamine (UDP-GlcNAc) which provide the

building blocks for the assembly of peptidoglycan. The second stage (Figure 1.2) takes place at the membrane and leads to the synthesis of the precursor lipid intermediates. At this stage, the phosphor-MurNAc-pentapeptide segment is assembled with undecaprenyl phosphate to yield lipid I. Then, UDP-GlcNAc is attached to lipid I with release of UDP to yield lipid II (GlcNAc- β -(1, 4)-MurNAc-(pentapeptide)-pyrophosphoryl-undecaprenol), which is the monomeric subunit of peptidoglycan. With the aid of its lipid group, lipid II is transported from the cytoplasm, through membrane, into extracellular environment. This transportation is catalyzed by flippase, which then exposes lipid II to suitable sites of the polymerase for polymerization in the final stage.

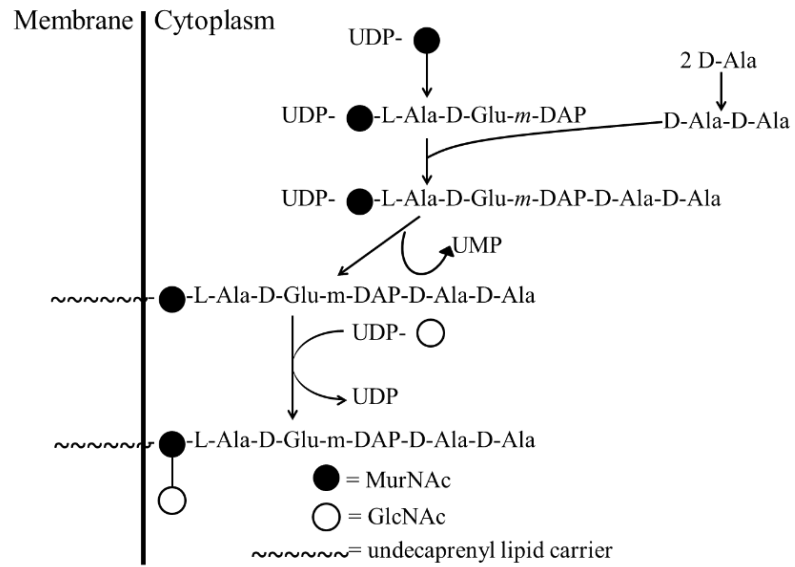


Figure 1.2 Cytoplasmic steps of peptidoglycan biosynthesis (adapted from [31])

The final stage takes place outside the cell membrane and it involves two processes, transglycosylation which polymerizes the disaccharide-peptide monomers and transpeptidation which cross-links the peptide residues between different growing peptidoglycan chains. The final stage is achieved mainly by the penicillin-binding proteins (PBPs), which contain two domains, glycosyltransferase (GT) and transpeptidase (TP), responsible for transglycosylation and transpeptidation respectively. In transglycosylation, the C-1 carbon of MurNAc of the growing PG strand is attached to the C-4 carbon of the glucosamine residue of lipid II with a release of the lipid chain at the same time as shown in Figure 1.3. The leaving group goes into the second round of lipid II synthesis. Scientists have not yet figured out the factors determining the length of peptidoglycan and how the growing glycan chain is released from the GT domain [32]. During transpeptidation, the D-Ala-D-Ala bond of one peptide is firstly hydrolyzed, which leads to the formation of the enzyme-substrate with release of the terminal D-Ala. Then, with the catalysis of transpeptidase, the peptidyl moiety is transferred to the non-alpha amino group of the dibasic amino acid in another pentapeptide to form a new peptide bond which results in the cross-linkage between different PG strands (Figure 1.3).

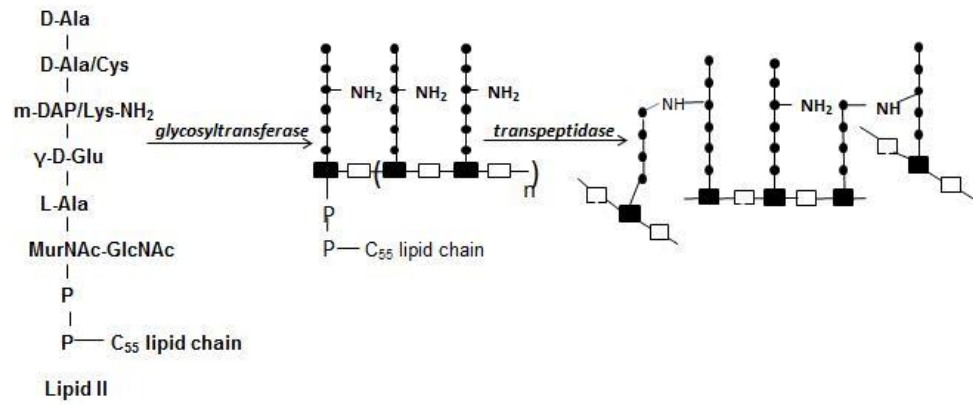


Figure 1.3 The extracellular processes of transglycosylation and transpeptidation (adapted from [31])

1.2.2 Enzymes involved in the last stages of peptidoglycan synthesis

Penicillin-binding proteins (PBPs), members of acyl serine transferases, are involved in the final stage of peptidoglycan biosynthesis [33]. PBPs are classified into two major groups, the high molecular mass (HMM) PBPs and the low molecular mass (LMM) PBPs. HMM PBPs consist of two domains: N-terminal domain and C-terminal domain. The C-terminal domain is responsible for transpeptidation. Depending on the structure and catalytical activity of N-terminal domain, the HMM PBPs are divided into class A and class B PBPs. N-terminal domain of class A is glycosyltransferase and it is responsible for transglycosylation, while the function of N-terminal domain of class B is related to cell morphogenesis and it interacts with other proteins involved in the cell cycle [34-36]. LMW PBPs are monofunctional DD-peptidases, most of which can hydrolyze peptide bond to control the extent of peptidoglycan cross-linking during cell wall biosynthesis [33, 37].

Numbering of PBPs is based on the migration pattern of them in SDS-PAGE (sodium dodecyl sulfate-polyacrylamide gel electrophoresis). The smaller the number, the higher the molecular weight of the PBPs. Each bacterium usually has several PBPs. For example, there are four PBPs in *S. aureus*. PBP1 belongs to class B HMW-PBP and plays an essential role in cell growth and division [38]. PBP2 is a class A HMW-PBP, a bifunctional enzyme which is responsible for peptidoglycan biosynthesis [39]. PBP3 belongs to class B HMW-PBPs which are responsible for maintenance of size and shape of the cell. PBP4 is a LMW-PBP which is believed to have relation with β -lactam resistance [40]. Moreover, 12 species of PBPs have been identified including three class

A PBPs (PBP1a, PBP1b and PBP1c), two class B PBPs (PBP2 and PBP3) and seven LMM PBPs in *E coli*. [41-43] Among them, PBP1a and PBP1b are responsible for the final stage in the peptidoglycan biosynthesis [41, 42].

1.3 Peptidoglycan glycosyltransferases as antibacterial target

In the biosynthetic pathway of peptidoglycan, membrane-associated glycosyltransferases incorporate lipid II into the growing glycan chain and transpeptidases enable the formation of peptide bonds between two glycan polymers. The two processes can be done under the catalysis of bifunctional PBPs which have two domains, glycosyltransferase and transpeptidase [44]. Previous work about peptidoglycan biosynthesis focused on the transpeptidation which provides a target for β -lactam antibiotics. Although penicillin and other β -lactams are still being used in clinical treatment currently, the serious bacterial resistance to β -lactams gives rise to an urgent need for novel antibiotic targets and antibacterial agents.

The glycosyltransferase domain of the bifunctional PBPs is an attractive target for novel antibiotics development [45, 46]. Comparing to TP inhibitors, the peptidoglycan glycosyltransferase (PGT) inhibitors may be less subjected to the development of antibiotic resistance, as comparing with the pentapeptide segment, the higher rigidity of saccharide group of lipid II makes it very difficult for bacteria to get resistance by modification of sugar segment of lipid II. The importance of PGT as a novel drug target has attracted many researchers to seek inhibitors of PGT for several decades. However, only one natural product moenomycin A (Moe A) was found to inhibit transglycosylation by direct binding to PGT, but the poor bioavailability restricted its use in clinic. The main reason of the slow development is due to the difficulties in protein purification and crystallization of the large membrane protein, PBPs [45]. In the recent decade, researchers have worked hard to uncover the mystery of the structural

information of PGT and their catalysis mechanism during peptidoglycan synthesis [47-51]. In 2007, Lovering *et al.* reported the first crystal structure of the bifunctional *S. aureus* PBP2 without transmembrane segment [47] and its complex with moenomycin (Figure 1.4a). In the same year, the crystal structure of the PGT domain of *Aquifex aeolicus* PBP1a was solved by Yuan *et al.* (Figure 1.4b) [48]. In 2009, Sung *et al.* revealed the crystal structure of complex of *E. coli* PBP1b with moenomycin A (Figure 1.4c) [49]. The three crystal structures revealed invaluable structural information of bifunctional PBPs and GT domain in detail. As shown in Figures 1.4a and 1.4c, the bifunctional PBPs including PBP2 and PBP1b consist of two separate lobes, N-terminal PGT and C-terminal TP domains, connected by a short linker. As shown in Figure 1.4b, PGT domain is rich in α -helices and has two regions: one globular head region next to the linker and a smaller jaw region behind it, located closer to the membrane. Interestingly, peptidoglycan glycosyltransferase has no similarities with other known glycosyltransferases, but it resembles bacteriophage λ lysozyme, which hydrolyzes glycosyl bond of peptidoglycan. The binding pose of Moe A and PBPs reveals that the sugar segment of Moe A extends into the cleft between the head and jaw segments by binding to many amino acid residues in that region, which explains the tight-binding model between PGTs and moenomycin. At the same time, one mechanism of peptidoglycan elongation has been proposed that the growing glycan chain as a donor is attacked at the reducing end by the receptor lipid II through deprotonation of the 4-OH nucleophile of GlcNAc under the catalysis of PGT [47, 48].

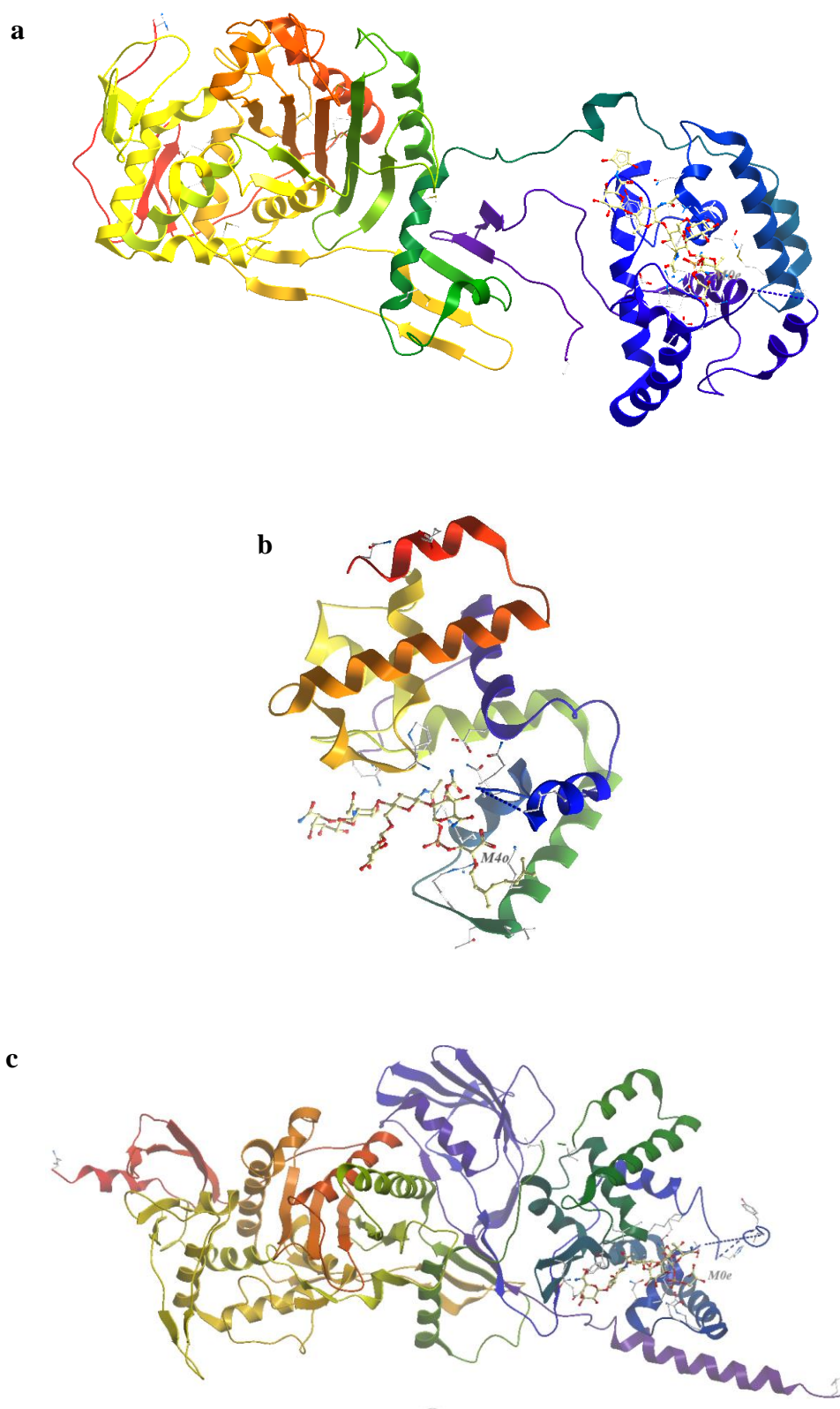


Figure 1.4 (a) Crystal structure of complex of *S. aureus* PBP2 with Moe A (PDB ID: 2OLV), (b) *Aquifex aeolicus* PBP1a PGT domain with Moe A (PDB ID: 3NB6) and (c) *E. coli* PBP1b with Moe A (PDB ID: 3FWL) [47-49]

In recent years, Huang *et al.* solved the crystal structure of *S. aureus* monofunctional glycosyltransferase (SaMGT) in complex with lipid II analogue shown in Figure 1.5 [51]. The structural information supports the previously proposed mechanism of transglycosylation. PGT domain has two active sites: glycosyl acceptor site and glycosyl donor site (Figure 1.6). During transglycosylation, several residues of SaMGT interact with lipid II at the acceptor site with stabilization through Mg^{2+} cations. Several residues in the donor site are responsible for binding to lipid II (or the growing glycan chain). The 4-OH of GlcNAc in lipid II at the acceptor site is attacked by C1 of the growing glycan chain, and the two segments are linked together through a glycoside bond with release of the pyrophosphate group. A new product lipid IV is produced after the formation of a β 1-4 glycoside bond, and then another transglycosylation commences as soon as lipid IV is transferred to the donor site and a new lipid II binds to the acceptor site [51]. Moe A as a PGT inhibitor is confirmed to perturb the elongation of the glycan chain by binding to the donor site of PGT. In summary, the elucidation of the mechanisms of transglycosylation and PGT inhibition has opened the door to the rational design of PGT inhibitors.

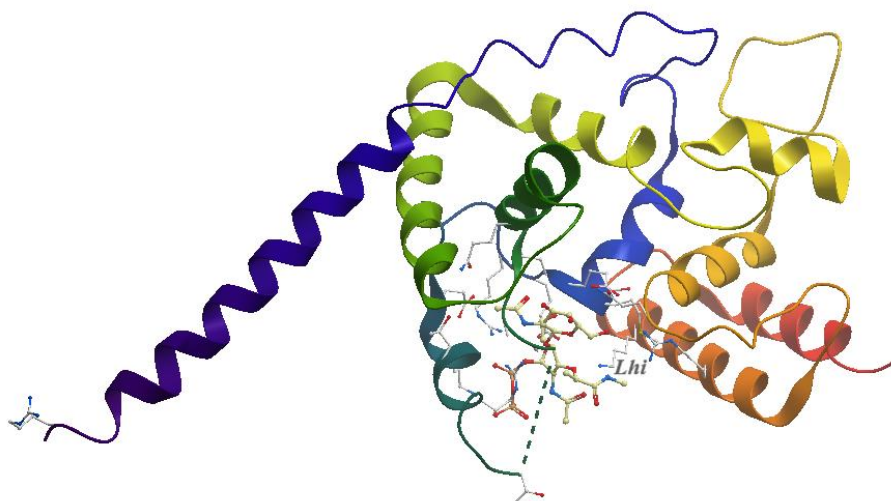


Figure 1.5 Crystal structure of complex of *S. aureus* monofunctional PGT (SaMGT) with Lipid II analogue (PDB ID: 3VMT) [51]

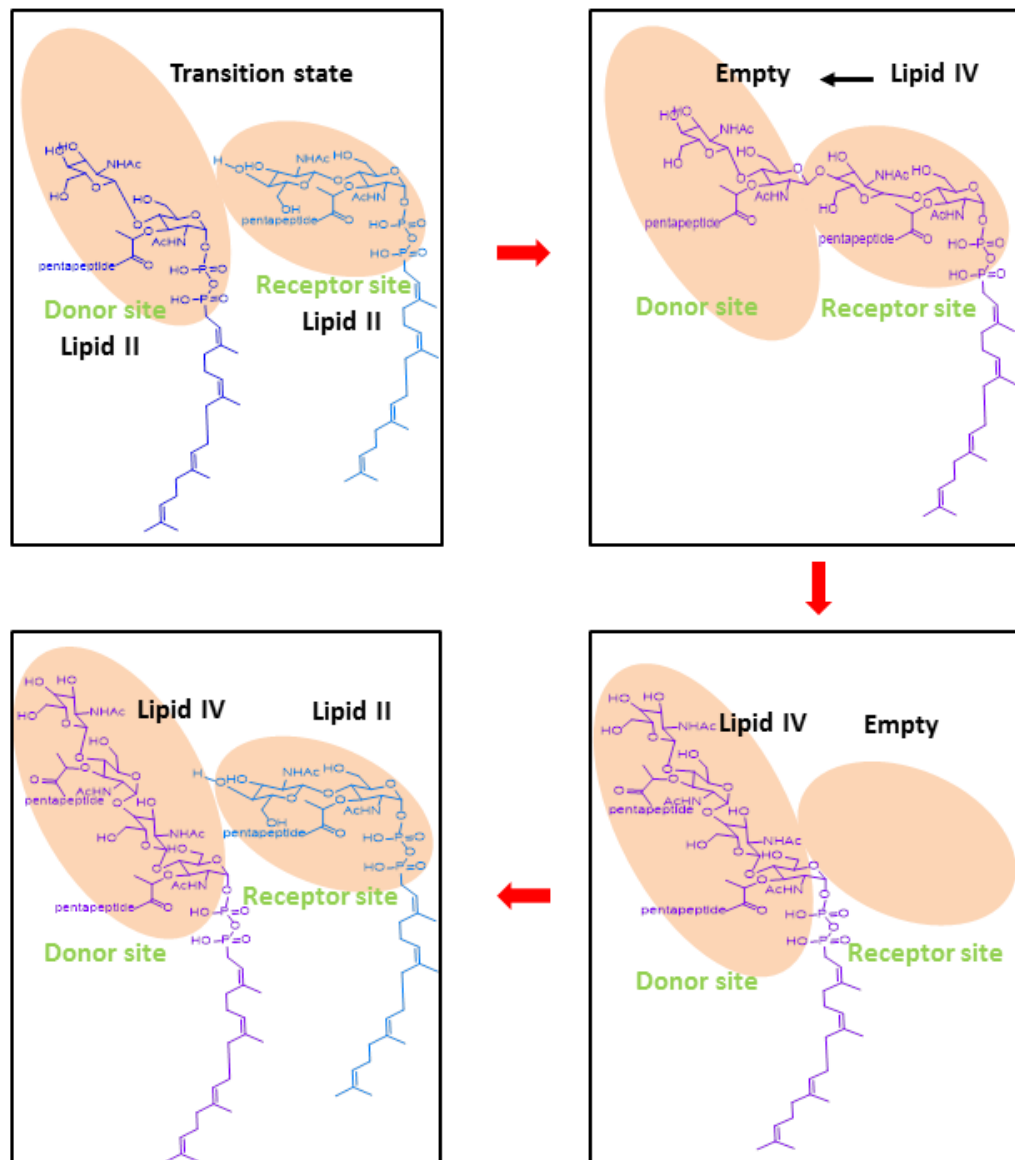


Figure 1.6 Mechanism of lipid II polymerization under the catalysis of PGT (adapted from [51])

1.4 Moenomycin A and its mimics as PGT inhibitors

1.4.1 Moenomycin A as a PGT inhibitor

Although several antibiotics that interfere with the polymerization of lipid II have been discovered, for example lantibiotics, ramoplanin and mannopeptimycins, these natural products inhibit the polymerization by acting on lipid II and only moenomycin A inhibits the polymerization by directly binding to the PGT domain of PBPs [45]. Moenomycin A (Moe A, shown in Figure 1.7), the major member of the moenomycin family antibiotics, was discovered in 1965 [52-54]. It is the only known antibiotic that inhibits peptidoglycan glycosyltransferase involved in the final stage of peptidoglycan biosynthesis by directly binding to the donor site of PGT. Moe A is a potent antibiotic against various Gram-positive bacteria, with the minimal inhibitory concentration (MIC) ranging from 1 ng/mL to 100 ng/mL, and is 10- to 1000-fold more potent than vancomycin [55]. Importantly, no pathogen isolated from human or animal is significantly resistant to Moe A [56]. Although *in vitro*-induced resistant strains were isolated, the process of resistance development is extremely slow with low-resistant frequencies [57]. Furthermore, no transferrable resistance between strains and no cross-resistance to other antibiotics were found [56, 58]. However, Moe A has no antibacterial effect in the human body because of its poor bioavailability. Furthermore, Moe A has quite a long half-life in bloodstream and causes some hemolysis in body. Therefore, it is currently used as a growth promoter in animal feed only [59].

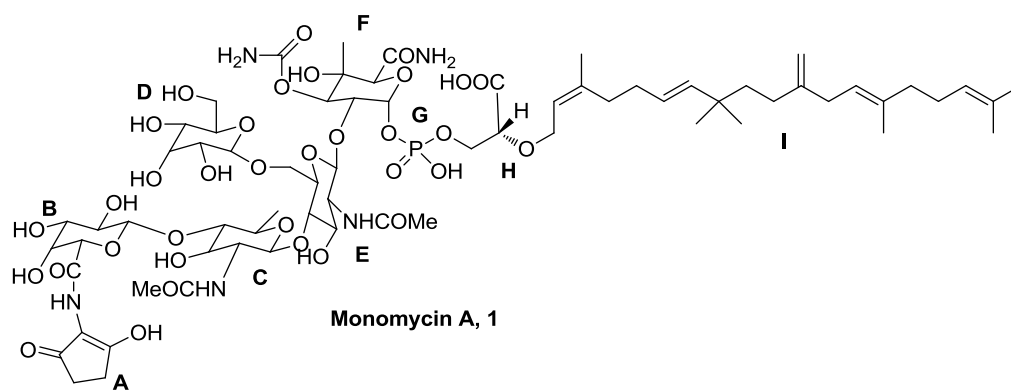


Figure 1.7 Structure of moenomycin A [52]

To improve its pharmacokinetic properties, researchers have studied extensively the structure-activity relationship (SAR) of moenomycin in the last two decades [60, 61]. Moenomycin A (Figure 1.7) consists of a chromophore unit A, a five-saccharide unit (B, C, D, E, F), and one C25 lipid chain attached to the sugar unit through a phosphate. The C25 lipid tail is essential for its bioactivity. Hydrogenation or shortening of the lipid chain reduces its antibacterial activity. Ring A is not essential for interaction with PGT and there is only a slight decrease in antibacterial activity after removing ring A. The C-E-F trisaccharide and E-F disaccharide segments are the minimal backbones for Moe A to maintain its antimicrobial activity *in vivo* and *in vitro* respectively.

In recent years, X-ray structures of different PGTs with moenomycin (Figures 1.4) have revealed that Moe A perturbs the binding of the growing glycan chain with PGT by binding to its donor site [47-49]. The pentasaccharide segment of Moe A extends to the active-site cleft of the PGT domain, and the E and F rings bind to the active residues through hydrogen bonds. It has also inferred from the binding pose of the phosphoglycerate unit that the lipid chain has a direct binding with PGTs [49]. The binding pose is confirmed by the SAR results of Moe A as mentioned above.

1.4.2 Synthetic PGT inhibitors based on moenomycin and lipid II

The structure-activity relationship of Moe A gives invaluable information for rational design of small molecule libraries with more drug-like structures based on the core structure of Moe A. Furthermore, design and synthesis of mimics of lipid II, the substrate of PGT, is another way to develop novel PGT inhibitors. C-Phosphonate disaccharides **2** and **3** (shown in Figure 1.8) were designed based on the core structures of Moe A and lipid II displayed modest (compound **2**) and no (compound **3**) PGT inhibition activity *in vitro* [62]. Compound **4**, which consisted of vancomycin segment and the disaccharide moiety of Moe A, was designed based on the concept that the main role of the lipid tail was to deliver Moe A to PGT which could be displaced by other groups with the same function. Vancomycin can bind to the peptide group of lipid II through hydrogen bonds. The hybrid compound **4** exhibited higher antimicrobial activity against several clinically relevant *cocci* than the two segments-disaccharide PGT inhibitors or vancomycin [63]. Lipid II analogue **5** containing an uncleavable 1-C-glycoside bond between the disaccharide segment and the pyrophosphonate showed a potent PGT inhibition with IC₅₀ of 25 μ M [64]. Recently, using PGT inhibitor Moe A as template, Zuegg *et al.* designed and synthesized two Moe A disaccharide mimics **6** and **7**, and both compounds showed potent antimicrobial activity against Gram-positive bacteria by targeting PGT. Then, based on the SAR of the disaccharide PGT inhibitors, two monosaccharide molecules **8** and **9** were screened out as extraordinary PGT inhibitors with a broad antibacterial spectrum, including multi-drug resistant methicillin-resistant *S. aureus*, vancomycin-resistant *S. aureus* and vancomycin

resistant *E. faecalis in vitro*, from a self-synthetic small molecule library of five hundred small molecules. Furthermore, compounds **8** and **9** also showed *in vivo* efficacy without toxicity in the tests of mouse model of septicemia and mouse mammary gland infection [65].

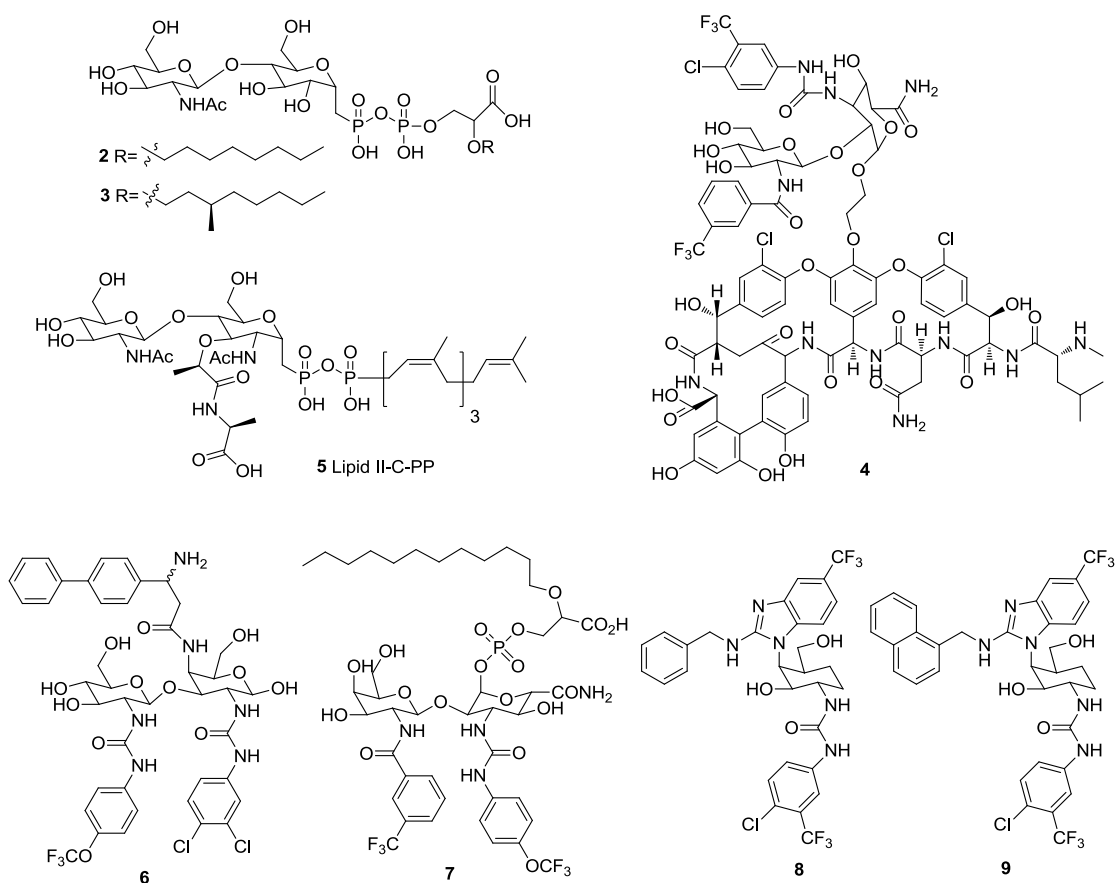


Figure 1.8 Synthetic PGT inhibitors inspired from Moe A and lipid II [62-65]

1.5 Assays for PGT inhibitors screening and potential PGT inhibitors from HTS

Peptidoglycan glycosyltransferase has been studied as a novel target for antibiotics development for more than 50 years, yet no antibiotics targeting PGT is available for the clinical treatment of bacterial infections. The slow progress of PGT inhibitors discovery is mainly due to the difficulty in obtaining the glycosyltransferase substrate, lipid II. In recent years, total synthesis of lipid II combined with crystal structures of different PGTs with lipid II or Moe A have advanced the development of assays for PGT inhibitors screening [47-49, 51]. On the following sections current assays that have been developed for PGT inhibitor screening and inhibitors screened out from these assays are discussed.

1.5.1 Lipid II-based peptidoglycan glycosyltransferase inhibition assays

This PGT inhibition assay used [^{14}C]-labeled or fluorophore-labeled lipid II as a reporter with glycosyltransferase [66, 67]. The fluorescent lipid II was obtained by attaching a fluorophore to the ϵ -amino group of the lysine residue of the pentapeptide unit via a sulfonamide linker and the modification of the peptide group of lipid II simultaneously prevents the molecules from cross linking, which facilitates the detection of the polymerization activity of the bifunctional PBPs. And for the [^{14}C]-labeled lipid II, penicillin was added to inhibit the occurrence of transpeptidation. The labeled lipid II acting as a reporter was incorporated into the growing glycan chain under the catalysis of glycosyltransferase, and then the assay results could be inferred

by detecting the amount of the radioactive or fluorescent products. Compounds that are able to reduce the productivity of the glycosyltransferases are PGT inhibitors.

Separation techniques such as paper or thin-layer chromatography (TLC), polyacrylamide gel electrophoresis and high-performance liquid chromatography (HPLC) are commonly used for isolation and detection of polymerized products. In 2013, Huang *et al.* designed a Forster resonance energy transfer (FRET)-based assay to detect inhibitors of transglycosylation without isolation of products. In this assay, they attached a coumarin (fluorophore) to the peptide segment as well as a dimethylamino-azobenzenesulfonyl quencher in the lipid tail of the same molecule [68]. At the beginning, the coumarin modified lipid II showed very weak fluorescence due to intramolecular FRET quenching. When the enzyme PGT was added and the lipid II analogues were incorporated into the growing glycan chain, the quencher-labeled lipid tail was released simultaneously. Therefore, FRET quenching was removed due to the release of the quencher, which would cause an increase in the fluorescence of the growing glycan products. As PGT inhibitors can prevent the biosynthesis of fluorescent growing glycan products, they can be detected by comparing the changes of fluorescence intensity before and after the addition of the PGT enzyme.

1.5.2 Moenomycin A-based displacement assays

SAR information of Moe A indicated that ring A is not an essential but a feasible moiety to provide reactive groups such as thiol and amine. A surface plasmon resonance

(SPR) based assay was developed using a ring A modified moenomycin [69]. In the assay, the Moe A derivative was immobilized on a sensor chip surface through an amide bond. PBP1b solutions at different concentrations were injected and the SPR signals resulting from the interaction between the PBP1b enzyme and the immobilized moenomycin derivative were concentration dependent. Free Moe A was then injected resulting in complete elution of PBP1b, which caused the SPR signal to return to the original level. This method allows PGT inhibitors to be screened based on the SPR signal resulting from elution of the PBP1b from the sensor chip surface.

Following the SPR assay, a fluorescence polarization (FP) based displacement assay was developed by Cheng *et al.* using a fluorescein labeled Moe A [70]. In the assay, fluorescence polarization of the fluorescein labeled Moe A increased due to the interaction between the PGT and the fluorescent Moe A which slowed down movement of the fluorophore. FP was recovered by adding some small molecules which could displace the probe from the binding site. Finally, six compounds (**10-15** as shown in Figure 1.9) from two databases of small molecules (57,000 compounds and 2 million compounds) were found to have both antimicrobial activity and PGT binding inhibition activities [71, 72]. However, the limitation of the assay is that detection of compounds with low affinity will be precluded from the drug candidate list as a result of the strong affinity of Moe A and PGTs. In 2013, Gampe *et al.* made an improvement of the FP assay by using a fluorescent labeled trisaccharide derivative of moenomycin with a lower binding affinity comparing to Moe A as the probe in the FP assay [67]. And one compound **15** was screened as an antibacterial agent inhibiting PGT. Although this

approach improved the sensitivity of the assay, the complexity of the chemical manipulations restricted its wide application. In recent years, computer-aided rational design is widely used in the early stage of drug discovery [73, 74]. In particular, the structure-based virtual screening of small molecule libraries provides a novel method for drug discovery more quickly and at a lower cost than the conventional way. In our group, using structure-based virtual high-throughput screening for PGT inhibitors, a lead compound, an isatin derivative **16** (Figure 1.9) screened out from a library of 3 million small molecules was shown to possess antibacterial activity by targeting PGTs [75].

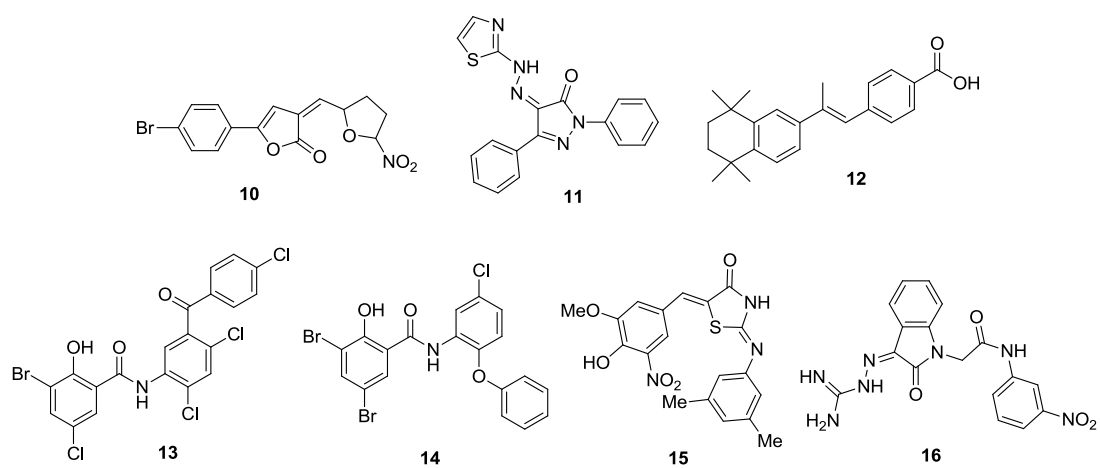


Figure 1.9 Some potential small molecule PGT inhibitors from HTS [67, 71, 72, 76]

1.6 Photoinduced electron transfer (PET) based biosensor

Biosensors are commonly used as analytical devices, which consist of a biological sensing element responsible for sensing a specific analyte, a transducer which converts the signal of interaction between analyte and biological element into a detectable and measurable signal, and a signal processor that is responsible for the display of the transferred signal in a user-friendly way. The advances in the synthesis of fluorescent dyes and the fluorescent imaging technologies in the past decades have prompted the fast development of fluorescent biosensors. Our research group has been developing novel biosensors based on fluorophore-labeled proteins for antibiotic residues detection. In recent years, we have developed a novel biosensor for β -lactam antibiotics detection by labeling the omega-loop of the enzyme β -lactamase with the environmentally sensitive fluorescein [77, 78]. In the construction of the biosensor, a β -lactamase E166C mutant was made by site-directed mutagenesis (SDM). The mutation resulted in a dramatic decrease in hydrolytic activity while the enzyme-substrate complex was stable enough for analysis. Environmental changes due to the binding between the mutant and its substrate resulted in an increase in fluorescence intensity. Recently our group has also developed a fast, simple and specific biosensing system for chloramphenicol determination based on photoinduced electron transfer (PET). In construction of the biosensor, a fluorescent chloramphenicol derivative labeled with fluorescein which had the same binding pose with chloramphenicol acetyltransferase as chloramphenicol was made. At the same time, a chloramphenicol acetyltransferase V28W/E140W mutant which quenched the fluorescence of fluorescein was constructed. The fluorescence of

the probe could be quenched by the tryptophan residue of the mutant while the complex of fluorescent chloramphenicol and acetyltransferase mutant formed, and then the fluorescent intensity would be mostly restored once the probe was displaced by chloramphenicol [79]. Besides the application in antibiotics detection, the PET based biosensors have been also applied in the detection of small anions (acetates, phosphates and amino acids) and biological molecules (DNA and ATP) [80-82].

1.6.1 Fluorescence quenching and photoinduced electron transfer

Fluorescence quenching is the decrease in fluorescence intensity caused by reactions or molecular interactions. Many molecular interactions can lead to fluorescence quenching, for example, ground-state complex formation, energy transfer, molecular rearrangements, and collisional quenching [83]. The quenching is mainly summarized into two types based on its process: collisional or dynamic quenching and static quenching. In the case of collisional quenching, the interaction between the excited fluorophore and an atom or molecule can facilitate non-radiative transitions to the ground state. The intensity decreases in the simplest case of collisional quenching is described by the well-known Stern-Volmer equation:

$$I_0/I = 1 + K_{SV}[Q]$$

I_0 and I are the fluorescence intensities in absence and presence of quencher respectively; $[Q]$ is the quencher concentration and K_{SV} is the Stern-Volmer quenching constant. Unlike collisional quenching, static quenching occurs when the fluorophore and another molecule form a stable complex in the ground state which is non-

fluorescent. This kind of quenching depends on the concentration of the quencher, as shown in the following equation which was firstly described by Gregorio Weber:

$$I_0/I = 1 + K_a[Q]$$

K_a is the association constant of the complex [83].

Fluorescence quenching by photoinduced electron transfer (PET) occurs when the photon excited fluorophore transfer electron with the other small molecule, through which the fluorescence of the fluorophore is quenched. The most classical mechanism of the PET is shown in Figure 1.10. The excited fluorophore is quenched by donating or accepting electrons, which gives rise to charge separation and formation of radical ion pair D^+A^- , and the ion pair goes back to the ground state by charge recombination without emission of a photon. Based on the mechanism, the quenching rate by PET depends on the efficiency of charge separation and recombination, which are mainly dependent on the energy of reactions, including the charge separation energy ΔG_{cs} , charge recombination energy ΔG_{cr} , and the distance between the donor and the receptor [84-88].

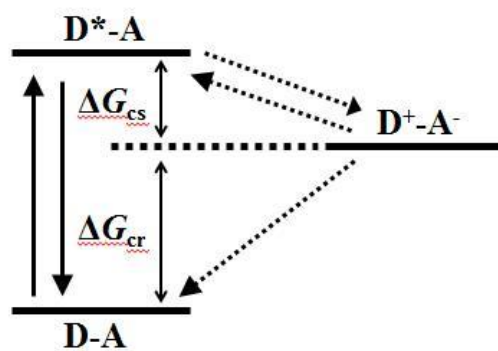
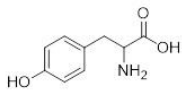
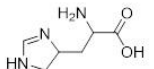
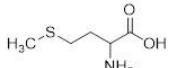
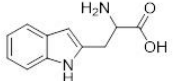


Figure 1.10 General mechanism of PET. D is the electron donor fluorophore, and A is the electron acceptor.

1.6.2 Fluorescence quenching by amino acids

Several natural amino acids including tryptophan (Trp), tyrosine (Tyr), histidine (His), and methionine (Met) have been identified as quenchers of Alexa dyes [89]. The structures of amino acid quenchers are shown in Table 1.1. The mechanism of the quenching was attributed to PET [86]. It occurs when the amino acids and the fluorophore are in close van der Waals contact and the electron is usually transferred to the amino acid (acceptor) from the excited fluorophore (donor). Then the excited fluorophore returns to its ground state by charge recombination without emitting a photon [86]. The natural amino acid tryptophan (Trp) is important in fluorescence-based study of peptides or proteins. For example, the quenching of the triplet state of tryptophan by cysteine has been used to measure formation rate of specific intramolecular interactions in disordered peptides [90]. Furthermore, Trp can be used as an efficient electron donor in PET reactions with some dyes, a property conferred by its indole group which is the most readily oxidized side chain among all natural amino acids [90].

Table 1.1 Structures of some reductive amino acids

Amino acid	Abbreviation	Structure
Tyrosine	Tyr, Y	
Histidine	His, H	
Methionine	Met, M	
Tryptophan	Trp, W	

1.6.3 Applications of PET based biosensors

The requirement of molecular contact for PET based quenching leads to a number of applications. For example, Sauer *et al.* developed a fluorescent assay for the ultrasensitive and specific detection of proteolytic enzymes using fluorophore-labelled peptide [91]. The conformation of the flexible peptide lied between the fluorophore and tryptophan residue which could quench the fluorescence. The contact resulted in an efficient fluorescence quenching through PET, and the fluorescence intensity increased dramatically in the presence of a protease which disturbed the contact by a specific cleavage of the peptide. Furthermore, Wang *et al.* designed a PET based sensing system to study the interaction between the anticancer drug mitoxantrone (MTX) and specific DNA [81]. The mechanism of the biosensor was that the MTX was absorbed on the surface of quantum dots (QDs), and the binding resulted in the fluorescence quenching of the QDs through PET. Then some extraneous DNA was added and some specific DNA could bind with MTX and remove the anticancer drug from QDs, which resulted in the restoration of the fluorescence. It was found that the fluorescence intensity was dependent on the concentration of the DNA. Recently, Wang *et al.* elucidated another novel biosensor using the fluorescent DNA/Ag nanoclusters and G-quadruplex/hemin based on photoinduced electron transfer [82]. This concept was further developed into a nanocluster-based molecular beacon for detection of target biomolecules such as DNA and ATP with high sensitivity and selectivity [92].

1.7 Aims and objectives

As mentioned above, the serious threat caused by bacterial drug resistance has provoked an urgent need for new antibiotics with novel targets. Peptidoglycan glycosyltransferase has been a well-proven target for development of new antibiotics to overcome the bacterial drug resistance. However, only one natural product, Moe A, has been identified as PGT inhibitor, but it can only be used as a growth promoter in the animal feed due to its poor bioavailability. The slow progress of the PGT inhibitor development mainly resulted from the lack of efficient and convenient method in the bioactivity assay.

The crystal structure of the complex of Moe A and PGTs revealed that Moe A can specifically bind to the donor site of PGTs tightly. This selective binding provides a good template for developing a new sensing system for PGT inhibitors. The construction of the new biosensor (Figure 1.11) for PGT inhibitors is as follows. Firstly, a fluorophore was attached to Moe A, and the modification of Moe A should make no change in its binding with PGTs. In this way, the fluorophore of the fluorescent Moe A can experience a huge change in solvation environment before and after the binding between the fluorescent Moe A and the PGTs. Furthermore, if a quencher of the fluorophore is introduced to a suitable site on PGT, the binding will lead to the fluorescent quenching of the fluorophore-labeled Moe A, and the dissociation of the fluorescent Moe A from PGT will remove the quenching and restore the fluorescent intensity. It is well-known that the natural amino acid tryptophan is an efficient quencher of fluorescein through a PET quenching process. Therefore, the new

biosensor can be set up by combination of a fluorescein labeled Moe A and tryptophan mutated PGT.

In construction of the sensing system, the fluorescent Moe A derivatives require a rational structure design. Based on previous SAR study, fluorescein should be attached to the ring A of Moe A, since modifications of ring A only cause a weak decrease in the bioactivity. Another important thing is the length of the linker between the fluorescein and Moe A, which plays a critical role to maximize the interaction between the fluorophore and the tryptophan residue of PGTs. Therefore, three fluorescein-labeled Moe A derivatives (**F-2-Moe A**, **F-3-Moe A** and **F-4-Moe A** with one, two and three carbons in the linker respectively) with linkers of different length will be synthesized. The synthesis and characterization of the fluorescent Moe A derivatives will be discussed in Chapter 2. Another important aspect in the construction of the biosensor is tryptophan mutation of PGT. In this study, the PGT domain of *S. aureus* PBP2 was expressed in *E. coli* BL21 with a vector pRSETk which was constructed from a commonly used vector pRSETA by changing AmpR to KanR. Five mutants with one amino acid close to the active site mutated to tryptophan by site-directed mutagenesis were expressed, purified and then characterized by mass spectrometry. The detailed construction of PGT mutants will be depicted in Chapter 3. After the preparation of the two components of the biosensor, the interaction between the probe and the PGT mutants and the performance of the sensing system was studied and the results will be discussed in Chapter 4.

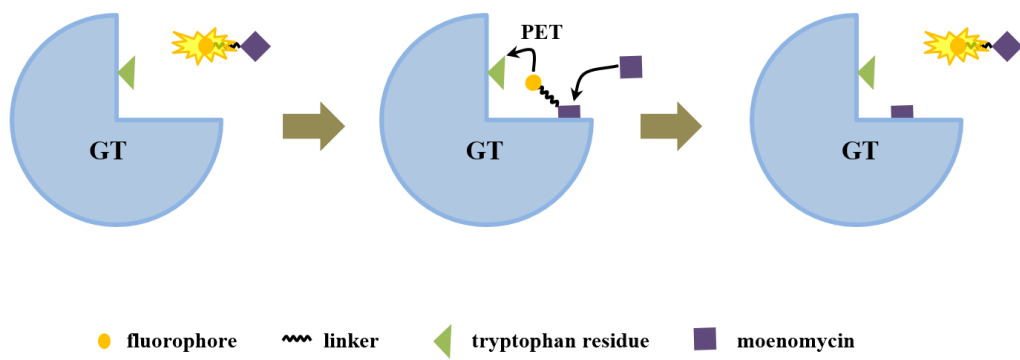


Figure 1.11 The concept of the PET-based biosensor for PGT inhibitors

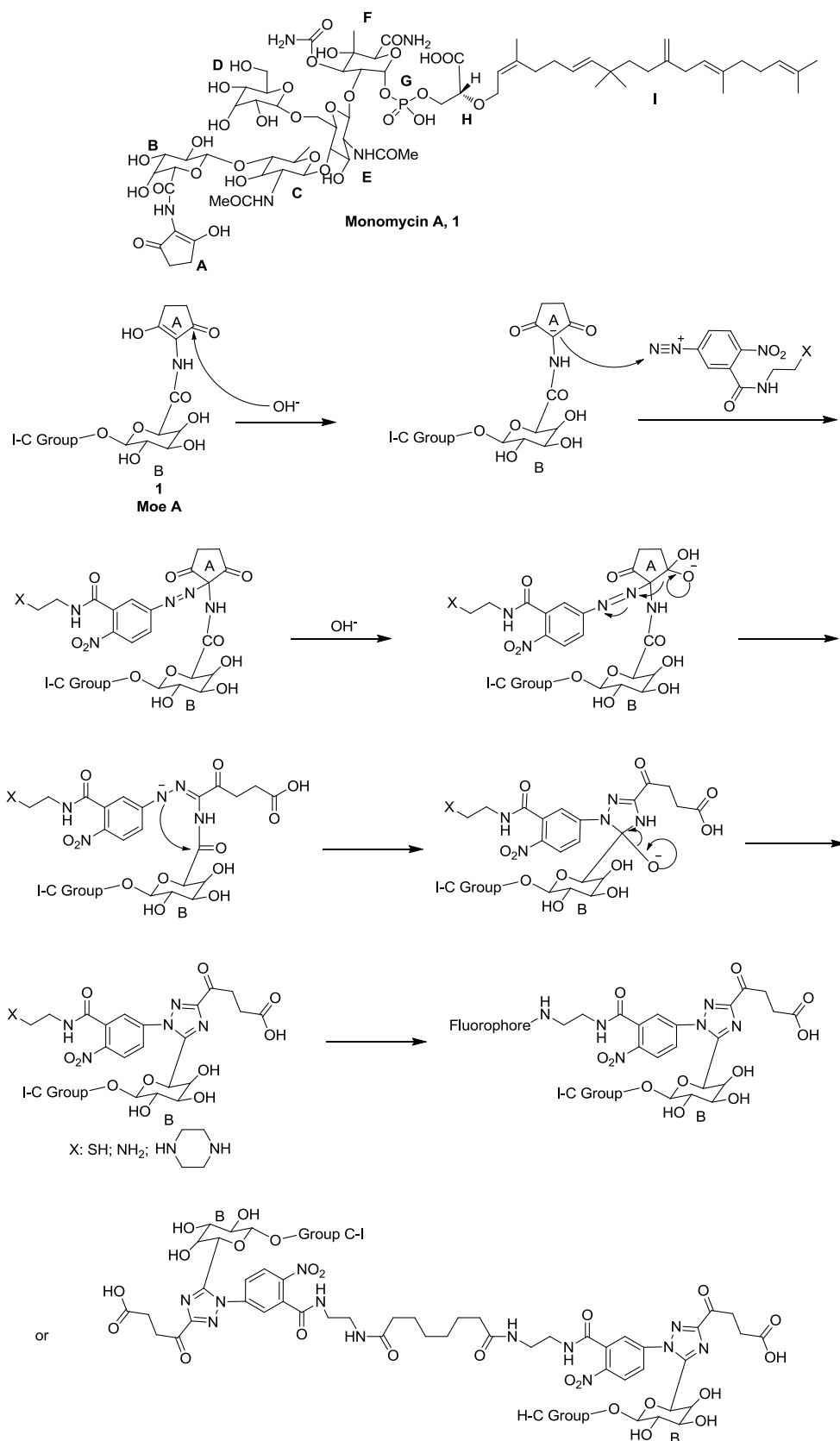
Chapter 2

Synthesis and characterization of fluorescein-labeled moenomycin A

2.1 Introduction

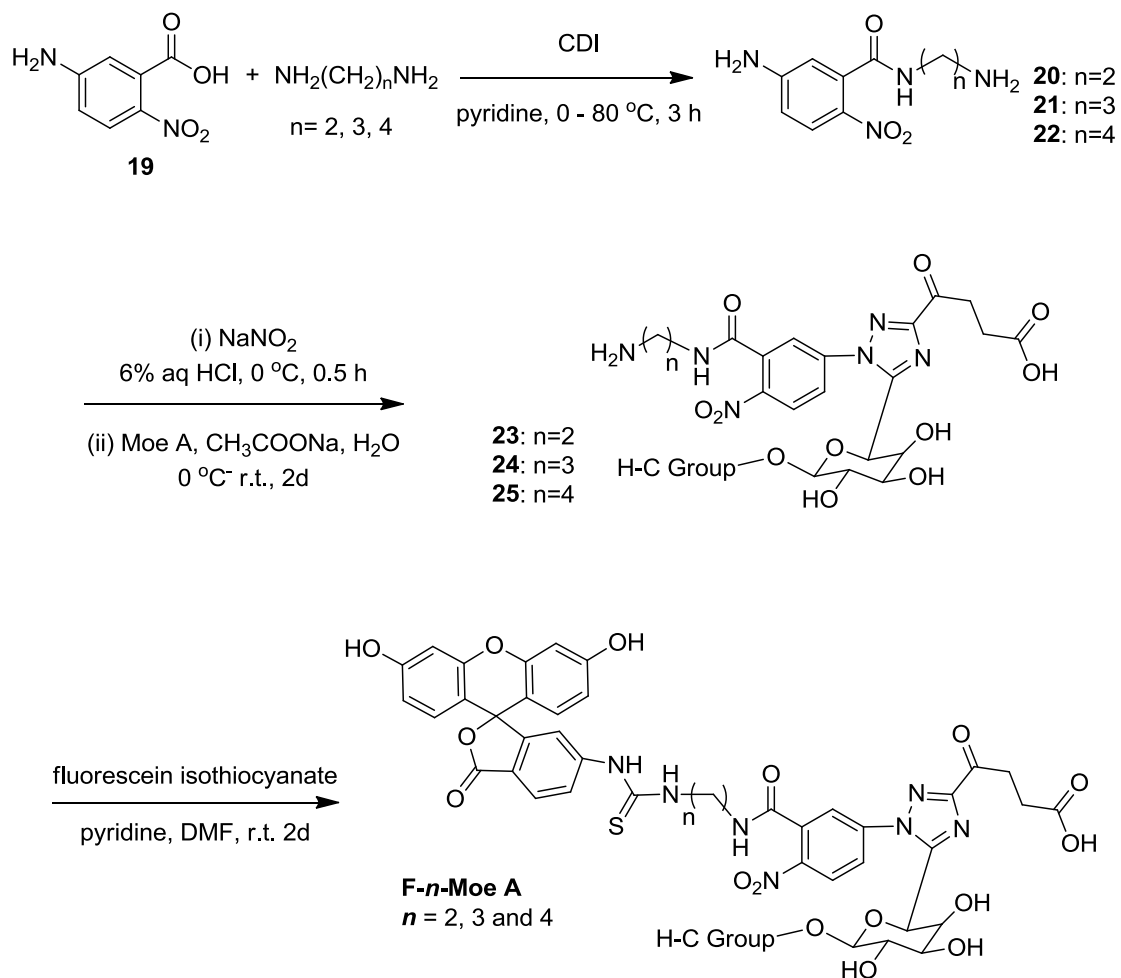
As mentioned in chapter I, in order for a fluorophore-labeled moenomycin to function as a probe in PGT inhibitor screening, it should have the following two properties: (i) the modified Moe A should be able to effectively bind to the same pocket of PGT as Moe A; (ii) the fluorescence intensity of the probe in free state should be strong enough for detection in PBS buffer solution and the fluorescence can be quenched efficiently by tryptophan.

Although the poor bioavailability of Moe A restricted its application in bacterial infection treatment, Moe A derivatives including fluorophore-labeled Moe A were employed in the study of inhibitory mechanism and inhibitor screening [67, 70, 93]. It is known that ring A of Moe A is not essential to its bioactivity [60, 61], so a series of moenomycin derivatives carrying different groups to replace ring A have been reported [94, 95], and these substituents provide reactive groups including free thiol and amine groups for further modifications. One of the approaches is by treating moenomycin with aryl diazonium salts to give products with substituted trizaole groups through Japp-Klingemann reaction. These products are featured with various active groups for moenomycin dimers construction as well as various fluorescence labels synthesis (Scheme 2.1).



Scheme 2.1 Synthetic scheme of Moe A derivatives and mechanism of Japp-Klingemann reaction

In this chapter, synthesis and characterization of three fluorescein-labeled Moe A derivatives with linkers of different lengths are discussed. Fluorescein isothiocyanate isomer I (FITC) was chosen because of its strong fluorescence, ease of availability and quenchability by tryptophan. Ring A of Moe A is a versatile group for modification, and most importantly, modification of this part does not change the binding pose of its derivatives to PGT. Therefore, a linker was introduced to ring A through Japp-Klingemann reaction and fluorescein was attached to the terminus of the linker. PET based quenching is highly dependent on the distance between the fluorophore and tryptophan, so the linker between Moe A and fluorescein should be of appropriate length and be flexible enough to allow the fluorophore to enter the binding pocket and be able to access the fluorescence quencher. In this study, three fluorescent Moe A derivatives (**F-*n*-Moe A**, *n* = 2, 3 and 4) with linkers of different lengths were designed and synthesized. The synthetic route is outlined in Scheme 2.2.



Scheme 2.2 Synthetic route of fluorescent Moe A derivatives. CDI: 1,1' - Carbonyldiimidazole

2.2 Experimental

2.2.1 Materials

Moenomycin A was isolated from crude flavomycin purchased from International Laboratory (ILD). Dimethylformamide (DMF), pyridine, aqueous HCl, NaNO₂, CH₃COONa and N,N'-Carbonyldiimidazole (CDI) were purchased from Sigma-Aldrich. Fluorescein isothiocyanate isomer I (FITC) was obtained from Acros. HPLC grade acetonitrile, dichloromethane and methanol were obtained from DUKSAN. Deuterated solvents were purchased from Cambridge Isotope Laboratories, Inc. Silica gel (70-200 μ m, Grace) was used for flash chromatographic separations. All these chemicals and solvents were used directly without further purification.

2.2.2 Instruments

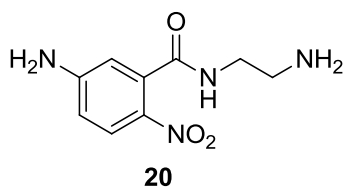
NMR spectra were recorded on a Bruker 400 MHz spectrometer (400 MHz for ¹H, 100 MHz for ¹³C and 162 MHz for ³¹P). All high resolution mass spectra were obtained on a Finnigan MAT 95S mass spectrometer. A preparative HPLC system (Waters) was used to isolate the products and an analytical HPLC system (Agilent) was employed to analyze the purity of the products. The eluent consisted of phosphate buffer (0.6 g of KH₂PO₄, 26.2 g of K₂HPO₄, and 1 L water, pH 8.0) and acetonitrile (60 : 40). UV-vis spectra were obtained with an Agilent Cary 8454 UV-vis spectrometer. Fluorescence measurements were performed with a Horiba FluoroMax-4 spectrofluorometer.

2.2.3 Preparation of moenomycin A

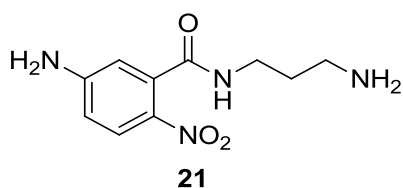
Moe A was extracted and isolated from crude flavomycin based on a published procedure [61]. Crude flavomycin (50 g) was dispersed in CH₂Cl₂ (200 ml) and the mixture was stirred and washed at room temperature overnight. The undissolved solid which contained Moe A was collected by filtration, and then extracted twice with MeOH (100 ml) at 40 °C for 5 h. The extracts were combined and concentrated *in vacuo* to obtain a yellow solid. The solid was purified by flash column chromatography with an eluent of 2-propanol and 2 M ammonium hydroxide (7 : 3) to give the crude Moe A. The crude Moe A was further purified using preparative HPLC with an eluent of CH₃CN and phosphate buffer (4 : 6) to give a white product (200 mg). ¹H NMR (400 MHz, MeOD) δ 5.95 (s, 1H), 5.95 (s, 1H), 5.47 (t, *J* = 6.6 Hz, 1H), 5.39 (d, *J* = 15.6 Hz, 1H), 5.35 – 5.25 (m, 1H), 5.20 – 5.09 (m, 1H), 5.05 (d, *J* = 10.6 Hz, 1H), 4.68 (d, *J* = 4.2 Hz, 1H), 4.64 (d, *J* = 7.2 Hz, 1H), 4.51 (d, *J* = 11.6 Hz, 1H), 4.44 (dd, *J* = 20.7, 8.1 Hz, 1H), 4.32 – 4.09 (m, 1H), 3.96 (dd, *J* = 22.3, 14.5 Hz, 1H), 3.85 – 3.78 (m, 1H), 3.77 – 3.35 (m, 2H), 2.71 (d, *J* = 7.3 Hz, 1H), 2.36 (s, 1H), 2.23 – 1.99 (m, 2H), 1.96 – 1.88 (m, 1H), 1.78 (s, 1H), 1.69 (s, 1H), 1.63 (s, 1H), 1.62 (s, 1H), 1.44 (d, *J* = 5.7 Hz, 1H), 1.42 – 1.34 (m, 1H), 1.28 (s, 1H), 0.98 (s, 1H); ¹³C NMR (100 MHz, MeOD) δ 198.78, 176.00, 174.00, 172.90, 172.66, 168.81, 157.84, 149.68, 140.39, 140.12, 135.96, 130.82, 125.52, 123.98, 122.12, 121.86, 109.73, 107.87, 103.55, 103.38, 102.97, 101.88, 94.72, 83.20, 80.99, 79.92, 78.59, 76.82, 75.32, 74.08, 73.71, 73.47, 73.05, 72.61, 72.46, 71.37, 71.02, 70.05, 69.37, 68.01, 65.14, 61.03, 55.83, 54.10, 41.49, 39.49, 35.06, 34.53, 32.14, 31.39, 30.96, 30.32, 26.49, 26.45, 26.31, 24.58, 22.71, 22.15,

22.00, 16.70, 16.42, 14.85, 14.74; ^{31}P NMR (162 MHz, CD_3OD) -2.25. HRMS (ESI) calcd for $\text{C}_{69}\text{H}_{107}\text{N}_5\text{O}_{34}\text{P}$ $[\text{M}-\text{NH}_3-\text{H}]^-$ 1580.6541, found 1580.6495.

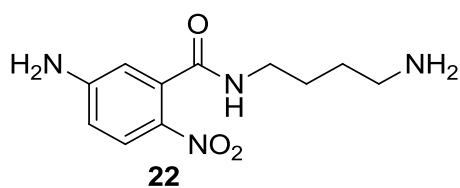
2.2.4 Synthesis of fluorescein-labeled Moe A



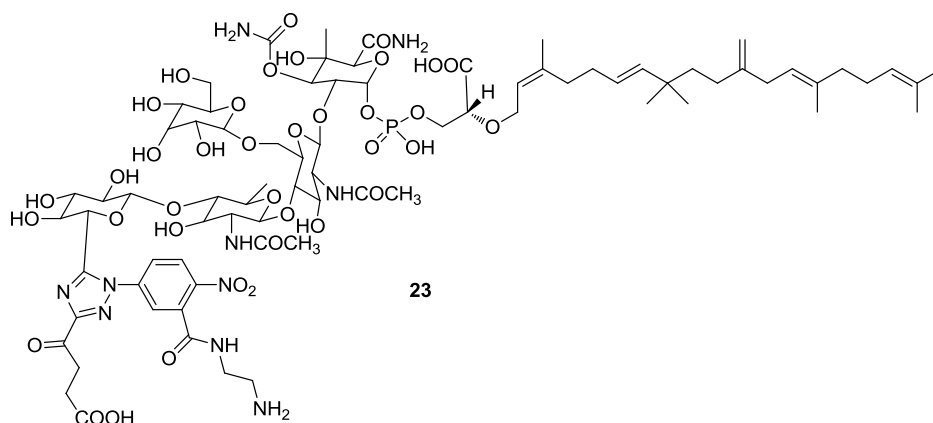
1,1'-Carbonyldiimidazole (CDI, 668 mg, 4.2 mmol) was added to a solution of 5-amino-2-nitrobenzoic acid (500 mg, 2.7 mmol) in pyridine (10 ml) and the mixture was stirred for 1 h at room temperature. A solution of ethylenediamine (194 mg, 3.2 mmol) in pyridine (1 ml) was then added slowly in an ice bath. The solution was stirred at 0 °C for 1 h and then at 80 °C for 3 h. The reaction was monitored by TLC until no starting reagent was left in the solution. The solvent was removed under reduced pressure to give a yellow oil. The mixture was purified by flash silica column chromatography (FC) to obtain a yellow solid (450 mg, 74 % yield). ^1H NMR (400 MHz, MeOD) δ 7.98 (d, $J = 9.1$ Hz, 1H), 6.67 (dd, $J = 9.1, 2.5$ Hz, 1H), 6.56 (d, $J = 2.5$ Hz, 1H), 3.59 (t, $J = 6.1$ Hz, 2H), 3.52 (t, $J = 6.1$ Hz, 2H); ^{13}C NMR (100 MHz, MeOD) δ 170.19, 154.90, 136.20, 133.53, 127.33, 112.68, 111.38, 40.36, 39.91. HRMS (ESI) calcd for $\text{C}_9\text{H}_{12}\text{N}_4\text{O}_3$ m/z : $[\text{M}+\text{H}]^+$ 225.0977, found 225.0982.



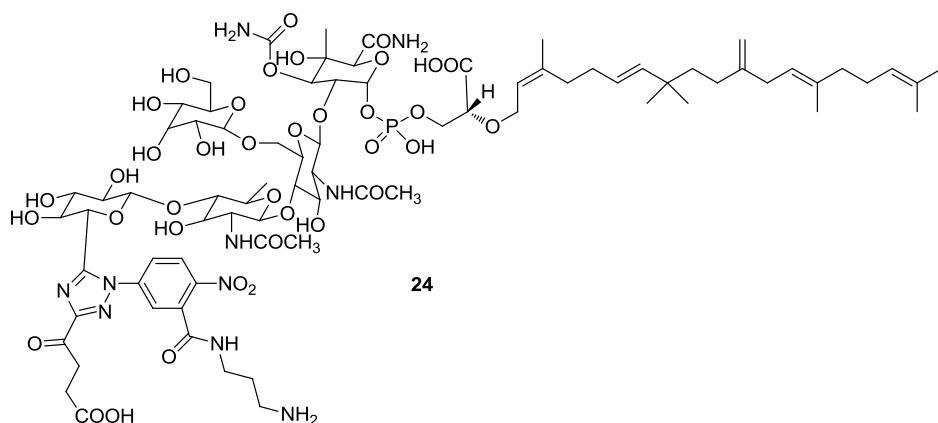
1,3-Diaminopropane was used instead of ethylenediamine to give product **21** (452 mg, 75%). ^1H NMR (400 MHz, MeOD) δ 7.98 (d, J = 9.1 Hz, 1H), 6.67 (dd, J = 9.1, 2.5 Hz, 1H), 6.56 (d, J = 2.4 Hz, 1H), 3.45 – 3.35 (m, 4H), 1.93 m, J = 6.8 Hz, 2H); ^{13}C NMR (100 MHz, MeOD) δ 169.74, 154.81, 136.28, 133.60, 127.26, 112.63, 111.85, 37.55, 29.37. HRMS (ESI) calcd for $\text{C}_{10}\text{H}_{14}\text{N}_4\text{O}_3$ m/z : $[\text{M}+\text{H}]^+$ 239.1139, found 239.1137.



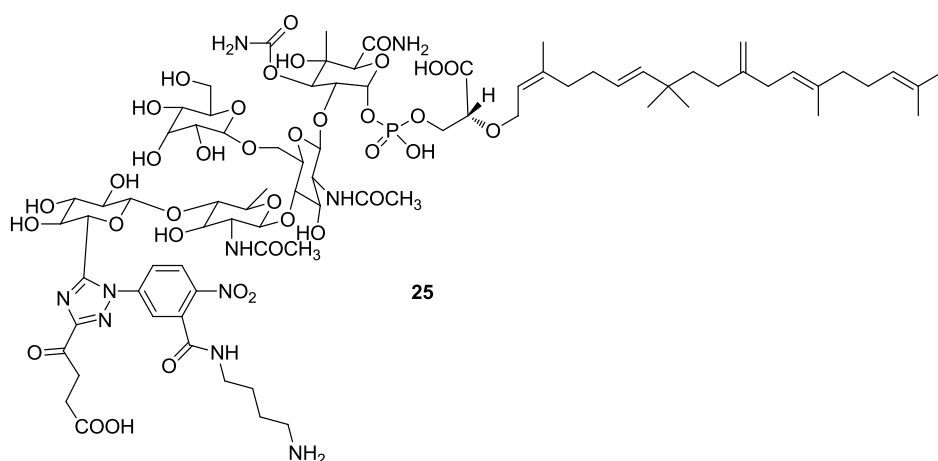
1,4-Diaminobutane was used instead of ethylenediamine to give product **22** (451 mg, 73%). ^1H NMR (400 MHz, MeOD) δ 7.99 (d, J = 9.1 Hz, 1H), 6.67 (dd, J = 9.1, 2.5 Hz, 1H), 6.57 (d, J = 2.5 Hz, 1H), 3.37 (t, J = 6.7 Hz, 2H), 2.71 (t, J = 7.0 Hz, 2H), 1.71 – 1.55 (m, 4H); ^{13}C NMR (100 MHz, MeOD) δ 169.70, 154.82, 136.33, 133.59, 127.28, 112.65, 111.90, 40.81, 39.19, 29.53, 25.96. HRMS (ESI) calcd for $\text{C}_{11}\text{H}_{17}\text{N}_4\text{O}_3$ m/z : $[\text{M}+\text{H}]^+$ 253.1295, found 253.1283.



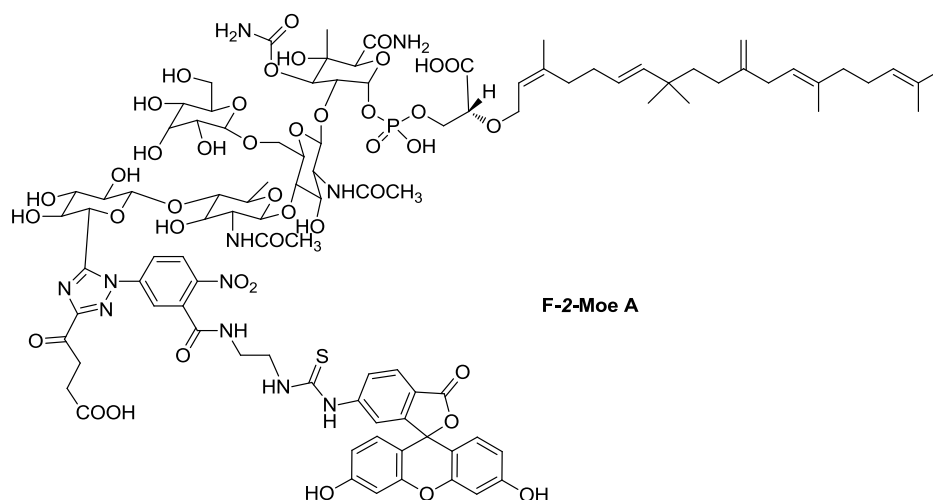
Compound **20** (67 mg, 0.3 mmol) was dissolved in 6% aqueous HCl (2 ml), and NaNO₂ (25 mg, 0.36 mmol) in H₂O (1 ml) was then added. The mixture was stirred for 30 min in an ice bath. The resulting solution was added slowly to a solution of Moe A (**1**, 100 mg, 0.06 mmol) and CH₃COONa (3 g, 36.6 mmol) in H₂O (100 ml) in an ice bath, and the mixture was stirred at 0 °C for 1 h. Then, the solution was further stirred at room temperature for 48 h. The solution was filtered and evaporated under reduced pressure to remove the solvent. Inorganic salts were removed by reverse phase flash column, and the crude product was purified by normal phase silica-gel column chromatography to obtain the target compound **23** (78.5 mg, 71%). HRMS (ESI) calcd for C₇₈H₁₁₇N₁₀O₃₇P [M-H]⁻ 1815.7246, found 1815.7174.



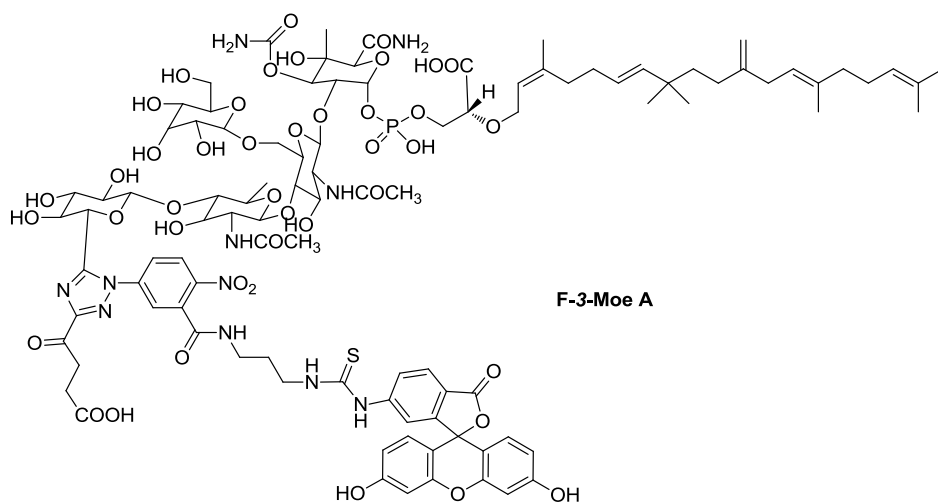
Compound **21** was treated by similar procedures as described for **20** to give product **24** (432 mg, 70 %). HRMS (ESI) calcd for $C_{79}H_{119}N_{10}O_{37}P$ $[M-2H]^{2-}$ 914.3665, found 914.3638.



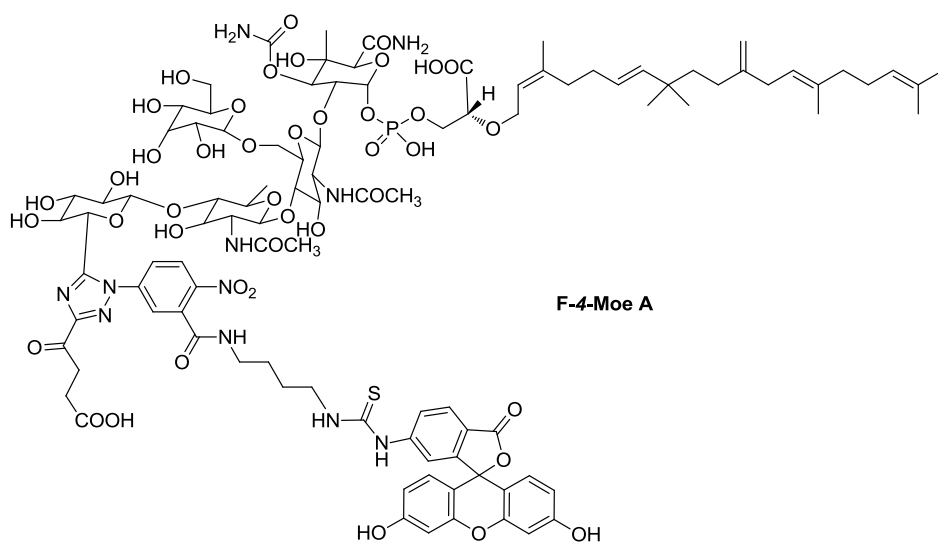
Compound **22** was treated by similar procedures as described for **20** to give product **25** (440 mg, 72%). HRMS (ESI) calcd for $C_{80}H_{121}N_{10}O_{37}P$ $[M-2H]^{2-}$ 921.3743, found 921.3728.



A solution of fluorescein isothiocyanate (isomer I, 10 mg, 0.023 mmol) in DMF (2 ml) was added to a solution of **23** (50 mg, 0.03 mmol) in DMF (1 ml) and pyridine (0.5 ml). The mixture was stirred in dark at room temperature under nitrogen for 2 days until TLC indicated no starting reagent was left in the reaction solution. The solvent was removed under reduced pressure to give a yellow residue which was then purified by prep-HPLC with a buffer system of phosphate solution (0.6 g of KH_2PO_4 , 26.2 g of K_2HPO_4 , and 1 L water, pH=8.0) and acetonitrile (60 : 40). Removal of organic solvent under reduced pressure and water by lyophilization gave a yellow powder **F-2-Moe A** (8 mg, 21%). HRMS (ESI) calcd for $\text{C}_{99}\text{H}_{128}\text{N}_{11}\text{O}_{42}\text{PS}$ $[\text{M}-2\text{H}]^{2-}$ 1101.8766, found 1101.8752.



Compound **24** was treated similarly as described for **F-2-Moe A** to give product **F-3-Moe A** (9 mg, 20%). HRMS (ESI) calcd for $C_{100}H_{130}N_{11}O_{42}PS$ $[M-2H]^{2-}$ 1108.8844, found 1108.8788.



Compound **25** was treated similarly as described for **F-2-Moe A** to give product **F-4-Moe A** (10 mg, 21%). HRMS (ESI) calcd for $C_{101}H_{130}N_{11}O_{42}PS$ $[M-2H]^{2-}$ 1115.8911, found 1115.8927.

2.2.5 Fluorescence quantum yield measurement

The absorption, excitation and emission spectra of the three probes were recorded. The absorption spectra of 1 μ M of fluorescent probes in PBS buffer were first obtained for wavelength 400 nm to 530 nm, which were followed by fluorescence measurement with excitation wavelength set to the maximum absorption wavelength (\sim 495 nm). Excitation and emission spectra were obtained with a slit width of 2 nm and a scan rate of 120 nm/min. Standard fluorescein dye in PBS buffer (0.5 μ M) was used as reference. The emission spectra of the samples and standard were obtained and integrated. The quantum yields of fluorescent probes were calculated by the following equation.

$$\Phi_x = \Phi_{st} \left(\frac{I_x}{I_{st}} \right) \left(\frac{A_{st}}{A_x} \right) \left(\frac{n_x^2}{n_{st}^2} \right)$$

Where Φ_{st} is the reported quantum yield of the standard, I is the integrated emission spectra, A is the absorbance at the excitation wavelength and n is the refractive index of the solvent used ($n = 1$ if same solvent). The subscription x denotes sample, and st denotes standard.

2.2.6 Fluorescence lifetime measurement

A time-correlated single photon counting (TCSPC) spectrofluorometer (PTI-QuantaMaster Spectrofluorometer) equipped with a Hamamatsu R928 photomultiplier tube was used for fluorescence lifetime measurement. A pulsed 460 nm LED was used

as the excitation source. The emission counts of the samples were recorded at 520 nm with 1 nm slit width. The instrument response function (IRF) was measured with a diluted Ludox solution. Time-resolved decay curves of the samples and Ludox were plotted. The lifetime of the three fluorescent Moe A were calculated by fitting the decay curves of the samples with reference to the Ludox standard.

2.3 Results and discussion

Moe A was isolated from crude flavomycin with a yield of 0.4 %. Purified Moe A was characterized by high-resolution mass spectrometry (HRMS), ^1H NMR, ^{13}C NMR and ^{31}P NMR and its purity was determined by analytical HPLC. All intermediates were characterized by HRMS, ^1H NMR and ^{13}C NMR. Fluorescent Moe A (**F-2-Moe A**, **F-3-Moe A** and **F-4-Moe A**) with linkers of various lengths were successfully obtained through 3 steps with yields of 11%, 10% and 11% respectively. The target compounds **26**, **27** and **28** were named as **F- n -Moe A** where n ($n = 2, 3$ and 4) is the number of carbon in the linker. The **F- n -Moe A** ($n = 2, 3$ and 4) were characterized by HRMS and their purities were determined by analytical HPLC (Appendix I).

2.3.1 Spectral properties of fluorescein-labeled Moe A

The absorption, excitation and emission spectra of the three fluorescent probes are shown in Figures 2.1, 2.2 and 2.3 respectively. All these probes show similar spectral properties to fluorescein. As shown in Figure 2.1, the maximum absorption wavelength of the probes were around 495 nm. Furthermore, as shown in Figures 2.2 and 2.3, the maximum excitation and maximum emission wavelengths of the three fluorescein-labeled Moe A derivatives were found to be around 494 nm and 517 nm respectively which are also similar to those of fluorescein. The excitation and emission wavelengths of the three probes are summarized in Table 2.1.

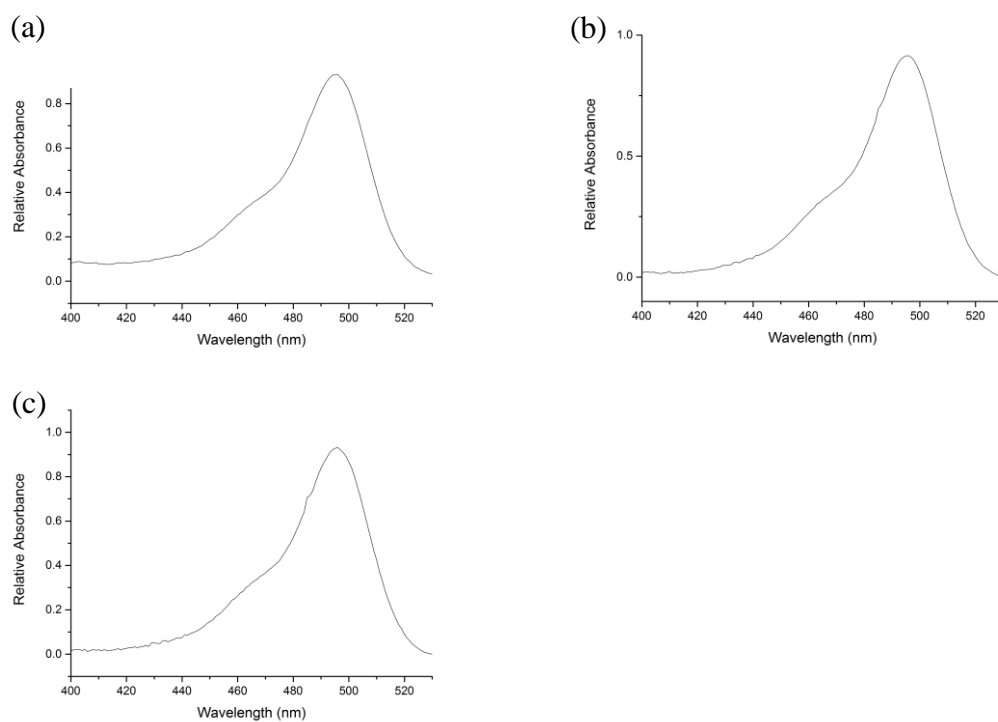


Figure 2.1 UV-vis absorption spectra of (a) 1 μ M of **F-2-Moe A**, (b) **F-3-Moe A** and (c) **F-4-Moe A** in PBS buffer (pH 8.0) at 25 °C.

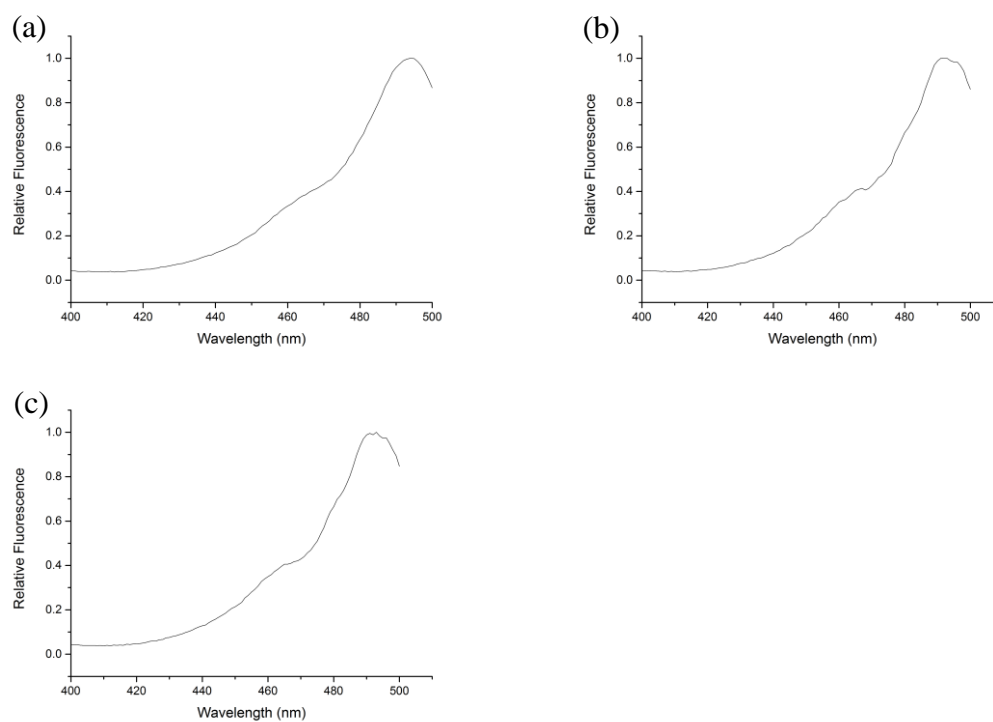


Figure 2.2 Excitation spectra of 1 μ M of (a) **F-2-Moe A**, (b) **F-3-Moe A** and (c) **F-4-Moe A** in PBS buffer (pH 8.0) at 25 $^{\circ}$ C with the emission wavelength set at 520 nm and the slits at 2 nm for both excitation and emission.

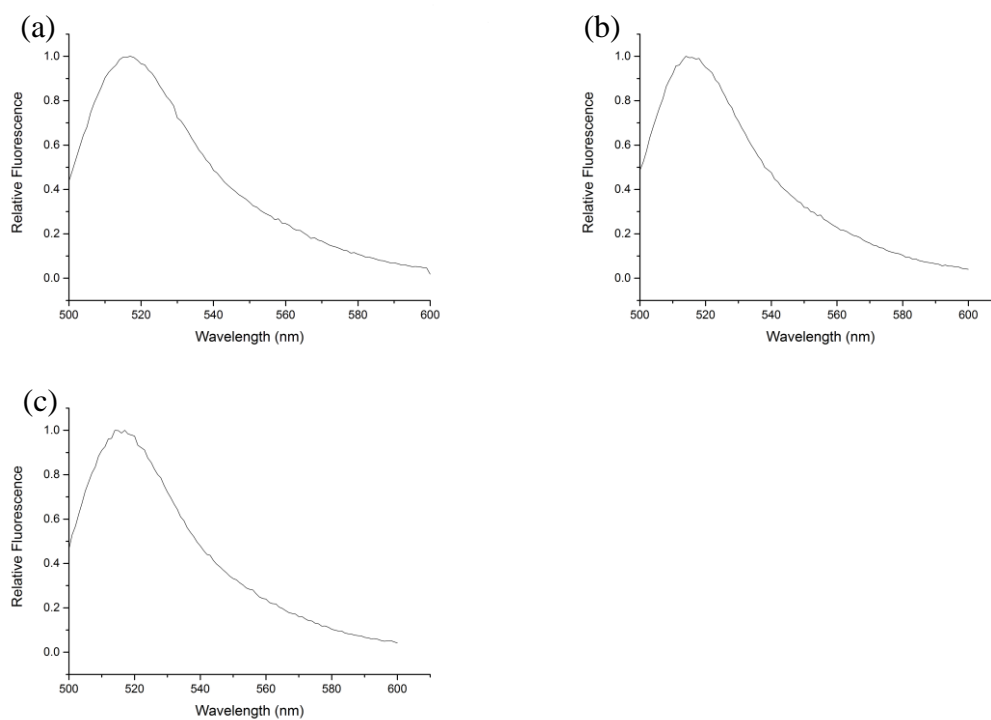


Figure 2.3 Emission spectra of 1 μ M of (a) **F-2-Moe A**, (b) **F-3-Moe A** and (c) **F-4-Moe A** in PBS buffer (pH 8.0) at 25 °C with the excitation wavelength set at 495 nm and the slits at 2 nm for both excitation and emission.

Table 2.1 Excitation and emission wavelength of the fluorescein-labeled Moe A derivatives

Fluorophores	Excitation Wavelength	Emission Wavelength
	λ_{max} (nm)	λ_{max} (nm)
F-2 -Moe A	494	517
F-3 -Moe A	491	514
F-4 -Moe A	493	517

2.3.2 Quantum yield and lifetime of the fluorescent probes

The quantum yield of fluorescent Moe A derivatives are summarized in Table 2.2. With fluorescein ($\Phi=0.79$) as reference [96], the quantum yield of the three probes (**F-2-Moe A**, **F-3-Moe A** and **F-4-Moe A**) were obtained with values of 0.52, 0.53, 0.55 respectively. Comparing to standard fluorescein, the quantum yields of the three probes are decreased by about 30%, which indicate that more energy of the excited probes are given off in a non-radiative manner. A possible explanation could be due to the presence of nitro-benzene group which is a quencher of certain fluorophores [97, 98]. Although the quantum yields of the probes are less than that of fluorescein, the fluorescence intensities of the probes are still strong enough for fluorescence assay.

The fluorescence lifetime of the three probes were also studied. The time resolved decay curves of the three probes are shown in Figure 2.4. The fluorescence decay curves of the three probes were fitted by a mono-exponential decay model to obtain the lifetime, and their lifetime were determined to be about 3 ns (Table 2.2). The decay model of **F-*n*-Moe A** is accordance with that of FITC reported before [99].

Table 2.2 Quantum yields and lifetime of the fluorescent probes

Fluorophores	Quantum Yield (Φ)	Lifetime (τ , ns)
Fluorescein	0.79 [#]	4.10 [#]
F-2 -Moe A	0.52	3.20
F-3 -Moe A	0.53	3.15
F-4 -Moe A	0.55	3.36

[#]The quantum yield and lifetime of fluorescein in the PBS buffer were reported to be 0.79 [96] and 4.10 [99].

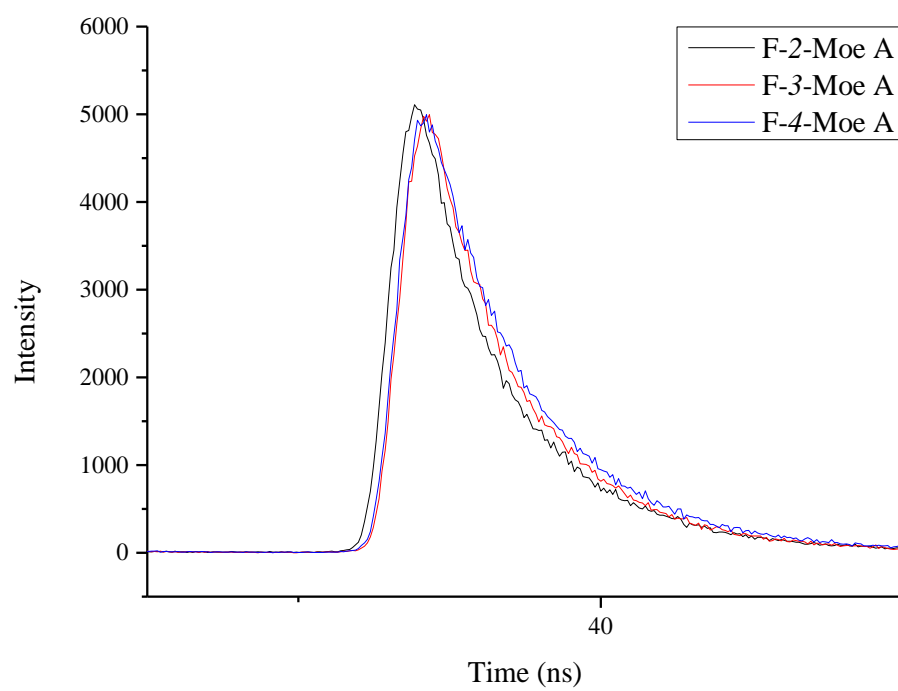


Figure 2.4 Time resolved decay curves of probes **F-2-Moe A**, **F-3-Moe A** and **F-4-Moe A**

2.4 Concluding remarks

In this chapter, three fluorescent probes (**F-2-Moe A**, **F-3-Moe A** and **F-4-Moe A**) with different linkers were designed, synthesized and characterized by high resolution mass spectrometry. Moreover, the spectral properties of the probes were also studied. These three probes possess similar absorption, excitation and emission properties. The photophysical properties of the probes are similar to those of fluorescein. The lifetime of three probes are around 3 ns. The quantum yield of the probes decreased by about 30% compared to fluorescein, which may be caused by the nitrobenzene group introduced to the linker. However, the quantum yields are still high enough for the three probes to be applied in fluorescence assay.

Chapter 3

Rational design, preparation and characterization of PGT mutants

3.1 Introduction

Since peptidoglycan glycosyltransferase is a promising target for antibiotic development, having a high performance assay for screening PGT inhibitors is of utmost importance. In recent years, several crystal structures of complexes of PGT with Moe A or lipid II have been solved, which greatly advanced the development of assays for screening PGT inhibitors [67, 68, 70]. From a biomedical perspective, fluorescent biosensors based on fluorescence intensity, polarization or lifetime, can provide a sensitive means for probing ions, metabolites, and protein biomarkers. These biosensors are widely used in disease diagnosis and monitoring, study of enzyme kinetics, and high throughput screening in drug discovery [100-103].

Several natural amino acids, including tryptophan, tyrosine, histidine and methionine, can induce fluorescence quenching of certain dyes through photoinduced electron transfer (PET) when the quencher amino acids are in van der Waals contact with the dyes [89]. Among them, tryptophan (Trp) is the most efficient quencher of commonly used dyes such as fluorescein [90]. Tryptophan, a natural amino acid, can be easily introduced into a specific site of a protein by site-directed mutagenesis. On the other hand, fluorescein is commonly used in fluorescence measurements due to its desirable absorption and emission characteristics as well as high fluorescence intensity and

quantum yield. Therefore, a biosensing system containing a tryptophan-mutated protein and its binding partner labeled with fluorescein can be constructed and be employed in areas such as small molecules detection, drug discovery and protein-protein interaction studies.

In this study, *S. aureus* PBP2 PGT domain was transformed into a fluorescent quencher by mutation of some amino acids near its binding pocket into tryptophan. Fluorescence quenching by photoinduced electron transfer is highly dependent on the distance between the fluorophore and the quencher. In order to find the best PGT mutant for constructing the biosensing system, five amino acid residues at different locations close to the binding pocket were selected for mutation to tryptophan based on the crystal structure of the complex of *S. aureus* PBP2 and Moe A. These five sites are shown in Figure 3.1, which include glutamine at position 161 (Gln-161, Q161), histidine at position 162 (His-162, H162), aspartic acid at position 199 (Asp-199, D199), tyrosine at position 210 (Tyr-210, Y210) and aspartic acid at position 241 (Asp-241, D241).

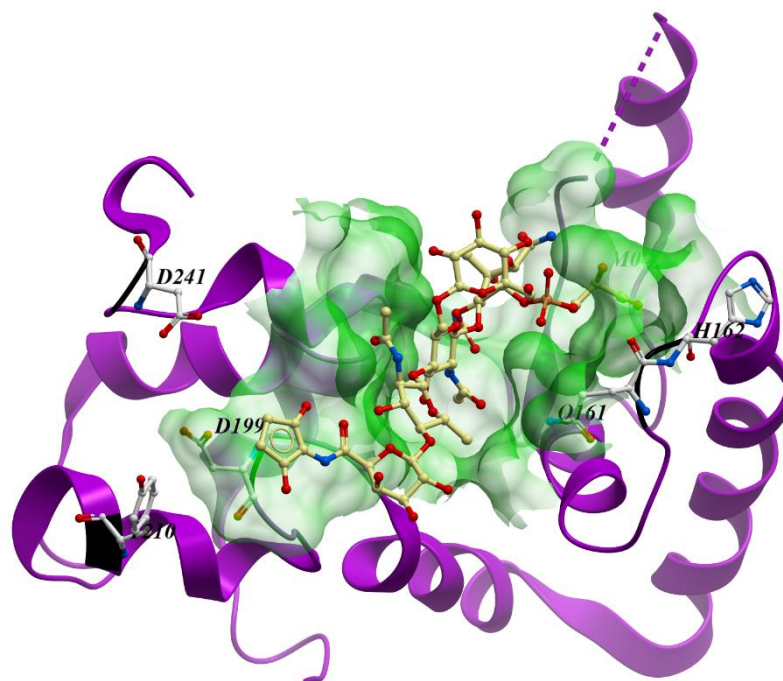


Figure 3.1 The five amino acid residues selected for mutation based on the crystal structure of complex of *S.aureus* PBP2 and Moe A [47]

3.2 Experimental

3.2.1 Materials

3.2.1.1 Chemicals

Kanamycin sulfate, ethylenediaminetetraacetic acid (EDTA), sodium phosphate monobasic dihydrate, sodium hydroxide, sodium chloride and sodium dodecyl sulfate (SDS) were purchased from Sigma-Aldrich Co. Tris(hydroxymethyl)aminomethane (Tris) was bought from ACROS. Isopropyl β -D-1-thiogalactopyranoside (IPTG) was obtained from USB Corporation. Reagents for Bradford protein assay were purchased from Bio-Rad Laboratories. HBS-EP buffer (0.01 M HEPES, pH 7.4, 0.15 M NaCl, 3 mM EDTA, 0.005% surfactant P20) as running buffer for SPR assay and regeneration scouting kit were obtained from GE Healthcare.

3.2.1.2 Media

Nutrient agar, tryptone and yeast extract were purchased from Oxoid Ltd. (Nepean, Ontario, Canada). Luria-Bertani (LB) medium was prepared by adding yeast extract (0.5 g), sodium chloride (0.5 g) and tryptone (1 g) in 100 mL deionized water and sterilized. It was used during the transformation of recombinant plasmid, preparing *E. coli* competent cells, and growing of pre-culture before protein expression. 2 \times TY medium for protein expression was prepared by mixing yeast extract (2.0 g), tryptone (3.2 g) and sodium chloride (1.0 g) in 200 mL deionized water and sterilized. Kanamycin (50 μ g/ml) was used for selection of plasmid containing *E. coli*.

3.2.1.3 Bacterial strains and plasmids

E. coli Top 10 was used for routine propagation and genetic modification of plasmids. *E. coli* BL21 (DE3) was used for overexpression of PGT wild type (WT) and its mutants. Plasmid pRSETk was employed for production of wild type PGT and mutants in *E. coli* expression system. The map of PGT-pRSETk is shown in Figure 3.2. The vector carries a pUC replication origin (ORI) and a fl origin for replication in *E. coli*, T7 promoter and T7 terminator. Antibiotic selective marker includes Kan^R gene for kanamycin resistance. The recombinant gene of PGT was inserted into the multiple cloning sites of the plasmid between *Bam*HI and *Xho*I restriction sites for overproduction of N-terminal 6-histidine tagged PGT.

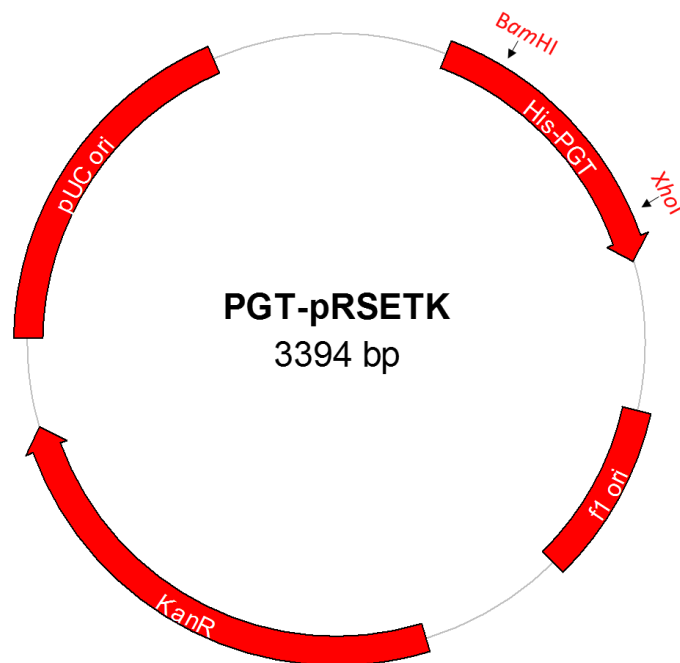


Figure 3.2 Plasmid map of PGT-pRSETk.

3.2.1.4 DNA manipulation reagents

Primers for site-directed mutagenesis (SDM) were obtained from Integrated DNA Technologies, Inc. PfuUltra High-Fidelity DNA polymerase for PCR and SDM and its corresponding PfuUltra buffer were purchased from Stratagene. Wizard® Plus SV Minipreps DNA Purification System, T4 DNA ligase, dNTPs, restriction enzymes including *Bam*HI, *Dpn*I, *Nde*I and *Xho*I were purchased from Promega and the Agarose Gel DNA Extraction Kit was obtained from Roche.

3.2.2 Cloning and expression of PGT mutants

3.2.2.1 Preparation of competent cells

A single colony of *E.coli* Top 10 or *E. coli* BL21 (DE3) was picked and cultured in 5 ml of sterilized LB medium at 37 °C overnight with shaking at 250 rpm. 1 ml of overnight culture was added to 100 ml of fresh LB medium and subjected to a further incubation at 37 °C with shaking at 250 rpm. When OD₆₀₀ of the culture reached about 0.4, the cells were harvested by centrifugation at 4000 rpm at 4 °C for 20 min. After discarding the supernatant, the cell pellet was resuspended gently in 10 ml of ice-cold CaCl₂ (100 mM), and then the mixture was incubated in ice for 30 min. The cells were harvested by centrifugation at 4000 rpm at 4 °C for 20 min again. Then, the cells were resuspended gently in a solution containing 1 ml of ice-cold CaCl₂ (100 mM) and 0.5 ml of 50 % glycerol. The competent cells were aliquoted into 100 µl portions and used

immediately or quickly freezed by liquid nitrogen and stored at -80 °C for later use.

3.2.2.2 Transformation of recombinant plasmid into *E. coli*

In the process of transformation, 2 µl of the target plasmid and CaCl₂ treated-competent cells (*E. coli* Top10 and *E. coli* BL21 (DE3)) were mixed gently in an ice-cold microcentrifuge tube, and the mixture was kept in ice for 30 min before heat shocked at 42 °C for 1 min. The mixture was kept in ice for 3 min. Then 1 ml of fresh LB medium was added, mixed gently, and the mixture was incubated at 37 °C for 1.5 hours. Finally, about 50 µl of the cells were plated onto the LB agar containing kanamycin and incubated at 37 °C overnight.

3.2.2.3 Site-directed mutagenesis (SDM)

The PGT domain without transmembrane region was amplified from the full length *S. aureus* PBP2 by PCR, and was then inserted into vector pRSETk. Site-directed mutagenesis of PGT gene was performed through the approach of whole plasmid mutagenesis. In this method, a pair of complementary mutagenic primers were designed and employed to amplify the whole plasmid in a thermocycling reaction using PfuUltra High-Fidelity DNA polymerase. After the reaction, the template DNA was eliminated by enzymatic digestion using the restriction enzyme *DpnI*, which can selectively digest methylated DNA. The template plasmid which is biosynthesized in *E. coli* is methylated while the mutated plasmid generated by PCR *in vitro* is not methylated. Therefore, the template plasmid was digested while the mutated plasmid was not digested.

Five different sites in wild type PGT were selected for mutation to tryptophan by SDM using different primer sets. Details of the primers used for the mutations are listed in Table 3.1. PCR was carried out in a MJ Research PTC-200 Peltier thermal cycler. A mixture of 50 μ l in total, containing sterile water (40 μ l), plasmid PGT-pRSETk (0.2 μ g, 1 μ l), 10 μ M forward primer (1 μ l), 10 μ M reverse primer (1 μ l), 10 mM dNTPs (1 μ l), PfuUltra High-Fidelity DNA polymerase (1 μ l) and 10X PfuUltra buffer (5 μ l) was subjected to PCR cycling. The condition for SDM was set as follows: pre-denaturation at 94 °C for 1 min; 18 cycles of denaturation at 94 °C for 1 min, annealing at 58 °C for 1 min and elongation at 68 °C for 4 min; and a final extension at 68 °C for 8 min, and then the product was kept at 4 °C. The PCR products were analyzed by agarose gel electrophoresis. *DpnI* (1 μ l) was subsequently added to the product mixture to eliminate the template plasmid. The solution was mixed gently and allowed to react at 37 °C for 2 h. Then, 10 μ l of the digested PCR product was transformed into *E.coli* Top 10 competent cells. All transformed cells were cultured in a LB agar plate containing kanamycin at 37 °C overnight after recovery in LB at 37 °C for 1 h. Several colonies were picked and inoculated into 5 ml of fresh LB medium individually and were allowed to grow overnight at 37 °C. Finally, mutated PGT-pRSETk were extracted using plasmid DNA mini-prep kits and then sent for DNA sequencing to confirm correct mutations. DNA sequencing was performed by BGI Ltd. using ABI 3730xl DNA analyzer based on Sanger sequencing method.

Table 3.1 PGT mutants construction

Mutant	DNA sequence	Resultant plasmid
Q161W	Forward: 5'-AAAGATGCATTTTATCAT TGG CATAAAATCTATTGGACGT-3' Reverse: 5'-ACGTCCAATAGATTTATG CCAT GATAAAAAATGCATCTTT-3'	PGT-pRSETk/Q161W
H162W	Forward: 5'-ATGCATTTTATCACAT TGG AATTCTATTGGACGTAAAG-3' Reverse: 5'-CTTTACGTCCAATAGATTT CCA TTGTGATAAAAAATGCAT-3'	PGT-pRSETk/H162W
D199W	Forward: 5'-CTAAATAAAATTTACTATTCT TGG GGCGTAACAGGTATTAAAGC-3' Reverse: 5'-GCTTTAATACCTGTTACGCC CCA AGAATAGTAAATTTTATTAG-3'	PGT-pRSETk/D199W
Y210W	Forward: 5'-GCTGCTGCTAAGT TGG TACTTTAATAAAG-3' Reverse: 5'-CTTTATTAAAGTAC CCA CTTAGCAGCAGC-3'	PGT-pRSETk/Y210W
D241W	Forward: 5'-CAACTATAATATTTAT TGG CATCCAAAAGCTGCTG-3' Reverse: 5'-CAGCAGCTTTTGGATG CCA ATAAATATTATAGTTG-3'	PGT-pRSETk/D241W

Note: the bold and underlined sequences correspond to the sites for mutagenesis

3.2.2.4 Expression and purification of PGT mutants

Wild type PGT and its five mutants were transformed and overexpressed in *E. coli* BL21 (DE3). Glycerol stock of BL21 (DE3) cells containing the recombinant plasmid were streaked on LB plate containing kanamycin and incubated at 37 °C overnight. A single colony was picked and inoculated into 5 ml of fresh LB medium with kanamycin. It was then incubated at 37 °C with shaking at 250 rpm overnight for about 16 h. The pre-culture was transferred into a fresh 2×TY medium containing kanamycin in 1:100 dilution (2 ml pre-culture into 200 ml 2×TY medium), followed by incubation at 37 °C with shaking at 250 rpm for about 2-3 h. Cell growth was monitored by measuring the optical density at wavelength 600 nm (OD₆₀₀). When the OD₆₀₀ reached 0.8, 200 µl of 1 M isopropyl-β-D-thiogalactopyranoside (IPTG) was added to induce expression of PGT protein. Then, the culture was allowed to grow for an additional 4 h at 37 °C with shaking at 250 rpm. The cells were harvested by centrifugation at 6000 rpm at 4 °C for 20 min. After the supernatant had been discarded, the cell pellets were resuspended in 20 ml of phosphate-buffered saline (PBS, 20 mM sodium phosphate, 500 mM NaCl, pH 7.4). Prior to purification of the PGT protein, cell lysis was performed by a 30 s sonication for 5 cycles using a Soniprep 150 ultrasonic disintegrator. Cell debris containing PGT was collected by centrifugation (9000 rpm at 4 °C for 1 h). The insoluble PGT protein was solubilized with the assistance of detergent Fos-choline-14. 20 ml starting buffer (20 mM sodium phosphate, 500 mM NaCl, pH 7.4) with 20 mM Fos-choline 14 was added to the cell debris. The PGT protein was solubilized by rolling the mixture gently at 4 °C overnight. The mixture was then centrifuged at 13,500 rpm

at 4 °C for 1 h. The supernatant containing solubilized PGT was collected for purification.

Purification of PGT was performed with an Amersham-Pharmacia Ä KTA Fast Protein Liquid Chromatography (FPLC) system using a 5 ml HiTrap chelating column (Amersham-Pharmacia). The column was firstly washed with three column volumes (CV) of double deionized water (diH₂O). Then three CV of 0.1 M nickel (II) sulfate was passed through the column and unbound nickel (II) was subsequently washed away by water. The column was then pre-equilibrated with starting buffer (500 mM NaCl, 20 mM NaH₂PO₄, 1 mM Fos-choline-14, pH 7.4). The 0.45 µm filtered supernatant was loaded onto the column. The column was washed with 6 CV of starting buffer and 2 CV of mixture of 10 % elution buffer (20 mM sodium phosphate, 500 mM NaCl, 500 mM imidazole, 1 mM Fos-choline-14, pH 7.4). Finally, the His-tagged protein was eluted by a linear gradient of elution buffer from 10 % to 100 %. All fractions were collected and a small portion of them were analyzed by SDS-PAGE (Section 3.2.3). The fractions containing the target protein were collected and its buffer was changed to 20 mM sodium phosphate buffer (pH 7.4) by dialysis and stored at -80 °C for future use.

3.2.3 Sodium dodecyl sulfate-polyacrylamide gel electrophoresis (SDS-PAGE)

The protein samples collected in different tubes were analyzed using 12 % SDS-PAGE in a Mini-PROTEAN III dual slab cell (Bio-Rad Laboratories). 20 µl of samples

were mixed with loading buffer (65.8 mM Tris-HCl (pH 6.8), 2.1% SDS, 26.3% (w/v) glycerol, 0.01% bromophenol blue, 2.5 % β -mercaptoethanol (w/v)). Then the mixture was boiled for 8 min. 20 μ l of mixtures were loaded into the lanes of the SDS-PAGE gel, which comprised of 5 % stacking gel (pH 6.8) and 12 % separating gel (pH 8.8). The SDS-PAGE gel was then subjected to electrophoresis in 1X running buffer (25 mM Tris-HCl, 192 mM glycine, 3.5 mM SDS, pH 7.4) at 150 V for 1 h. Finally, the gel was stained with Coomassie blue for 5 min, and then was destained in the destain solution (methanol: glacial acetic acid: diH₂O 2: 1: 7) to get a clear background of the gel.

3.2.4 Electrospray ionization-mass spectrometry (ESI-MS)

ESI-MS was used to analyze the molecular weight of the PGT mutants. The protein was concentrated and buffer-exchanged into 20 mM ammonium acetate using the 10 kDa Amicon Ultra filter centrifuge tubes (Millipore Corp.) before MS analysis. ESI-MS analysis was performed using a VG Platform quadrupole-time-of-flight (Q-TOF2) mass spectrometer (Micromass, Altrincham, Cheshire, UK). The protein was diluted in H₂O/CH₃CN (1: 1) with 1 % formic acid to a final concentration of 5 μ M. Mass spectrum at the range of m/z 500 to 2000 was scanned.

3.2.5 Determination of protein concentration

Bradford assay was employed to determine the concentrations of the PGT mutants

[104]. 200 μ l of Bradford reagent dye purchased from Bio-Rad was mixed with 799 μ l of water and 1 μ l of the protein sample. The mixture was incubated for 10 min at room temperature to allow the formation of the stable protein-dye complexes. Then the absorbance of the sample was measured by a UV-vis spectrometer at 595 nm. The concentration of the target protein was determined by comparison with a calibration curve constructed using bovine serum albumin (BSA).

3.2.6 SPR assay for determining PGT mutants-Moe A binding affinity

A BIACORE[®]3000 surface plasmon resonance (GE Healthcare Life Sciences) system was employed to investigate the binding affinities of PGT mutants to Moe A. Amine derivative of Moe A (compound **23**) was immobilized on a sensor chip CM5 (GE Healthcare Bio-Sciences AB, Uppsala, Sweden) by covalent bond as described by Stempera *et al.* [69]. A mixture of NHS (0.05 M) and N-ethyl-N'-(3-dimethylaminopropyl)-carbodiimide hydrochloride (EDC, 0.2 M) was injected into both the analytical flow cell and the reference cell for 5 min to activate the carboxymethyl groups on the sensor chip surface by forming an N-hydroxysuccinimide ester. A solution of **23** (0.5 μ M) in running buffer was injected into the analytical cell for over 10 min while the reference cell was treated with the blank running buffer. Then the residual active ester groups in both cells were blocked with a 10 min flow of 1 M ethanolamine. All the above steps were performed at a flow rate of 10 μ l/min.

Following the immobilization of **23**, the whole system was washed with running

buffer at a rate of 50 $\mu\text{l}/\text{min}$ for 5 min. PGT mutants and WT were diluted in SPR running buffer and injected into the sensor surface for 120 s, followed by a 40 s of regeneration by injection of 10 mM glycine-HCl (pH 1.5) at a flow rate of 10 $\mu\text{l}/\text{min}$. Then the system was washed by the running buffer for 5 min at a flow rate of 50 $\mu\text{l}/\text{min}$. For the wild type protein and its mutants, a series of different protein concentrations (50 nM, 100 nM, 150 nM, 200 nM, 250 nM, 300 nM) were injected into both cells and analyzed. Finally, sensorgrams were described by response data which were obtained by subtraction of reference cell without Moe A immobilization versus time. K_D values of each protein were calculated by the SPR system.

3.3 Results and discussion

3.3.1 Preparation of wild type PGT and mutants

The glycosyltransferase domain of *S. aureus* PBP2 and its five mutants, namely Q161W, H162W, D199W, Y210W and D241W, were successfully cloned into pRSETk vector. The sequences of these recombinant PGT-pRSETk were confirmed by DNA sequencing and the sequencing results are shown in Appendix II . The protein purification chromatograms and images of SDS-PAGE gel of purified His-tagged PGT are shown in Figure 3.3 and Appendix III. In the FPLC chromatogram, the third blue peak was the target protein with His-tag while the first and second blue peaks were non-specific proteins. In SDS-PAGE, the protein bands in lanes 6-9 corresponded to the third blue peak in the chromatogram. The dominant bands in lanes 6-9 were in the similar level with the 5th bands of the low range molecular marker, which means that the proteins in these lanes should have a molecular weight around 21.5 kDa. So, it can be preliminarily concluded that PGT protein was obtained in the third blue peak of FPLC chromatography.

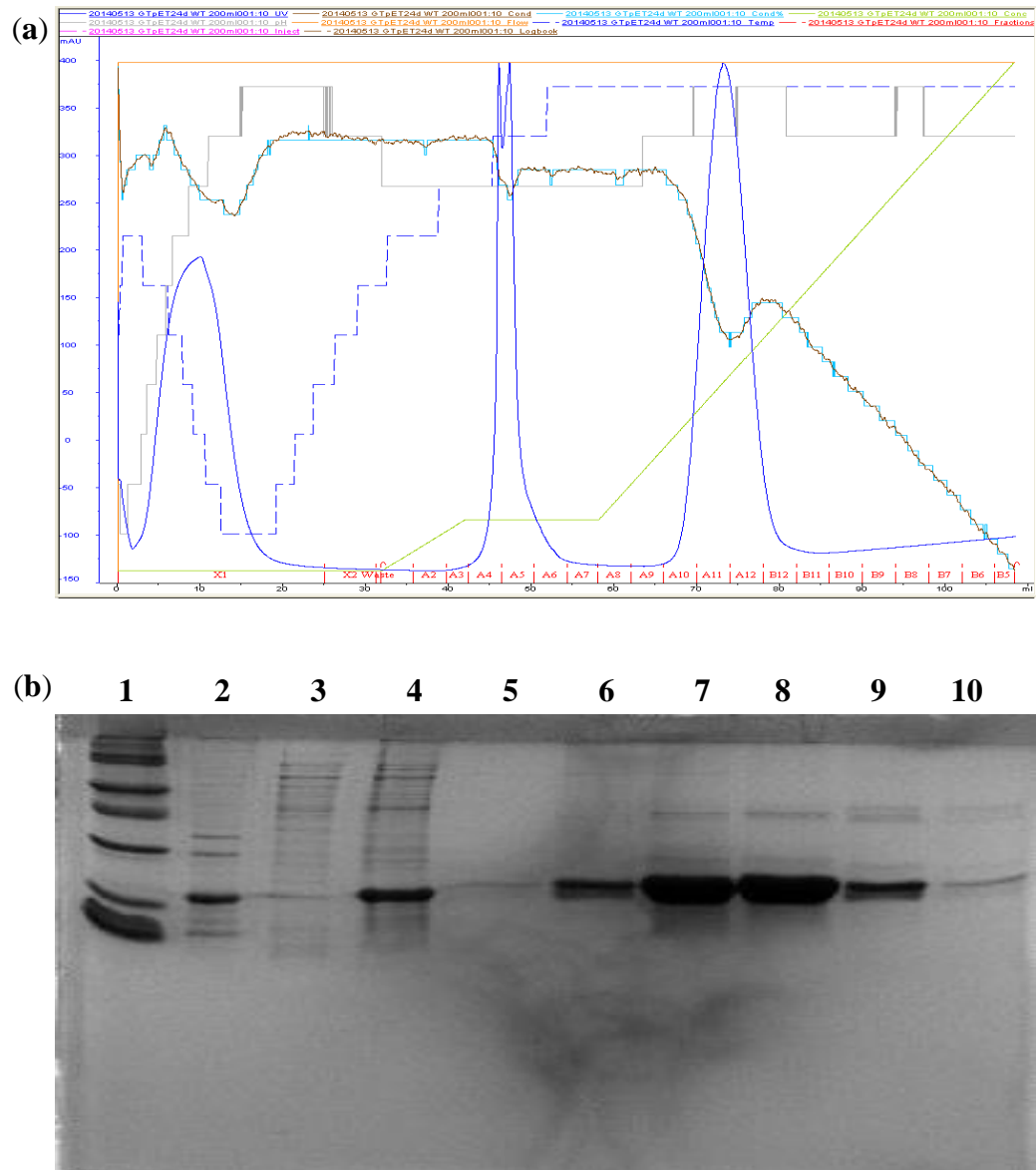


Figure 3.3 (a) FPLC chromatogram of 200 ml PGT-WT-pRSETk/BL21 (DE3) protein purification and (b) SDS-PAGE gel photo of various fractions from PGT-WT-pRSETk/BL21 (DE3) purification.

Note: Lane 1: Low range molecular marker: Phosphorylase b (97.4 kDa), Serum albumin (66.2 kDa), Ovalbumin (45 kDa), Carbonic anhydrase (31 kDa), Trypsin inhibitor (21.5 kDa), Lysozyme (14.4 kDa); Lane 2: supernatant after solubilization with fos-choline-14; Lane 3: supernatant before solubilization with Fos-choline-14; Lane 4: cell pellet after solubilization with Fos-choline-14; Lanes 5-10: 20 μ l of fractions A9-B11.

3.3.2 Characterization by ESI-MS

The accurate molecular mass of wild type PGT and mutants were obtained by ESI-MS as shown in Figure 3.4 and Appendix IV. Only a single peak was observed in the mass spectra of WT, D199W, Y210W and D241W. The additional peaks, 19728 Da in the MS spectrum of Q161W and 19720 Da for H162W corresponded to the mutants with the loss of three amino acids (DHP) at the C-terminal. Based on the structural information, the missing three amino acids are distant from its active site so their absence should not affect the bioactivity. A comparison of the calculated mass and the mass found in the ESI-MS results of WT and mutants is shown in Table 3.2. Data obtained from SDS-PAGE gel and ESI-MS of WT and mutants indicated that all PGT proteins were successfully obtained with correct sequence and high purity.

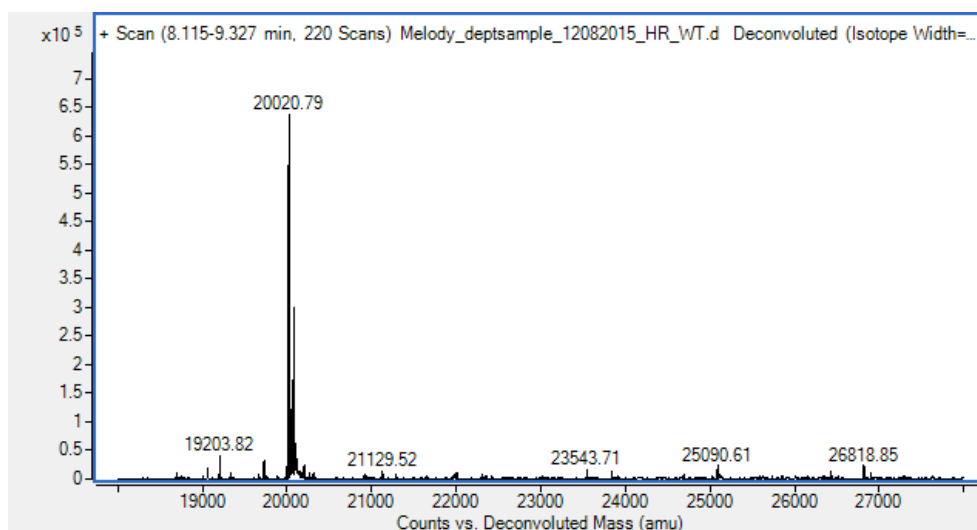


Figure 3.4 ESI-MS spectrum of wild type PGT

Table 3.2 Comparison of the calculated mass and measured mass of wild type PGT and mutants

Mutant	Calculated mass (Da)	Measured mass (Da)
WT	20020.39	20020
Q161W	20078.47	20078
H162W	20069.46	20071
D199W	20091.51	20091
Y210W	20043.42	20044
D241W	20091.51	20091

3.3.3 Binding affinity determination of the PGT mutants with Moe A by SPR

When an amino acid residue is mutated in the PGT, it is imperative to test their binding affinity with Moe A to ensure the alternation does not exert significant influences on their structure and bioactivity. A series of PGT solutions in running buffer ranging from 20 nM to 300 nM were used to analyze their binding to Moe A. Sensorgrams of the WT and five mutants were obtained and shown in Figure 3.5. Concentration dependent binding responses were observed in all PGT proteins including WT and the five mutants. The dissociation constant (K_D) was obtained by BIACORE 3000 Control Software. As shown in Table 3.3, K_D values of WT and five mutants including Q161W, H162W, D199W, Y210W and D241W are similar, being 200 nM, 300 nM, 300 nM, 220 nM, 180 nM and 160 nM respectively, which indicated that the mutations did not significantly alter the bind affinity. Comparing to wild type PGT ($K_D = 200$ nM), the binding affinities of three mutants Q161W ($K_D = 300$ nM), H162W ($K_D = 300$ nM) and D199W ($K_D = 220$ nM) showed a slight decrease while those of two mutants Y210W ($K_D = 180$ nM) and D241W ($K_D = 160$ nM) intensified a little bit. The main reason of the alternation could be conformational changes due to site mutations, which provided a more or less fitting pocket for Moe A binding comparing to the wild type PGT.

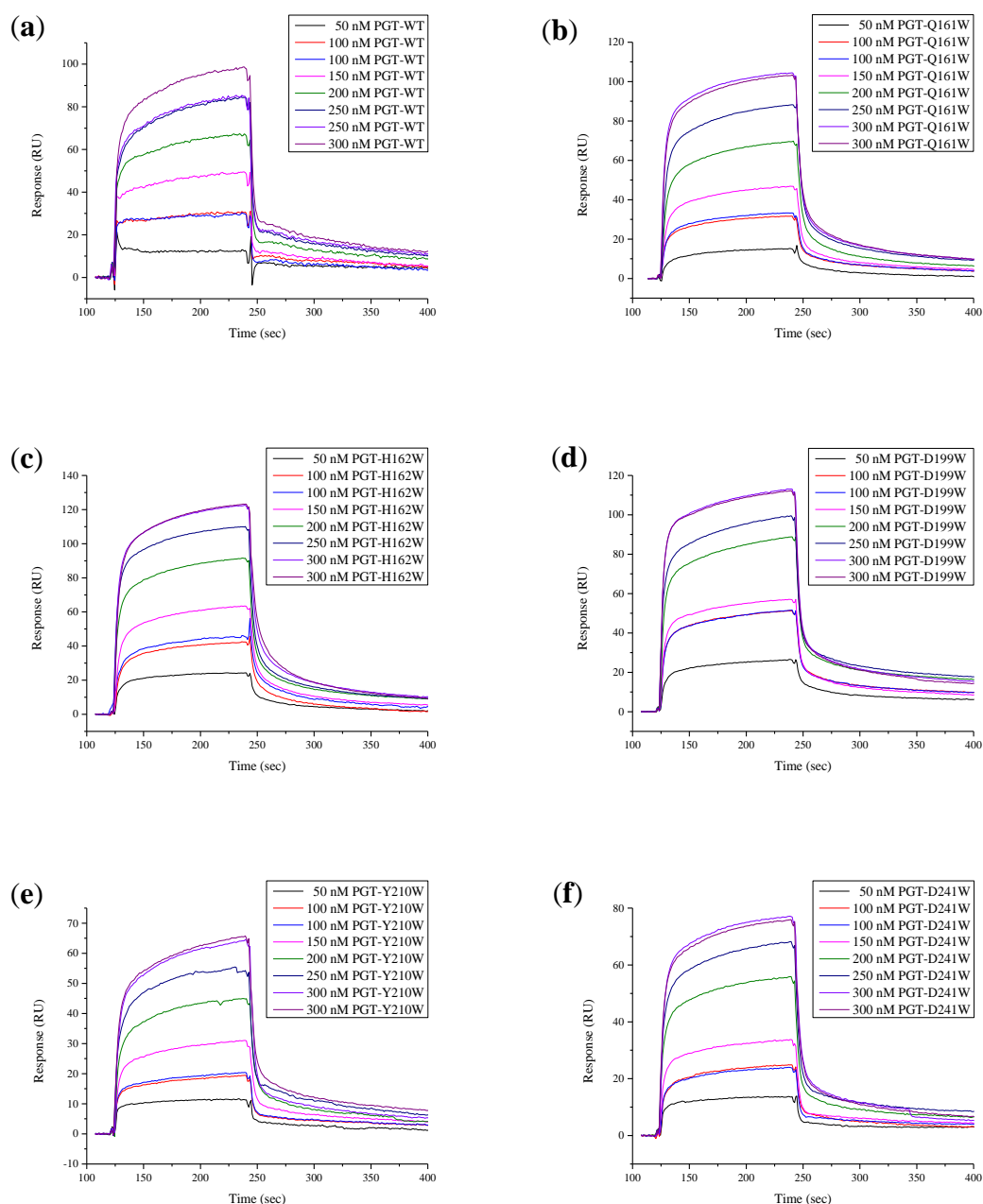


Figure 3.5 Sensorgrams of a concentration series of *S. aureus* PGT (a) WT and mutants (b) Q161W; (c) H162W; (d) D199W; (e) Y210W; (f) D241W binding to Moe A chip. Injection of the solutions starts at 107 s and lasts for 120 s.

Table 3.3 Binding affinities of PGT-WT and mutants calculated from SPR assay

PGT	Dissociation Constant (K_D, nM)
WT	200 ± 56
Q161W	300 ± 47
H162W	300 ± 64
D199W	220 ± 72
Y210W	180 ± 53
D241W	160 ± 69

3.4 Concluding remarks

In this chapter, we successfully cloned the peptidoglycan glycosyltransferase domain of *S. aureus* PBP2 into *E. coli* expression vector and created five mutants based on structural rational design.

Based on the binding pose of Moe A with PGT domain obtained from the crystal structure of the complex, amino acid residues near the active sites were selected for tryptophan mutation. Finally, five selected sites (Q161, H162, D199, Y210 and D241) were mutated to tryptophan by SDM to give the corresponding single-point mutants Q161W, H162W, D199W, Y210W and D241W. These mutants together with the WT were obtained with high expression level and purity. The SPR analysis results indicated that all the mutants had similar binding affinities to Moe A comparing to the WT, which meant the mutations did not cause significant structural change to the protein and Moe A can still bind to the active site. Therefore, the PGT mutants expressed can be employed in the construction of the biosensing system.

Chapter 4

Validation of the PET based biosensor for screening of PGT inhibitors

4.1 Introduction

In constructing the biosensor for detecting PGT inhibitors, fluorescein was attached to Moe A to make the fluorescent probe and several amino acid residues of PGT were mutated to tryptophan which serves as a quencher to the fluorophore. The biosensing system works by initial fluorescence quenching due to binding of fluorescein-labeled Moe A derivatives to the active site of PGT, which is followed by fluorescence recovery through displacement of the probe with potential PGT inhibitors which competitively bind to the same active site of PGT (Figure 1.12).

For a successful biosensor for PGT inhibitors, the probe should be able to bind to the active site of PGT mutants and the fluorescein group can interact with the tryptophan residue. The interaction between PGT mutant and fluorescent probe can be monitored through fluorescence changes. In order to find the best pair of mutant and fluorescent probe for constructing the biosensing system, the extent of quenching effect by PGT mutants and the restoration of the fluorescence by Moe A and inhibitors are discussed in this chapter. Furthermore, the specificity of the biosensor is also reported.

4.2 Experimental

4.2.1 Measurement of steady-state fluorescence intensity

Steady-state fluorescence intensity measurements were carried out with a Horiba FluoroMax-4 spectrofluorometer (HORIBA, Ltd.). The excitation wavelength was set at 495 nm with slit width of 5 nm at a scan rate of 200 nm/min. A solution containing 10 mM Tris (pH 8.0), 200 mM NaCl, 1 mM CHAPS, 100 nM probe and 0.5 μ M wild type PGT or mutants (Q161W, H162W, D199W, Y210W or D241W) was allowed to equilibrate for 30 min at 4 °C before measurement. BSA and lysozyme were used as negative controls.

4.2.2 Determination of the dissociation constant K_D by fluorescence titration of probes with PGT mutants

The probe / PGT mutant pairs selected from the results of steady-state fluorescence measurements were further studied for the concentration-dependent responses. A solution containing 10 mM Tris (pH = 8.0), 200 mM NaCl, 1 mM CHAPS, 100 nM probe, and 3.2 μ M PGT mutant was allowed to equilibrate for 10 min at 4 °C and then was serially diluted (1: 1 dilutions) into a solution containing 10 mM Tris (pH = 8.0), 200 mM NaCl, 1 mM CHAPS, 100 nM probes. After another 10 min of equilibration at 4 °C, 150 μ l of the mixture was transferred to a black 96-well plate (Corning 3650, Corning Inc.) and the fluorescence intensities (FI, ex: 485 nm; em: 520 nm) of the

samples in the 96-well plate were measured using a POLARstar OPTIMA microplate reader (BMG Labtech). Each series was performed in duplicate and the changes in fluorescence intensity were plotted against PGT mutant concentrations. The change in FI was defined as $[(FI_{max} - FI_{obs}) / FI_{max} \times 100 \text{ \%}]$. For determination of the K_D value, we assumed that the titration follows a standard binding equation describing an equilibrium $L + R \rightleftharpoons LR$ (L = ligand; R = receptor; LR = ligand receptor complex). Fitting the sigmoidal curve based on the equilibrium using GraphPad Prism 5.0 (GraphPad Software, Inc.) resulted in the K_D values.

4.2.3 Displacement assay with PGT inhibitors and K_I determination

The fluorescence spectra of probe / PGT mutant pairs after the addition of Moe A were recorded. A solution containing 10 mM Tris (pH 8.0), 200 mM NaCl, 1 mM CHAPS, 100 nM probes (**F-*n*-Moe A**, **n = 2, 3 and 4**) and 0.5 μ M PGT mutant (D199W, or D241W) was allowed to equilibrate for 10 min at 4 °C before measurement using Horiba FluoroMax-4 spectrofluorometer (HORIBA, Ltd.). Then Moe A was added into the solution with a final concentration of 5 μ M. After another 10 min of equilibration at 4 °C, the sample was subjected to fluorescence measurement. During fluorescence intensity analysis, the excitation wavelength was fixed at 495 nm with slit width of 5 nm at a scan rate of 200 nm/min.

To determine the inhibitory constant (K_I), various concentrations of Moe A were added into a solution containing 100 nM probe and 0.5 μ M PGT mutant with final

concentrations ranging from 0.05 μM to 51.2 μM . After a 10 min equilibration at 4 $^{\circ}\text{C}$, 150 μl of the solutions were transferred to a black 96-well plate. The fluorescence intensity (FI, ex: 485 nm; em: 520 nm) was measured using a POLARstar OPTIMA microplate reader (BMG Labtech).

We assumed that the displacement follows a complete competitive binding model “ $RL + L_S \xrightleftharpoons{K_D} R + L_S + L \xrightleftharpoons{K_I} RL_S + L$ ”, where R is receptor, L is ligand, L_S is competitive inhibitor, RL is the complex of ligand and receptor, and RL_S is the complex of inhibitor and receptor. The K_I value was determined by plotting the logarithm of inhibitor concentrations against the percentage changes in fluorescence intensity and fitting the resulting curve to the following equation using GraphPad Prism 5.0.

$$\frac{[RL]}{[R]} = \frac{1}{1 + \frac{K_D}{[L]} \left(1 + \frac{[M]}{K_i}\right)}$$

Where $[RL]$ is the concentration of enzyme-ligand complex, $[M]$ is the concentration of inhibitor, $[L]$ is the concentration of probe (100 nM), and K_D is the dissociation constant for the probe determined above.

The most efficient biosensing system was chosen for further validation based on the above displacement assay result using Moe A. Various inhibitors reported in literature and two other antibiotics ampicillin and kanamycin as negative controls were employed in the further validation test. The assay was carried out under the same condition as used above. The test samples stocked in DMSO were added with final concentrations ranging from 0.4 to 2.5 mM. After a 10 min equilibration at 4 $^{\circ}\text{C}$, 150 μl of the solutions

were transferred to a black 96-well plate and subjected to fluorescence intensity measurement.

4.3 Results and discussion

4.3.1 The effect of linker lengths and mutation locations on the fluorescence quenching of probes by PGT mutants

The principle of the biosensor is based on PET fluorescence quenching, which is triggered by a contact within van der Waals distance between the fluorophore group and the quencher tryptophan residue introduced to PGT mutants. Therefore, it is imperative to optimize the linker length of the probe and the location of tryptophan residue in the PGT mutant. Based on the crystal structure of the complex of PGT and Moe A, five amino acid residues close to the active sites of PGT were chosen for tryptophan mutation while three fluorescent Moe A derivatives with different lengths of linkers were synthesized. The aim was to find the best combination in which the fluorescence of the probe can be quenched efficiently by the PGT mutant to construct the biosensing system.

Three probes (**F-*n*-Moe A**, *n* = **2**, **3** and **4**) and five PGT mutants respectively (Q161W, H162W, D199W, Y210W and D241W) were subjected to the steady fluorescence measurement to study the fluorescence quenching effect. The fluorescence spectra of three probes before and after the addition of wild type PGT and mutants are shown in Figure 4.1-4.3. PGT WT does not show any quenching effect by the three

probes. Among the five PGT mutants, three of them (Q161W, H162W and Y210W) do not quench the fluorescence of the three probes, which indicates that the tryptophan residue introduced to these three mutants are not in the right position to have a close contact with the fluorophore group of the fluorescent Moe A derivatives. For the remaining two mutants D199W and D241W, the fluorescence intensity (FI) of the three probes decrease to different extent. The FI of probe **F-2-Moe A** decreased by 22 % in the presence of 0.5 μ M D199W, while the FI of probes **F-3-Moe A** and **F-4-Moe A** decreased by 20 % - 30 % after addition of 0.5 μ M D199W or D241W. Comparing to the nil fluorescence change of the wild type PGT, the fluorescence decrease caused by D199W or D241W indicate that the quenching should be induced by the tryptophan residue introduced into these two mutants.

The decrease in FI of probe **F-4-Moe A** (with four carbon in its linker) reaches the highest level (30 %) in the presence of mutant D199W, while that of probe **F-2-Moe A** (with two carbon in its linker) and **F-3-Moe A** (with three carbon in its linker) is about 20 %. The quenching effects on probes **F-3-Moe A** (23 %) and **F-4-Moe A** (28 %) by D241W are also stronger than that on probe **F-2-Moe A** (18 %). The results show that the weak quenching effect on probe **F-2-Moe A** is due to its short linker length and the quenching effect can be intensified by appropriate elongation of the linker. The longer linker increases the flexibility of the fluorophore group, which may allow it to have a closer contact with the tryptophan residue in PGT mutants.

Furthermore, the location of mutation also affect the quenching efficiency. The absence of quenching from Q161W, H162W and Y210W indicates that the tryptophan

residues in these three mutants are located in distant positions from the fluorophore group, which makes the tryptophan residue unable to quench the probes although the probe still binds to the active site of PGT. Two mutants D199W and D241W show efficient quenching, which means these two tryptophan residues are located close enough to the fluorophore group when the fluorescent probes are bound to the active site. It is known that the amino acid residues Y196 and P234 are in close contact with the A and B rings of Moe A in the PGT-Moe A complex (Rebets et al., 2013). As shown in the binding pose of Moe A with *S. aureus* PBP2 (Figure 4.4), the amino acid residues D199 and D241 are close to the residues of Y196 and P234, so the tryptophan mutations in these two positions can have close interaction with the ring A of Moe A, where the fluorophore group is attached. Consistent with this, mutants D199W and D241W exhibit efficient quenching on the fluorescent probes.

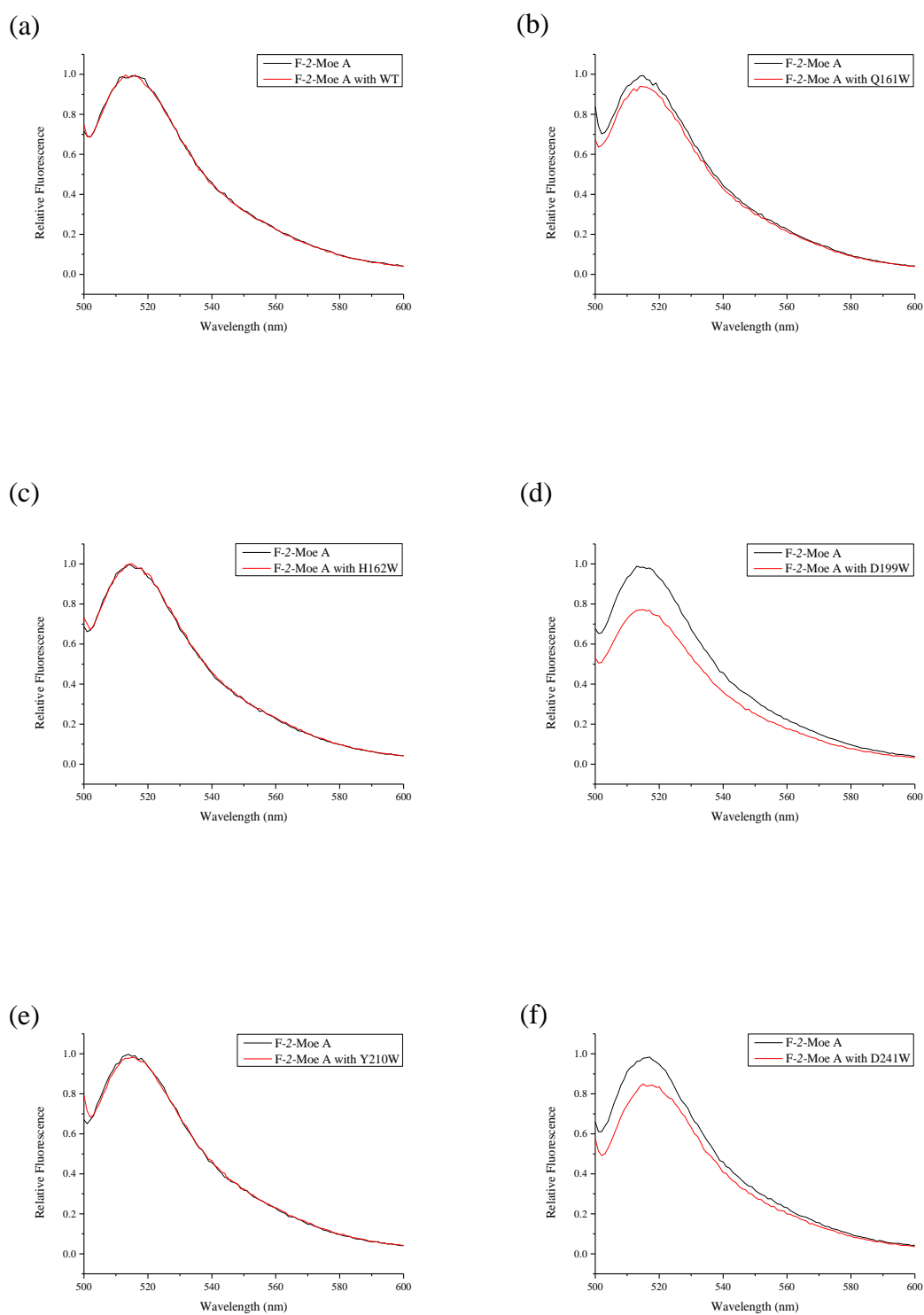


Figure 4.1 Fluorescence spectra of probe **F-2-Moe A** with (red) and without (black) 1 μ M of PGT (a) WT, (b) Q161W, (c) H162W, (d) D199W, (e) Y210W and (f) D241W

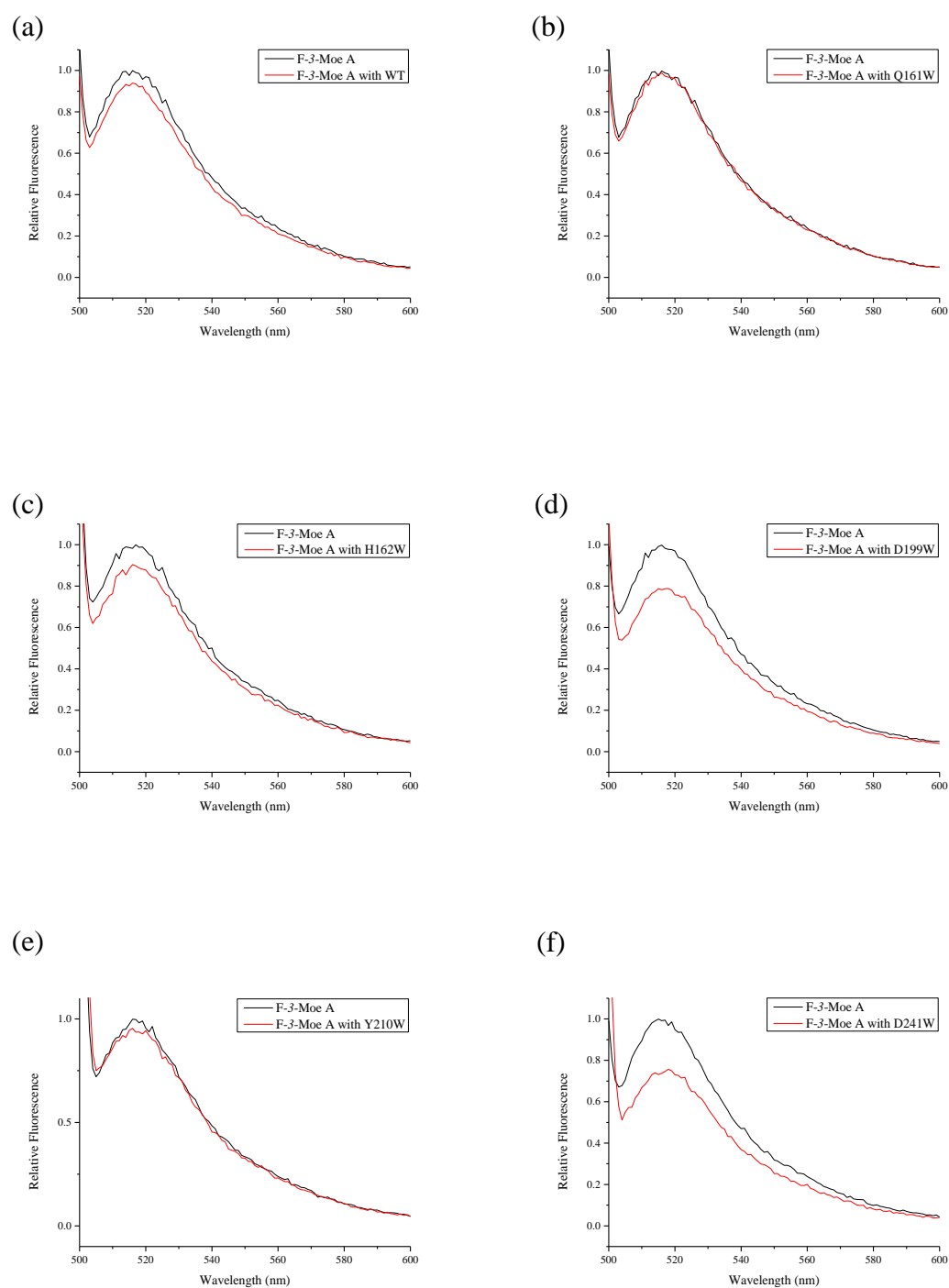


Figure 4.2 Fluorescence spectra of probe **F-3-Moe A** with (red) and without (black) 1 μ M of PGT (a) WT, (b) Q161W, (c) H162W, (d) D199W, (e) Y210W and (f) D241W

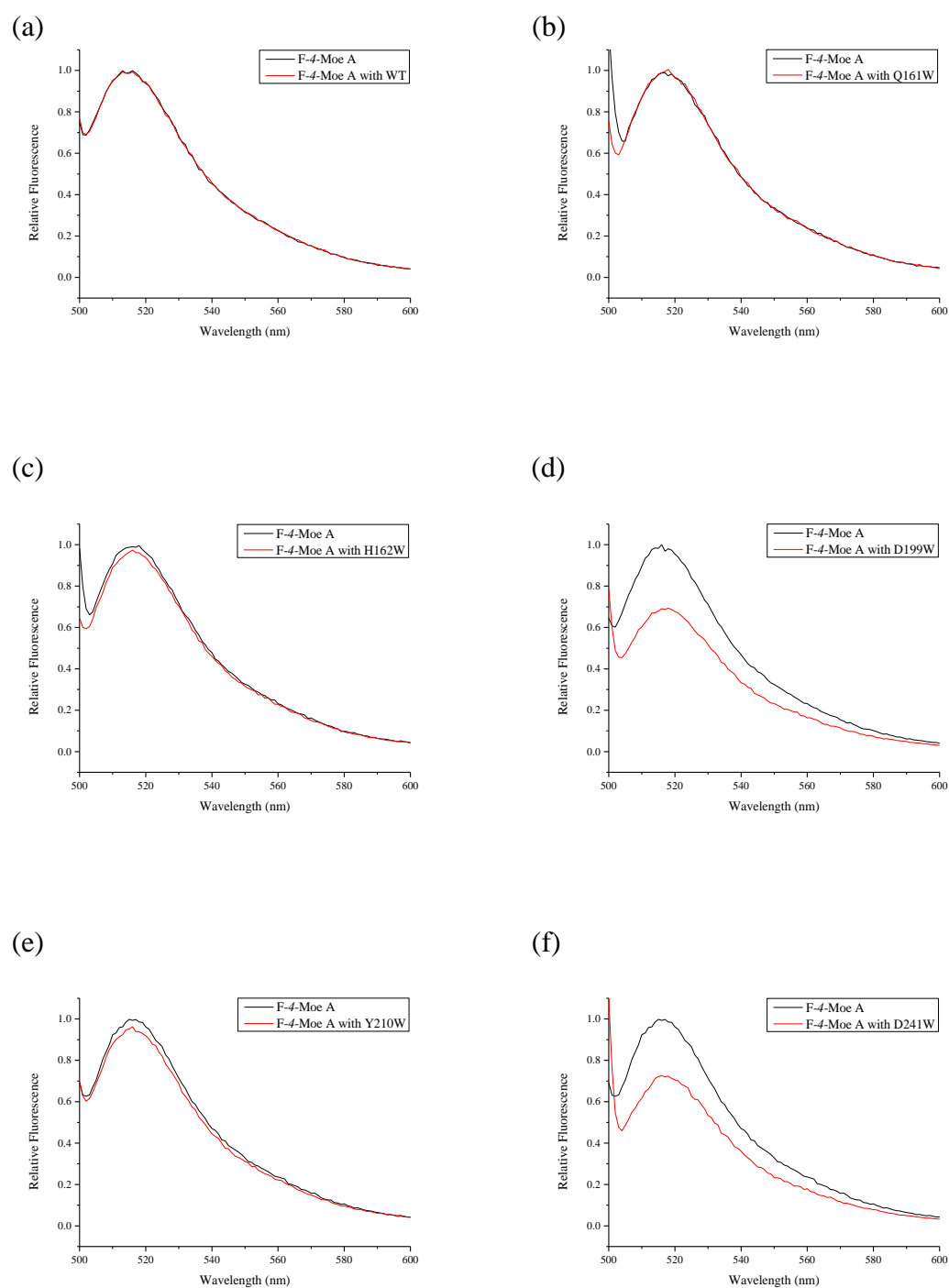


Figure 4.3 Fluorescence spectra of probe **F-4-Moe A** with (red) and without (black) 1 μ M of PGT (a) WT, (b) Q161W, (c) H162W, (d) D199W, (e) Y210W and (f) D241W

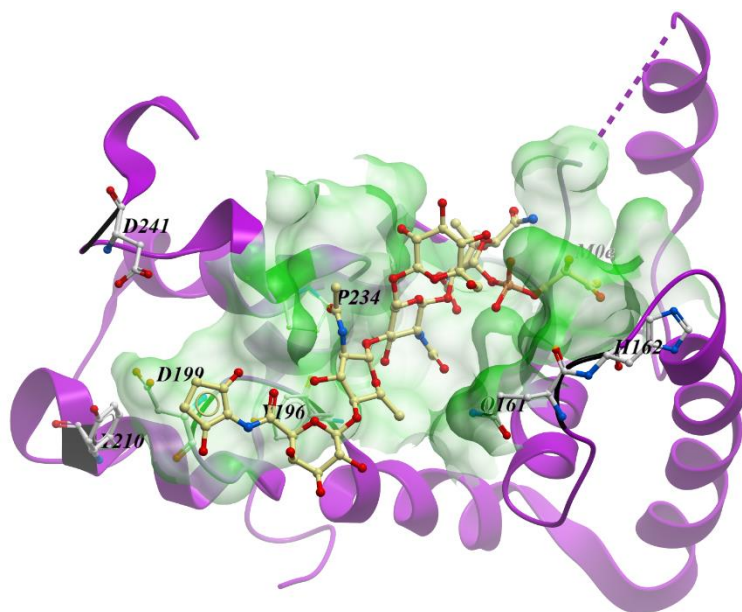


Figure 4.4 Binding pose of Moe A with *S. aureus* PBP2 PGT domain. Two amino acid residues Y196 and P234 interact with the ring A and B of Moe A, and the other five labeled amino acid residues are the selected mutation sites in this work [47].

4.3.2 Specificity of the quenching by PGT mutants

To verify that the fluorescence quenching is a result of the specific interaction between the probes and PGT mutants, two proteins including BSA (bovine serum albumin) and lysozyme were added instead of PGT into the probe-containing solutions as the control group, and then the solutions were subjected to the steady state fluorescence intensity analysis. The results are shown in the Figure 4.5 a-f. No FI changes were observed after addition of BSA or lysozyme though tryptophan residues are known to exist in the proteins. It can be concluded that either there is no interaction between fluorescent Moe A derivatives and the two proteins, or any unspecific binding which may exist between the probe and the two proteins cannot induce the fluorescence quenching, as the quenching effect of tryptophan occurs only under the condition of a van der Waals contact.

The standard dye fluorescein isothiocyanate isomer I (FITC) was also used to study the fluorescence response upon the addition of PGT mutants D199W and D241W. As shown in Figure 4.5 g, no fluorescence quenching effect was observed with the addition of PGT mutants. The results indicate that fluorescein alone cannot enter into the active site of the PGT to interact with the tryptophan residue in the PGT mutants. And for fluorescein-labeled Moe A, the fluorescein group can interact with the tryptophan group leading to fluorescence quenching under the aid of Moe A binding into the active site of PGT. Therefore, it is concluded that the quenching effect on the probes by PGT mutants is contributed by specific interaction between the fluorescein-labeled Moe A probe and the tryptophan residues on the PGT mutants.

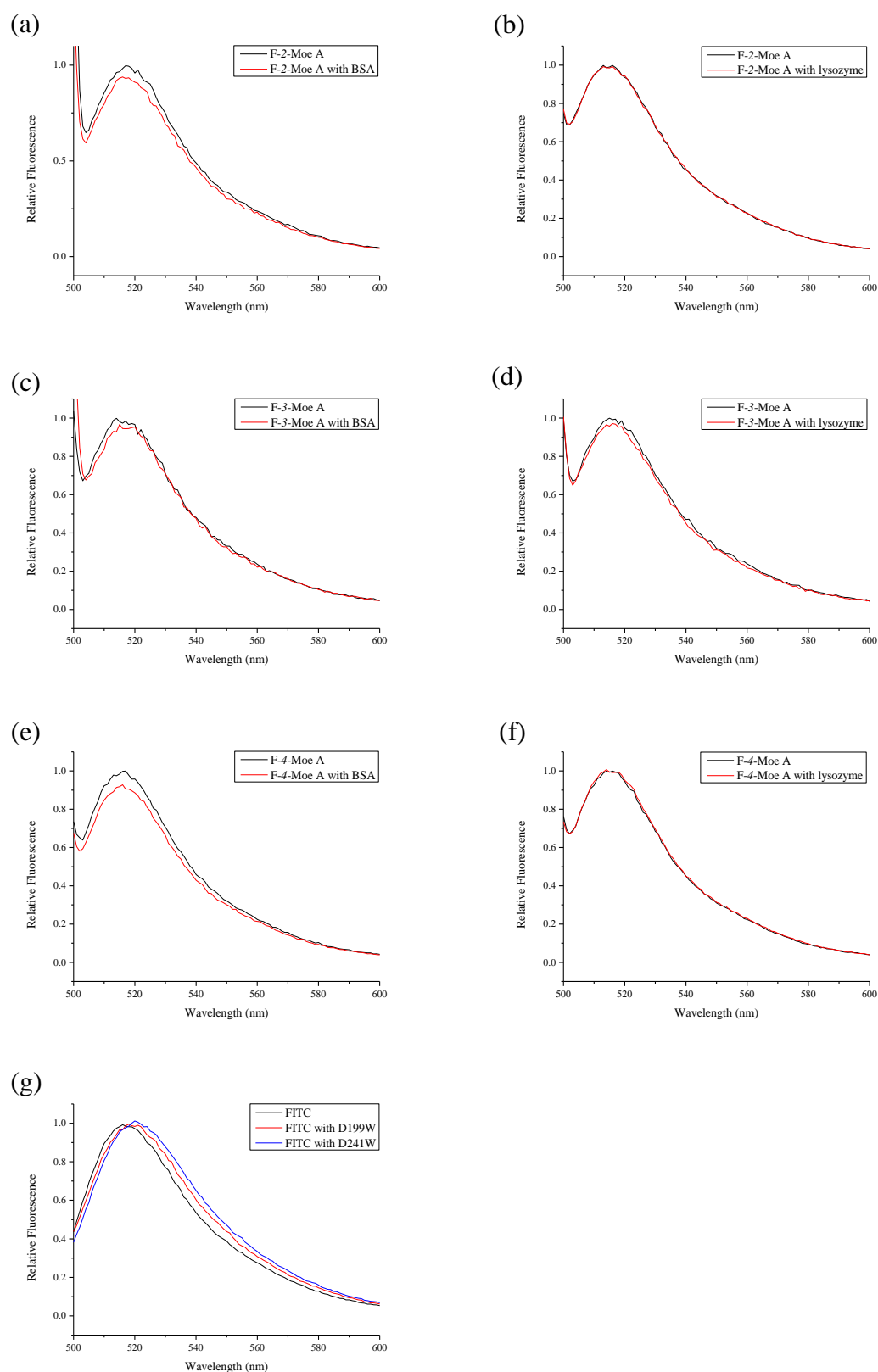


Figure 4.5 Fluorescence spectra of probe **F-2-Moe A** with (red) and without (black) 1 μ M of (a) BSA, (b) lysozyme; probe **F-3-Moe A** with 1 μ M of (c) BSA, (d) lysozyme; and probe **F-4-Moe A** with 1 μ M of (e) BSA, (f) lysozyme; (g) fluorescence spectra of FITC with and without (black) 1 μ M of D199W (red) and D241W (blue).

4.3.3 PGT proteins titration and determination of K_D values

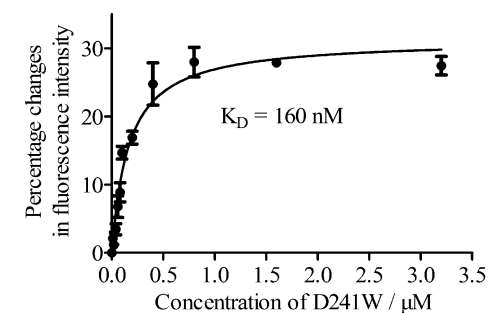
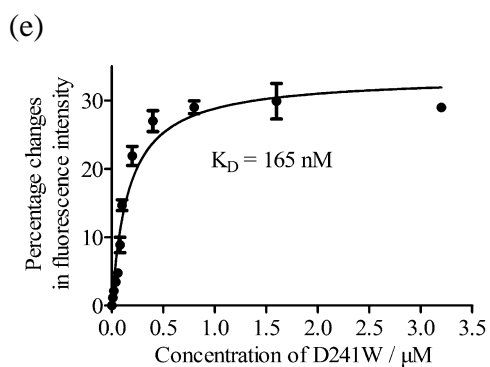
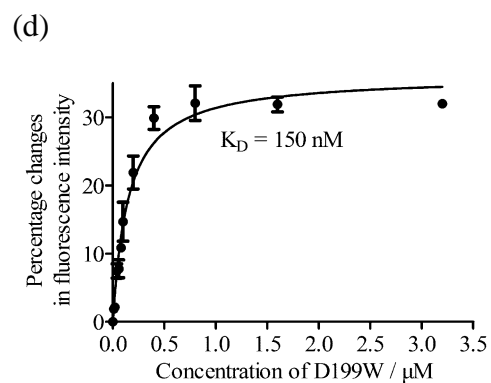
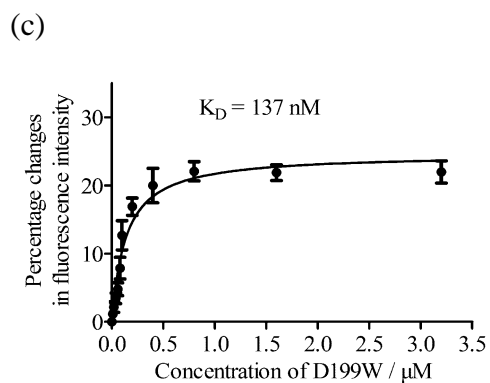
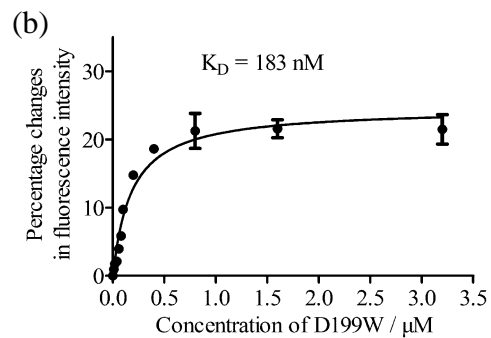
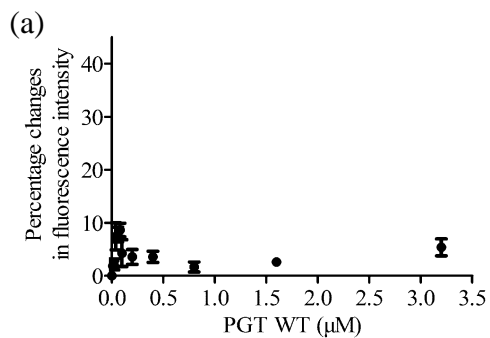
To select the best combination of PGT mutant and fluorescent probe to construct the biosensing system, the probe / mutant pairs with efficient fluorescence quenching were then investigated on the extent of their quenching effect. At the meantime, the dissociation constant K_D values of each pair were calculated. In this study, each probe of a fixed concentration (100 nM) was titrated against a series of protein concentrations ranging from 10 nM to 3.2 μ M. The percentage changes in fluorescence intensity were plotted against the protein concentrations. The changes in FI were defined as “ $(FI_{max} - FI_{obs}) / FI_{max} \times 100 \%$ ”. For the determination of K_D value, we assumed that the titration follows a standard binding equation describing an equilibrium $L + R \rightleftharpoons LR$ (L = ligand; R = receptor; LR = ligand receptor complex). Fitting the sigmoidal curve based on the equilibrium using GraphPad Prism 5.0 (GraphPad Software, Inc.) resulted in the K_D values, and the results are shown in Figure 4.6.

Sigmoidal fluorescence response curves were obtained by titrations of three probes against their pairing PGT mutants, while no fluorescence change of **F-4-Moe A** was observed when titrated against wild type PGT. This difference further confirms that wild type PGT cannot quench fluorescence of the probes, and the changes in FI is due to the introduction of tryptophan. Based on the sigmoidal titration curves, the whole process of titration consists of three stages: a steady stage at low protein concentration, an exponentially rising stage and an eventual plateau. In the first stage, the amount of protein is far less than that of probe and only a small number of fluorescent molecules are quenched, so the fluorescence change of the probe is hardly observed. As the

concentration of PGT mutant increases, an increasing number of probes bind to the active site of the protein, which leads to a strong quenching effect and a significant decrease in FI. The interaction between PGT mutant and probe is a reversible reaction. Increasing the amount of any reagent (protein or probe) leads to a shift of the equilibrium to the product side (complex of protein-probe). Finally, when an excessive amount of PGT mutant is present in the reaction solution, almost all the probes are in the form of adduct in the system and the equilibrium shifts to the product side to a great extent. The quenching effect reaches the maximum level, and the fluorescence intensity cannot change anymore with further increase in protein concentration, which results in the eventual plateau stage. In the titration process, the FI of all probe / PGT mutant pairs start to change at about 60 nM of PGT mutant, and reach a stable level at around 800 nM protein. As shown in Figure 4.6, the quenching effects for each combinations are different. The most efficient quenching reaches 32 % for the probe **F-4-Moe A** / mutant D199W pair. In the presence of D241W, the fluorescence quenching of probes **F-3-Moe A** (30 %) and **F-4-Moe A** (28 %) are similar, whereas the fluorescence quenching of probe **F-2-Moe A** was 20 %. Comparing to the quenching efficiencies of the five probe / mutant pairs, the probes (**F-3-Moe A** and **F-4-Moe A**) with a longer linker showed a better performance than the probe with a shorter linker (**F-2-Moe A**). It can be inferred from the results that the longer carbon chain of the probe makes the fluorophore more flexible to have a better interaction with the tryptophan residue. The three probe / mutant pairs of **F-3-Moe A** / D199W, **F-4-Moe A** / D199W, **F-4-Moe A** / D241W showed the best quenching efficiency.

The dissociation constant (K_D) of probes for PGT mutants shown in Table 4.1 were calculated from the titration data. The K_D values of different probe / mutant pairs are in the same order of magnitudes, which indicates that the mutations and the linker length did not severely change the binding affinities. Thus the core structure of Moe A (units C-E-F) which plays an essential role in binding to PBPs probably remains intact in each probe and the mutation sites do not have a direct interaction with the core structure of Moe A.

Moreover, the K_D of D199W and D241W with Moe A obtained from SPR assay were 220 ± 72 nM and 160 ± 69 nM respectively which are similar to the values obtained from the fluorescence titration. All the above results indicate that the fluorescein group linked to ring A does not interfere with the interaction between PGT and the core structure (units C-E-F) of Moe A.



(f)

Figure 4.6 The concentration-dependent changes in fluorescence intensity: (a) probe **F-4-Moe A** titrated against PGT WT; (b) probe **F-2-Moe A** titrated against PGT D199W; (c) probe **F-3-Moe A** titrated against PGT D199W; (d) probe **F-4-Moe A** titrated against PGT D199W; (e) probe **F-3-Moe A** titrated against PGT D241W; (f) probe **F-4-Moe A** titrated against PGT D241W.

Table 4.1 K_D inferred from the fluorescence titration and SPR

FI_ K_D (nM)		SPR_ K_D (nM)	
D199W + F-2 -Moe A	183 ± 15	WT + Moe A	200 ± 56
D199W + F-3 -Moe A	137 ± 21	D199W + Moe A	220 ± 72
D199W + F-4 -Moe A	150 ± 14	D241W + Moe A	160 ± 69
D241W + F-3 -Moe A	165 ± 22	PBP2 + Moe A	393 [#]
D241W + F-4 -Moe A	160 ± 21		

The K_D of PBP2 to Moe A obtained by SPR method was reported as 393 nM [71].

4.3.4 Fluorescence recovery upon the addition of Moe A

To each probe / PGT mutant pair (**F-2-Moe A** / D199W, **F-3-Moe A** / D199W, **F-3-Moe A** / D241W, **F-4-Moe A** / D199W and probe **F-4-Moe A** / D241W) in Tris solution, Moe A was added and then the changes in fluorescence intensity were recorded. As shown in Figure 4.7, the fluorescence intensity recovery of the five probe / mutant pairs were in the range of 15 % - 30 % of the original intensity upon the addition of 5 μ M of Moe A. **F-4-Moe A** / D199W and **F-4-Moe A** / D241W showed the most obvious fluorescence recovery which reached 30 % after adding 5 μ M of Moe A, while the fluorescence of **F-3-Moe A** / D241W restored by 20 %. The fluorescence of **F-2-Moe A** / D199W and **F-3-Moe A** / D199W recovered by about 15 %.

In order to ensure the fluorescence change was not caused by potential aggregation of probes upon the addition of Moe A, the fluorescent spectra of probes in the presence of Moe A but in the absence of PGT mutants were recorded. As shown in Figure 4.8, the fluorescence intensity of the three probes (100 nM) did not change after the addition of 5 μ M Moe A. It indicates that there are no interaction between the probe and Moe A in the absence of PGT mutants. So the fluorescence change was caused by the displacement of probes from the binding pocket of PGT mutants by Moe A. It can be concluded that Moe A competitively binds to the active site of PGT with the probes, the probes were released from the binding site and the PET-based quenching effect was removed, which led to the FI recovery of fluorescent probes.

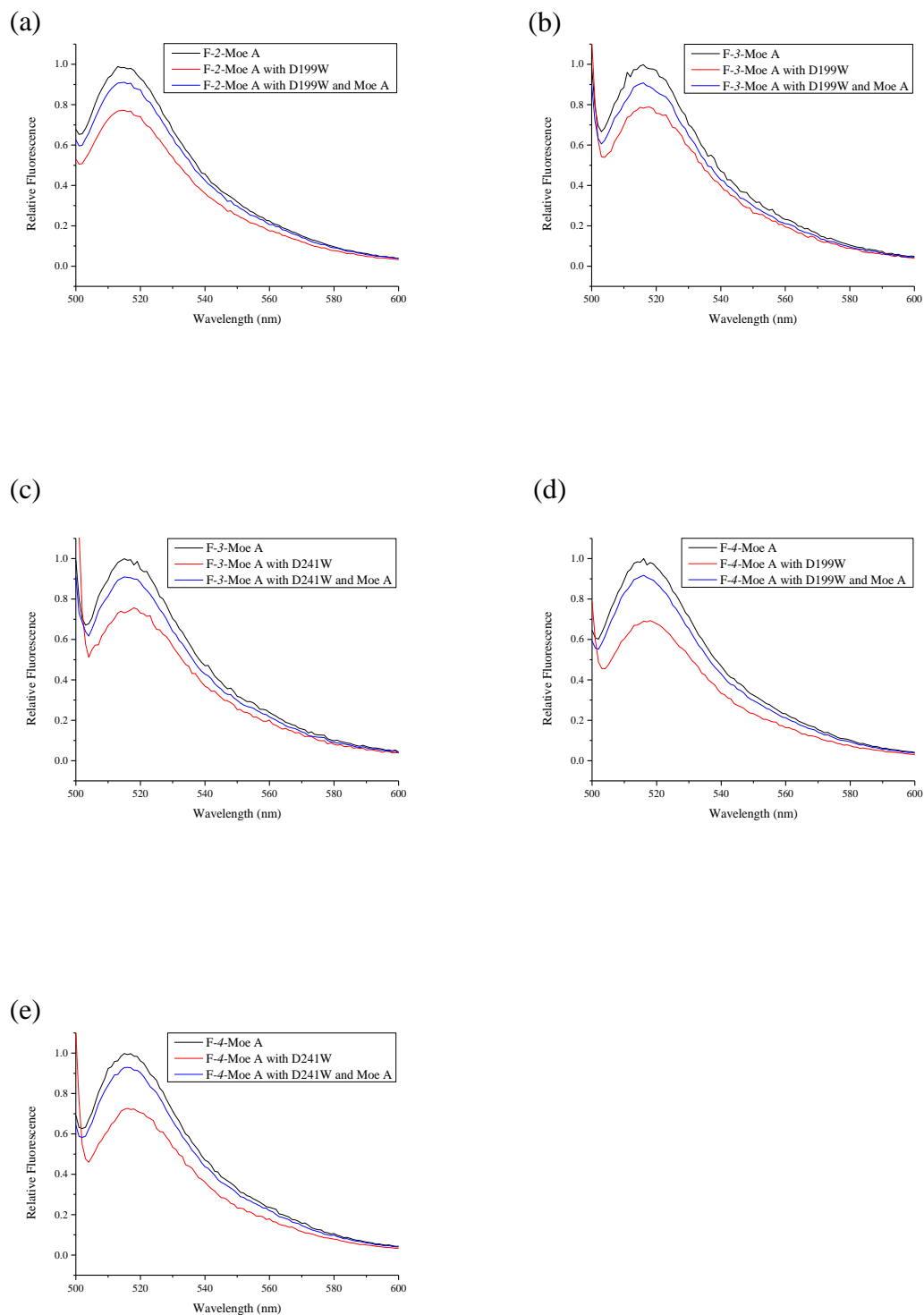


Figure 4.7 Fluorescence spectra of probe / PGT mutant pairs with the addition of 5 μ M Moe A (a) **F-2-Moe A** / D199W; (b) **F-3-Moe A** / D199W; (c) **F-3-Moe A** / D241W; (d) **F-4-Moe A** / D199W and (e) **F-4-Moe A** / D241W. Each pairs is consisted of probe (100 nM) and its quencher PGT mutant (0.5 μ M).

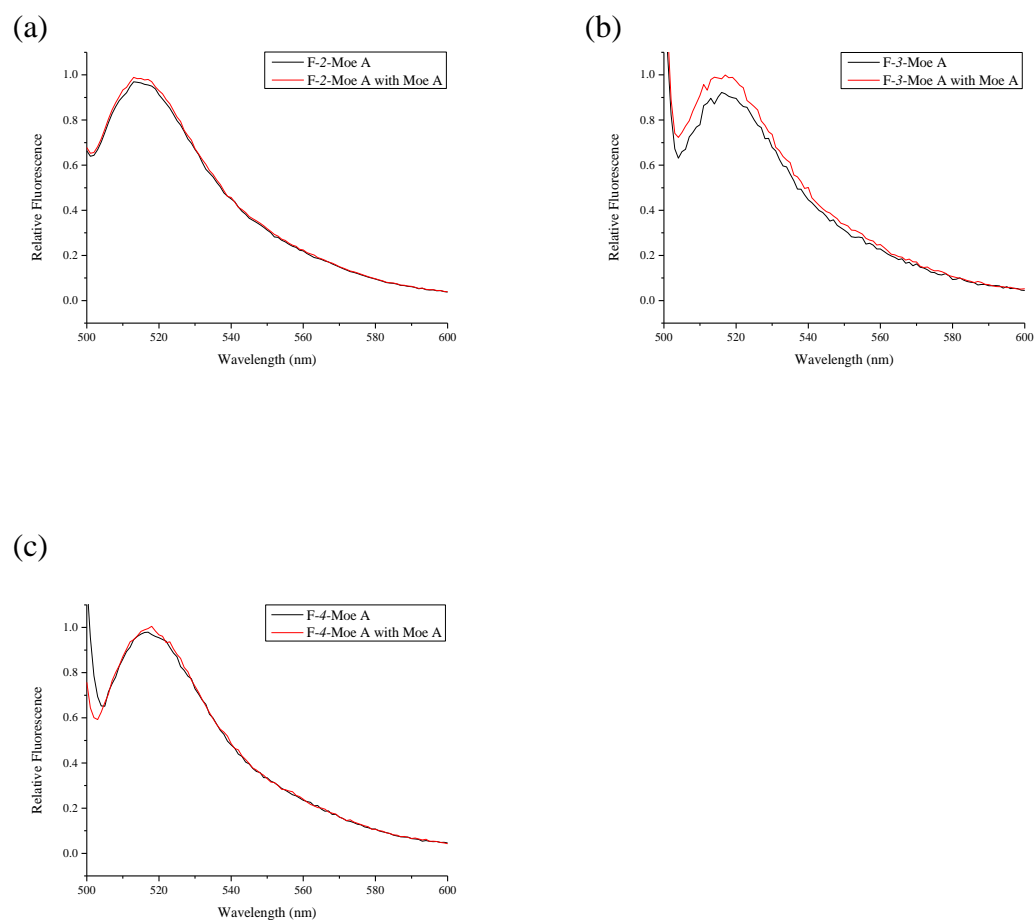


Figure 4.8 Fluorescence spectra of probes with (red) and without (black) 5 μ M Moe A (a) **F-2-Moe A**; (b) **F-3-Moe A** and (c) **F-4-Moe A**.

4.3.5 Determination of K_I of Moe A from the competitive displacement assay

As shown in Figure 4.9, the five probe / PGT mutant pairs showed a similar response with increasing concentrations of Moe A. At the beginning, the concentration of Moe A was low, and only a small number of probes were displaced from the active site of the quencher PGT mutant. So, a weak change in fluorescence intensity was observed. Upon an increasing amount of Moe A was added into the system, more probes were released from the active sites of PGT mutants. The fluorescence intensity of these probes were restored, which resulted in a stronger fluorescence changes. Most of the probes were in free state when the amount of Moe A was large enough to displace them from the active sites of PGT mutants. So, the fluorescence intensity leveled off in a plateau.

The K_I values of Moe A for different PGT mutants were calculated by fitting the observed data using Graphpad Prism 5.0. As shown in Table 4.2, the inhibitory constant K_I values of all mutants are of the same order of magnitude, which further confirms that the mutations do not cause a significant change in binding affinity of PGT to Moe A. Furthermore, the K_I value obtained from D199W is higher than that of D241W, which implies that the D199 mutation is favorable to the interaction between the probe and the mutants and higher concentration of Moe A is required to displace the probe from the PGT enzyme.

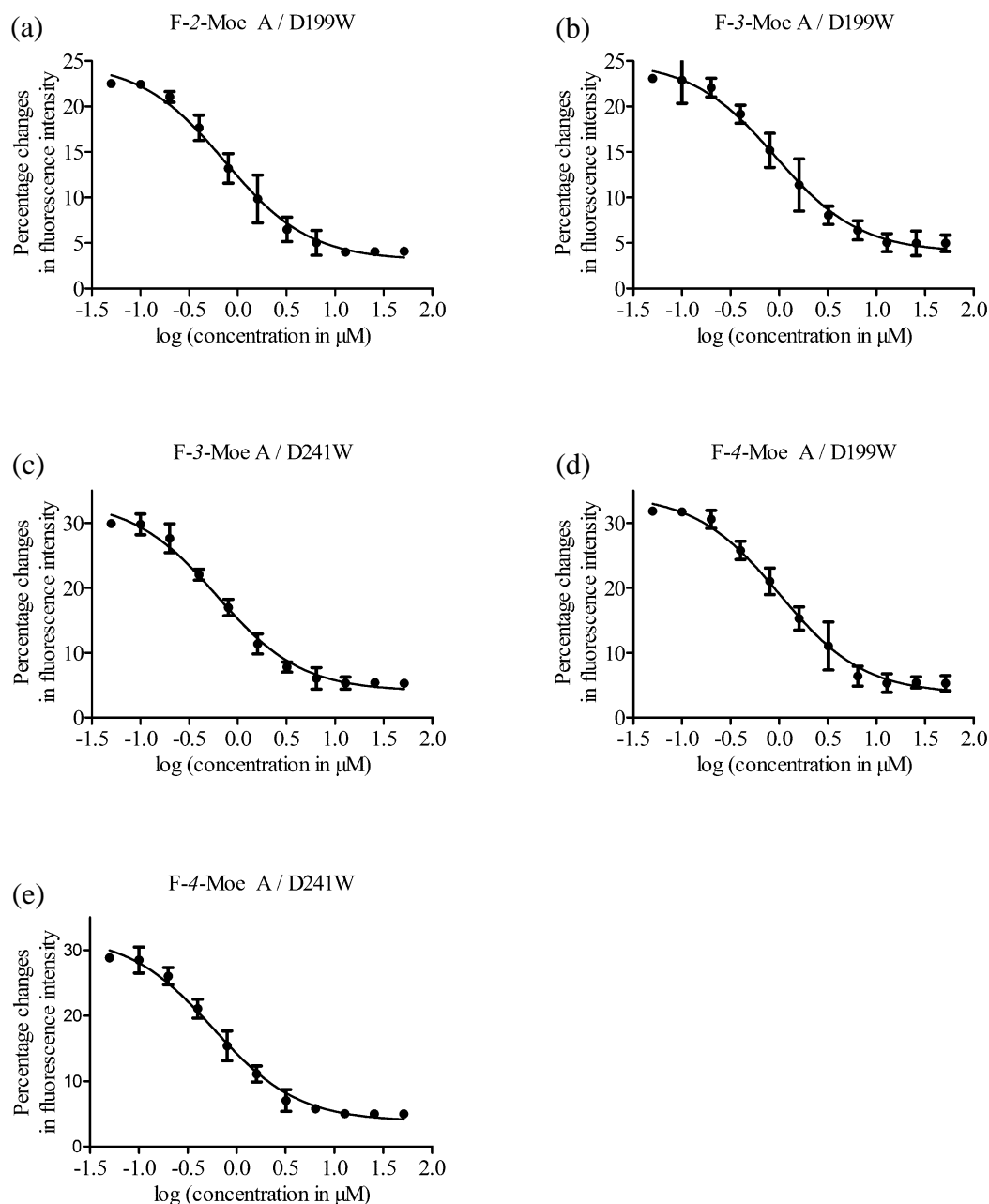


Figure 4.9 Fluorescence responses of five probe / PGT mutant pairs (a) **F-2-Moe A** / D199W; (b) **F-3-Moe A** / D199W; (c) **F-3-Moe A** / D241W; (d) **F-4-Moe A** / D199W (e) **F-4-Moe A** / D241W with addition of different concentrations of Moe A.

$$\#FI_{\text{change}} \% = (FI_{\text{max}} - FI_{\text{obs}}) / FI_{\text{max}} \times 100 \%$$

$\#FI_{\text{change}} \%$ is percentage change in fluorescence intensity, FI_{max} is the fluorescence intensity in absence of PGT mutants, FI_{obs} is the observed fluorescence intensity under one concentration of Moe A.

Table 4.2 K_I values of Moe A calculated from five probe / PGT mutant pairs

Biosensing systems	K_I values (μM)
F-2 -Moe A / D199W	0.72 ± 0.14
F-3 -Moe A / D199W	0.58 ± 0.14
F-3 -Moe A / D241W	0.52 ± 0.11
F-4 -Moe A / D199W	0.70 ± 0.17
F-4 -Moe A / D241W	0.51 ± 0.16

Note: K_I (Moe A) for *S. aureus* SgtB / Moe A trisaccharide analogue was reported as $0.64 \mu\text{M}$ [67].

4.3.6 The effect of DMSO on FI of F-4-Moe A in Tris solution (pH 8.0)

As shown in Figure 4.10, DMSO shows a dose-dependent quenching effect on **F-4-Moe A** in a 10 mM Tris solution (pH 8.0). The fluorescence intensity of the fluorescent probe decreases by 7 % in presence of 10 % of DMSO, which is a comparatively small change in the fluorescence-based assay. Importantly, it has been reported that *S. aureus* PBP2 can still efficiently catalyze polymerization of lipid II under the condition of 10 % DMSO [105]. Therefore, 10 % of DMSO was used in PGT inhibitors screening assay to improve the solubility of PGT inhibitor candidates in Tris solution.

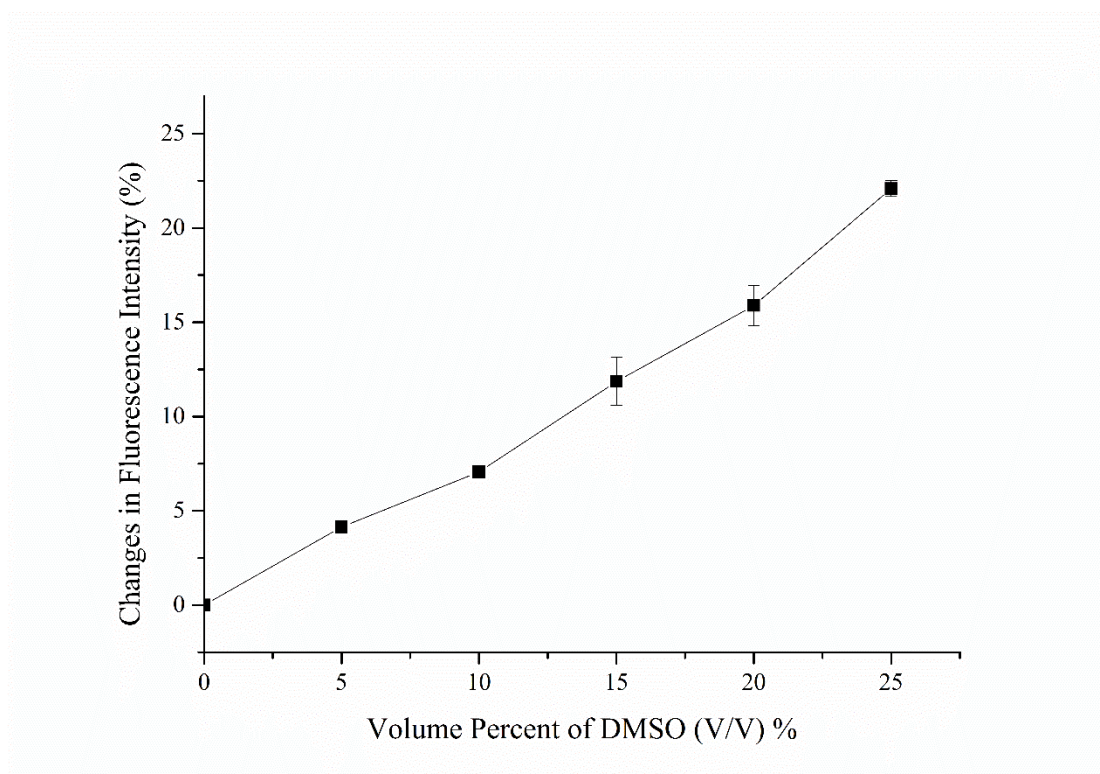


Figure 4.10 Quenching effect of DMSO on **F-4-Moe A**

4.3.7 Further validation of the best performed F-4-Moe A / D199W

Before the application of the biosensor in PGT inhibitor screening, it is imperative to characterize the specificity of the biosensing system towards the analyte. PGT inhibitors **14** and **16** (please refer to Figure 1.9 of chapter I), antibiotics including ampicillin and kanamycin which target on the process of transpeptidation or protein biosynthesis were used in specificity analysis. These four compounds were added into the biosensor instead of Moe A to monitor the fluorescence response of the biosensing system. As shown in Figure 4.11, the fluorescence intensity of **F-4-Moe A / D199W** did not recover even though both two negative controls (ampicillin and kanamycin) reached 2.5 mM. It can be inferred that antibiotics which cannot bind to the PGT active sites are not able to restore the fluorescence intensity. As for two reported PGT inhibitors, while nil fluorescence change was observed after the addition of **16**, a concentration-dependent increase in fluorescence intensity was recorded upon the addition of **14**. This increase reached a maximum at ~1.5 mM of **14**. Although **16** is known to bind to PGT, its binding affinity is relatively weak and the exact binding site has not yet been confirmed. That compound **16** is too weak to displace the probe from the active site of PGT may be the reason for its unobservable fluorescence change. On the other hand, inhibitor **14** is able to competitively bind to the enzyme with fluorescein-labeled Moe A and release the bound probe from PGT. Based on the above results, it can be concluded that only PGT inhibitors which are strong enough to displace the probes by binding to the active site can restore the fluorescence intensity. Therefore,

the designed biosensing system can provide a specific assay for screening PGT inhibitors.

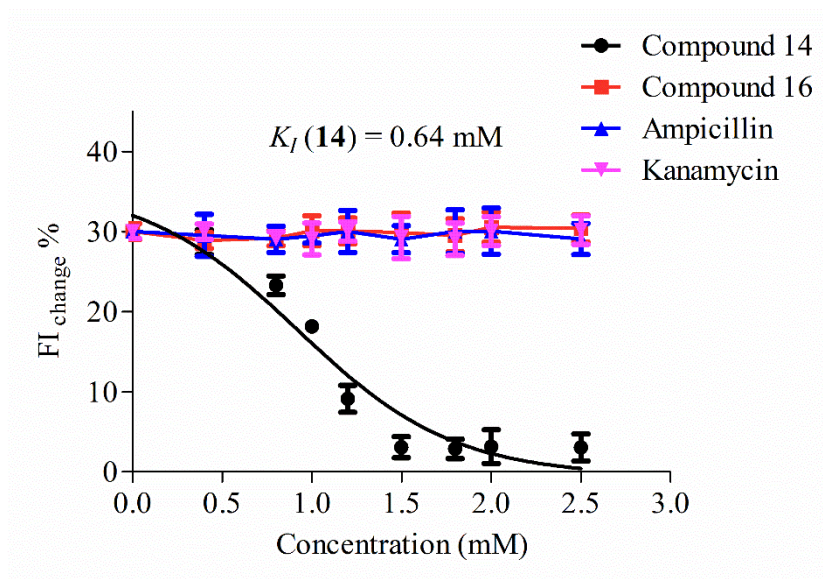


Figure 4.11 FI changes of F-4-Moe A / D199W with addition of PGT inhibitor **14**, **16**, ampicillin and kanamycin. $\#FI_{change} \% = (FI_{max} - FI_{obs}) / FI_{max} \times 100\%$

$\#FI_{change} \%$ is percentage change in fluorescence intensity, FI_{max} is the fluorescence intensity in absence of PGT mutants, FI_{obs} is the observed fluorescence intensity under one concentration of **14**, **16**, ampicillin and kanamycin.

4.4 Concluding remarks

The performance of all fluorescent probe / PGT mutant pairs are reported in this chapter. Three probe / mutant pairs including **F-3-Moe A** / D241W, **F-4-Moe A** / D199W and **F-4-Moe A** / D241W show better fluorescence quenching efficiency. The fluorescence intensity of these three pairs were restored upon the addition of Moe A. **F-4-Moe A** / D199W showed the best recovery and the fluorescence was restored in presence of 10 μ M of Moe A. Further validation assay indicates that both the PGT inhibitors Moe A and compound **14** can restore the fluorescence whereas no fluorescence was observed upon the addition of the negative controls ampicillin and kanamycin. Therefore the **F-4-Moe A** / D199W pair is the best choice for the construction of biosensor for PGT inhibitors discovery.

Chapter 5

Conclusions

In this study, a new biosensor based on photoinduced electron transfer for PGT inhibitors detection has been developed. In construction of this biosensor, three fluorescent Moe A derivatives (**F-*n*-Moe A**, *n* = 1, 2, 3) were synthesized by attaching fluorescein to ring A of Moe A through flexible linkers of different lengths. The binding affinity of these modified Moe A to the active site of PGT were not significantly altered compared to Moe A, which further confirms that ring A of Moe A is not essential for its binding to peptidoglycan glycosyltransferase. Five amino acid residues, namely Q161, H162, D199, Y210 and D241 of PGT were mutated to tryptophan which is an efficient quencher of fluorescein. These five amino acid residues are located near the Moe A binding site of PGT based on the crystal structure of complex of Moe A and PGT. Surface plasmon resonance (SPR) analysis of the interaction between Moe A and PGT mutants indicated that the active sites of the five mutants are intact and Moe A can still bind to the mutants with similar binding affinities as to the wild type. The tryptophan residue in the five mutants were demonstrated to interact with the bound probe through the changes in fluorescence intensity.

The fluorescence intensity of **F-*n*-Moe A** decreases with addition of certain PGT mutants and can be recovered by addition of Moe A and inhibitor compound **14**. The fluorescence intensity decreases when D199W is added to all three probes, as well as

when D241W is added to probes **F-3-Moe A** and **F-4-Moe A**. Upon the addition of Moe A to the probe / mutant pairs with fluorescence quenching, the fluorescence intensity is restored. It was found that two mutated sites (D199W and D241W) which can quench the fluorescence of probes are located close to the residues Y196 and P234, which directly binds to units A and B of Moe A during the interaction of PGT with Moe A. Furthermore, longer linkers of the probes provide more flexibility and facilitate the interaction between the fluorophore group and the nearby tryptophan residue resulting in a stronger fluorescence quenching effect. The decrease in fluorescence is attributed to the quenching effect of tryptophan residue introduced into the PGT by site directed mutagenesis. In the displacement assay, fluorescence intensity restoration was observed when Moe A was added to the probe / mutant pairs with fluorescence quenching effect, whereas no fluorescence change was observed for the negative controls ampicillin or kanamycin. Among the five pairs of **F-*n*-Moe A** and PGT mutants with quenching effect, the **F-4-Moe A** / D199W pair shows the strongest signal in fluorescence quenching and recovery. The results suggest that PGT inhibitors can be identified by the biosensing system when the inhibitors competitively bind to the active site of PGT and release the fluorescent Moe A from the binding pocket of PGT.

Comparing to the high price and tedious operation in SPR-based screening assay [69], our biosensor provides a fast and simple way for PGT inhibitors screening. Moreover, SPR-based assay is not very sensitive to small molecules and high binding affinity of substrate (inhibitor) to protein is required, which restricts the wide use of this method in discovery of enzyme inhibitors. Importantly, the method reported here can be

operated in microplate and applied in high-throughput screening. Fluorescence polarization-based assays for PGT inhibitors screening have been developed by Walker's and Wong's groups respectively [67, 71]. The FP-based assay depends on alternation of molecular mobility upon dissociation or formation of protein-inhibitor complex in solution phase, which makes FP assay not applicable to surface-bound chip-based assays. On the contrary, PET-based fluorescence techniques can be applied in assays which are operated in both solution phase and surface-bound assays [81]. The concept of protein engineering of PGT into a fluorescence quencher used for the detection of PGT inhibitors can be further developed into a chip-based biosensor for inhibitors screening.

In this study, a fast, simple and effective biosensor has been developed for PGT inhibitors screening. However, the performance of this biosensor may require further optimization to improve its efficiency. The quenching effect only reaches 32 % which can be improved by double mutation, mutation of other amino acid sites or modification of **F-n-Moe A**. Firstly, since two mutants (D199W and D241W) can quench the fluorescence of **F-n-Moe A**, double mutations (D199W and D241W) can be made to strengthen the quenching efficiency. Based on the crystal structure, D199 and D241 are both close to the active sites Y196 and P234, so more amino acids around Y196 and P234 can be selected for tryptophan mutation. Under this situation, fluorescence of bound **F-n-Moe A** can be quenched by two or more tryptophan residues, which can increase the quenching efficiency. PET based fluorescence quenching is dependent on the distance between the tryptophan residue and the fluorophore of **F-n-Moe A**, so a

longer linker between fluorophore group and Moe A can be made. With the increased quenching efficiency, the sensitivity of the biosensor for detecting PGT inhibitors can be further improved as the same amount of bound **F-*n*-Moe A** released from the active site of PGT can result in a higher fluorescence recovery.

Appendix I

NMR and HRMS spectra of **1**, **20-28** and HPLC spectra of probes **F-*n*-Moe A** ($n = 1, 2$ and 3)

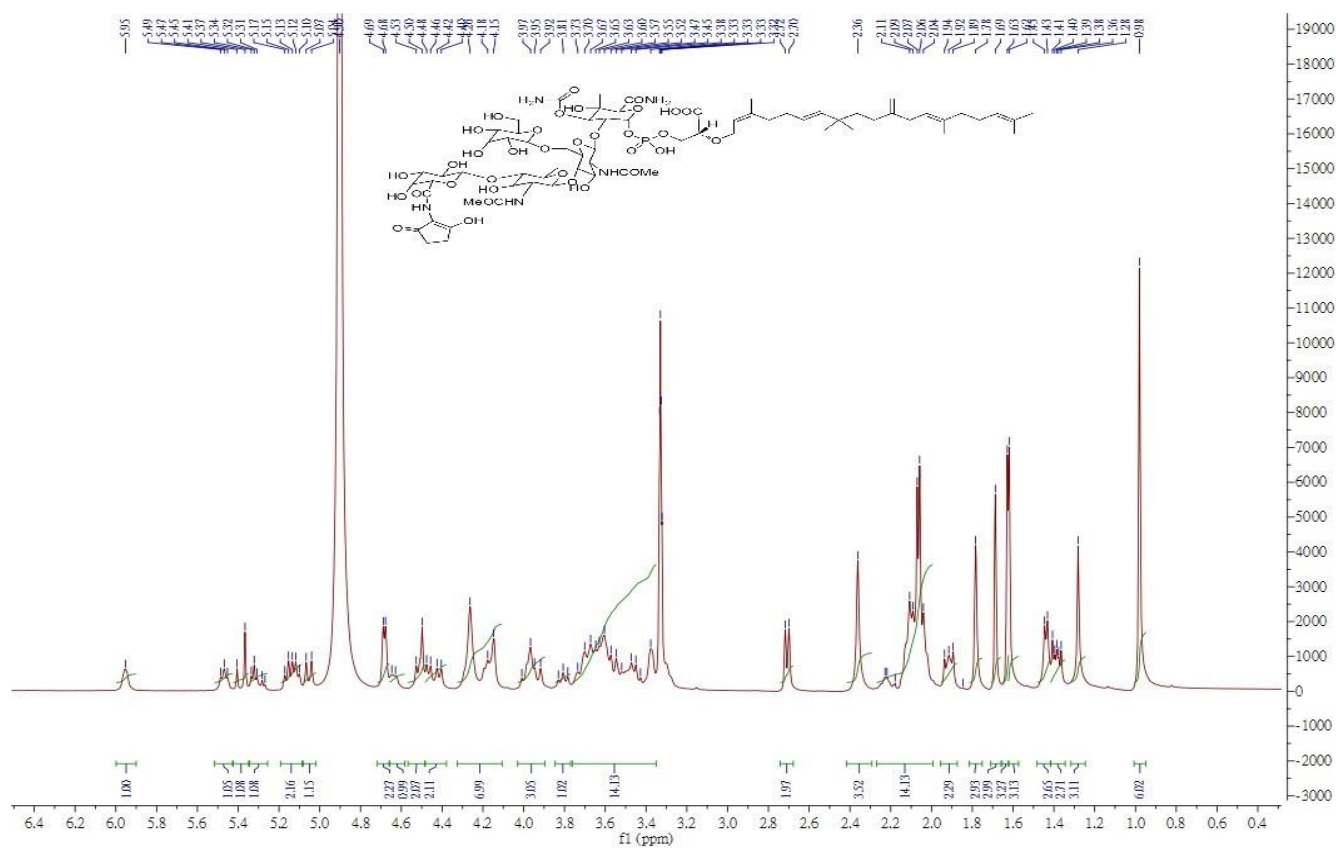


Fig. A1 ^1H NMR spectrum of **1**

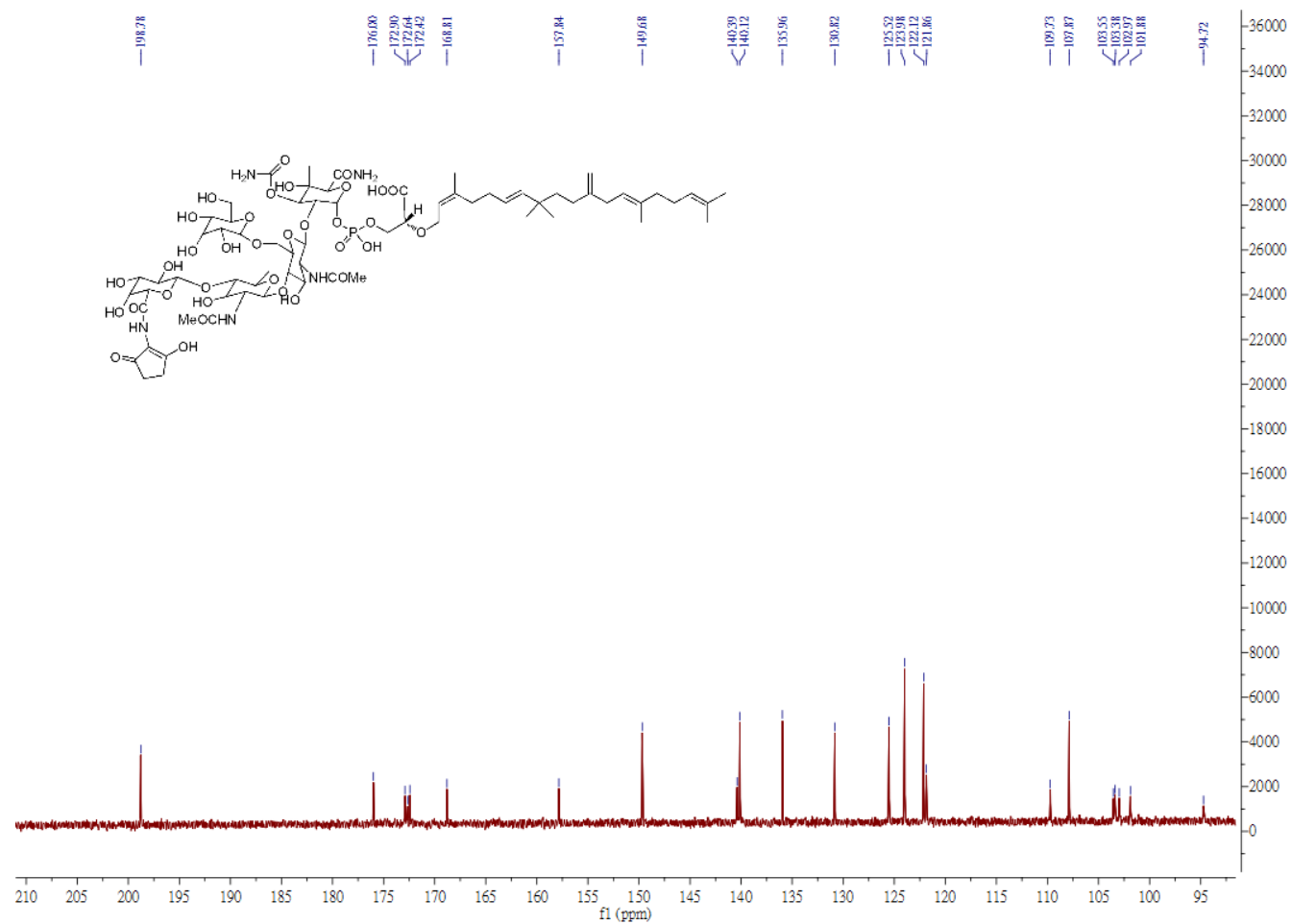


Fig. A2 ^{13}C NMR spectrum of **1**

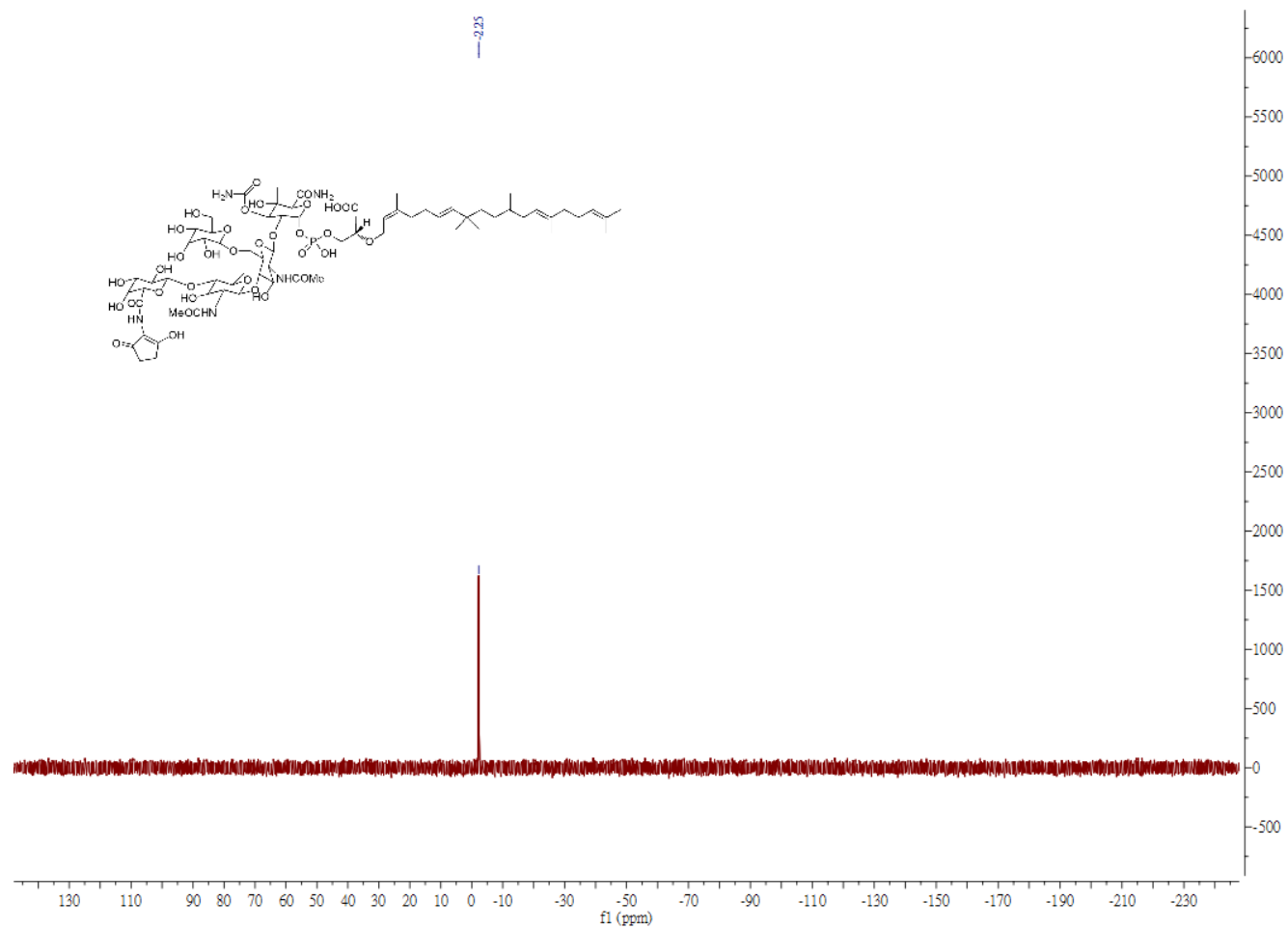


Fig. A3 ^{31}P NMR spectrum of **1**

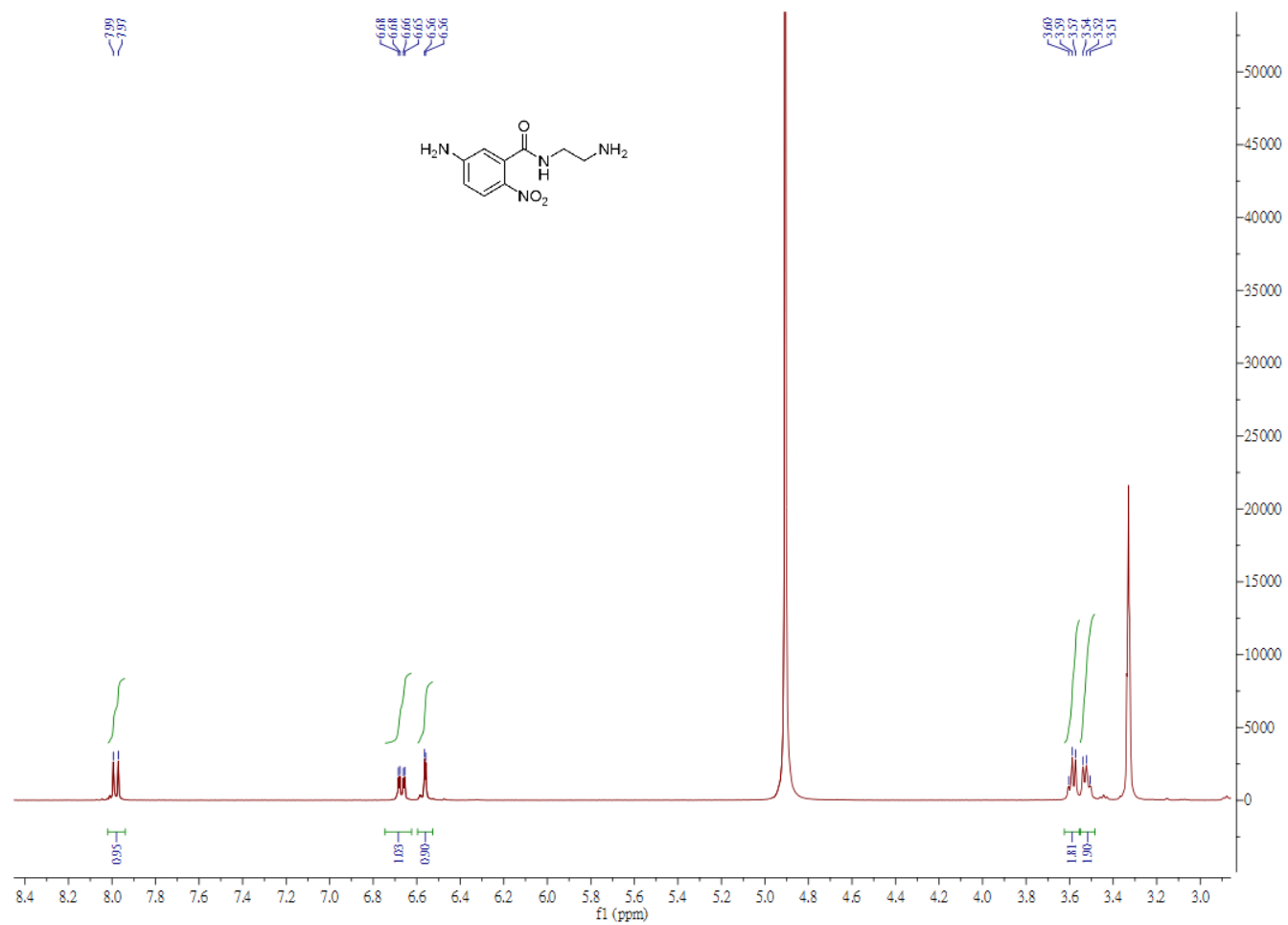


Fig. A4 ¹H NMR spectrum of **20**

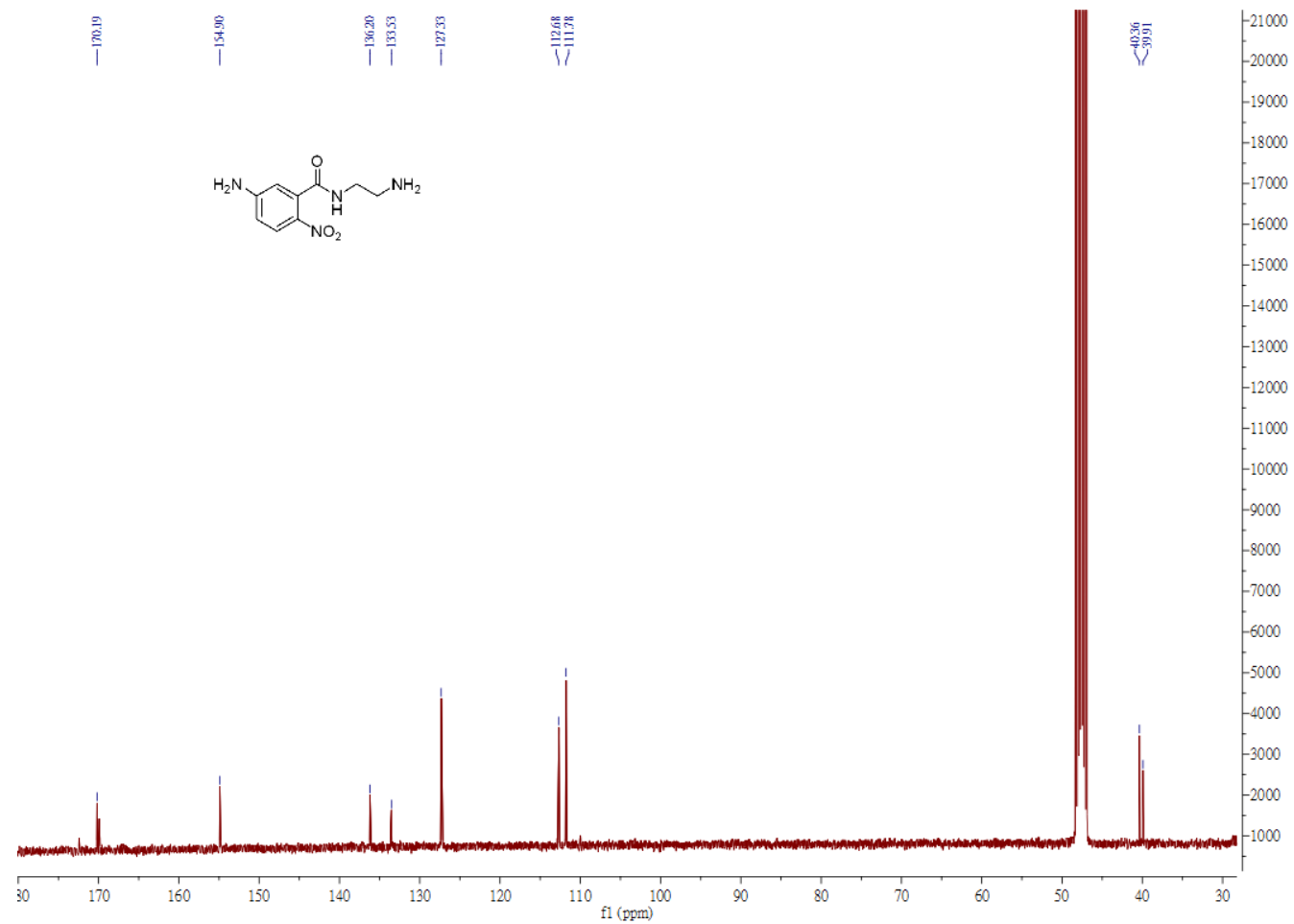


Fig. A5 ¹³C NMR spectrum of **20**

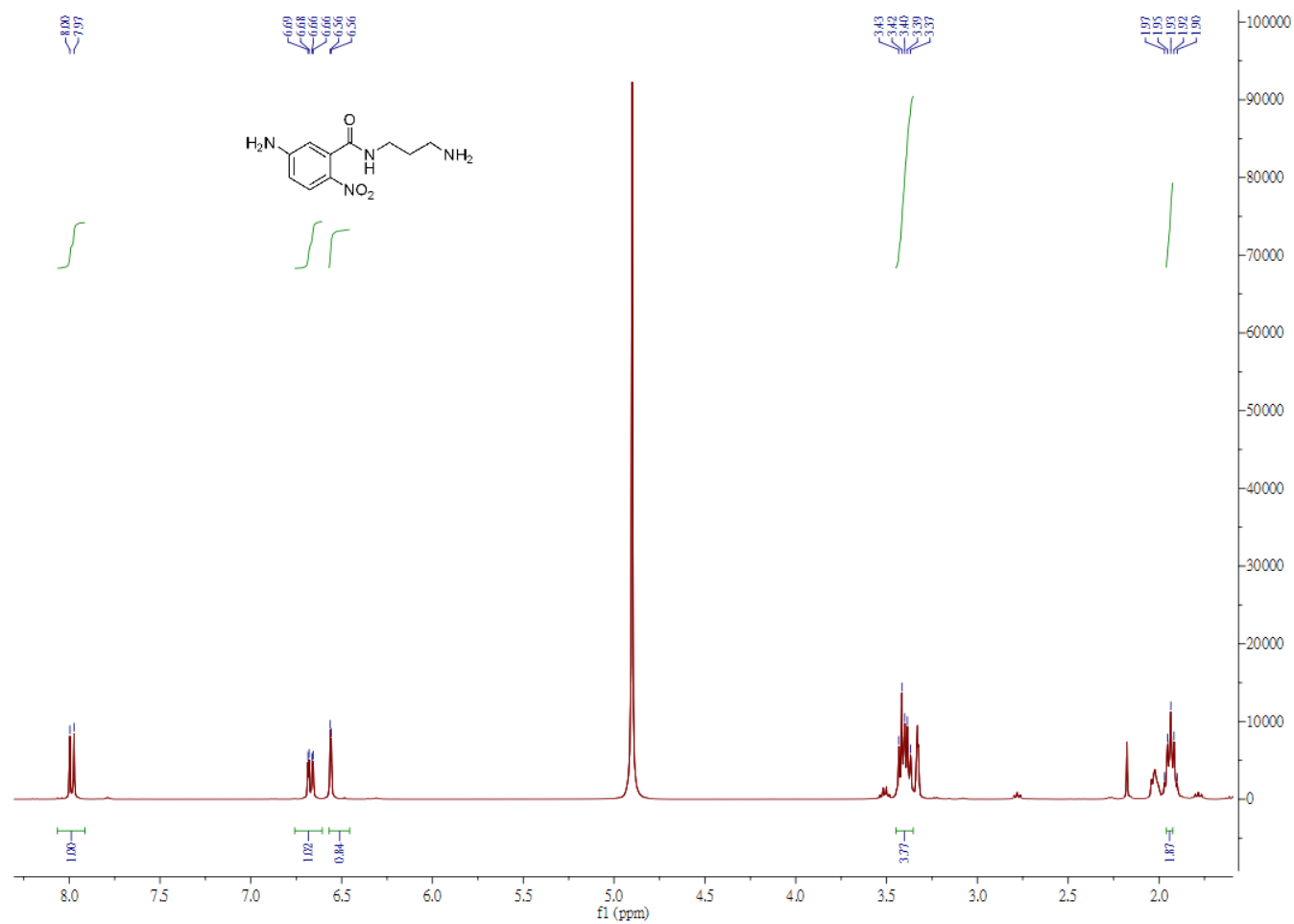


Fig. A6 ¹H NMR spectrum of **21**

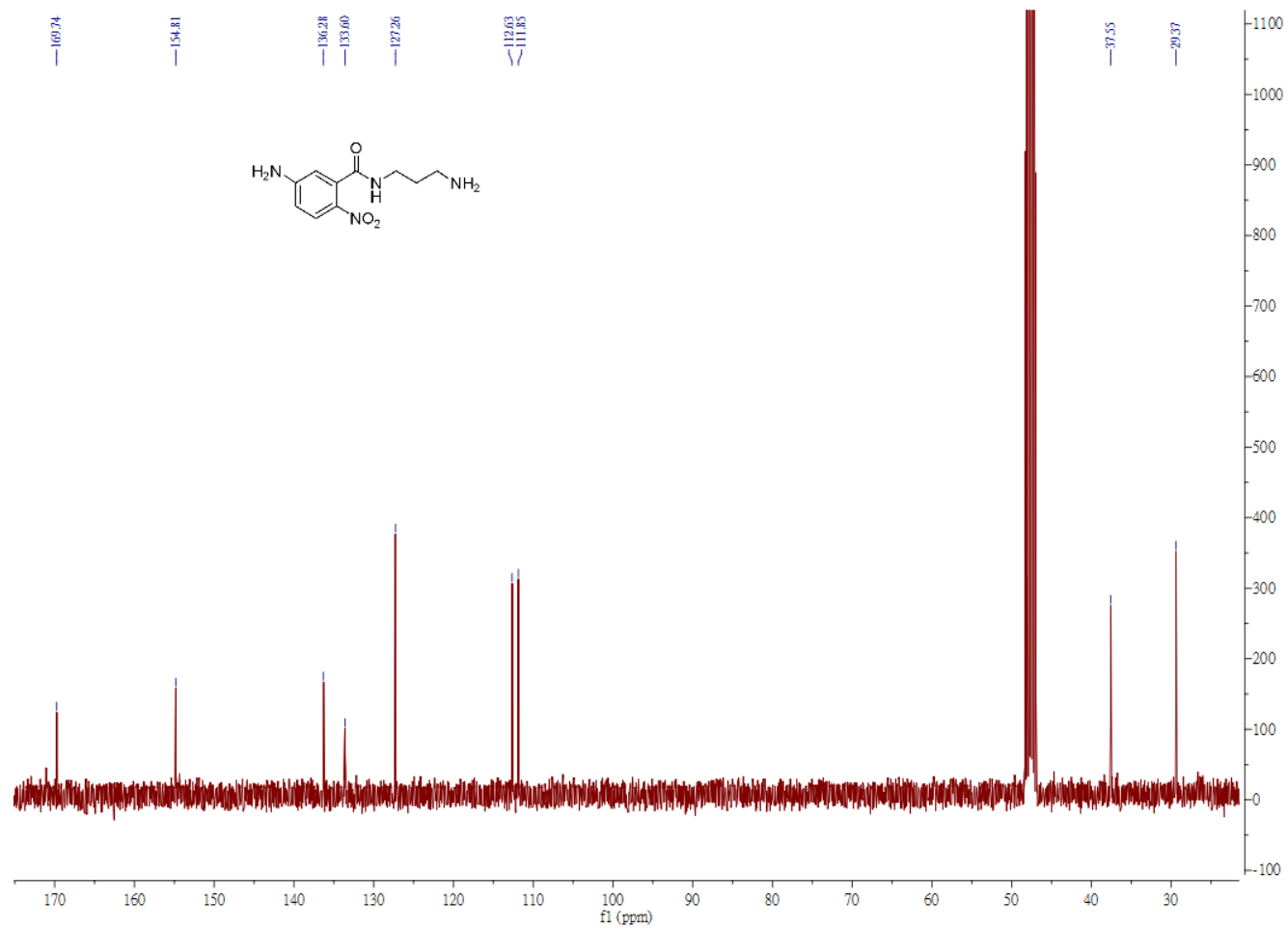


Fig. A7 ¹³C NMR spectrum of **21**

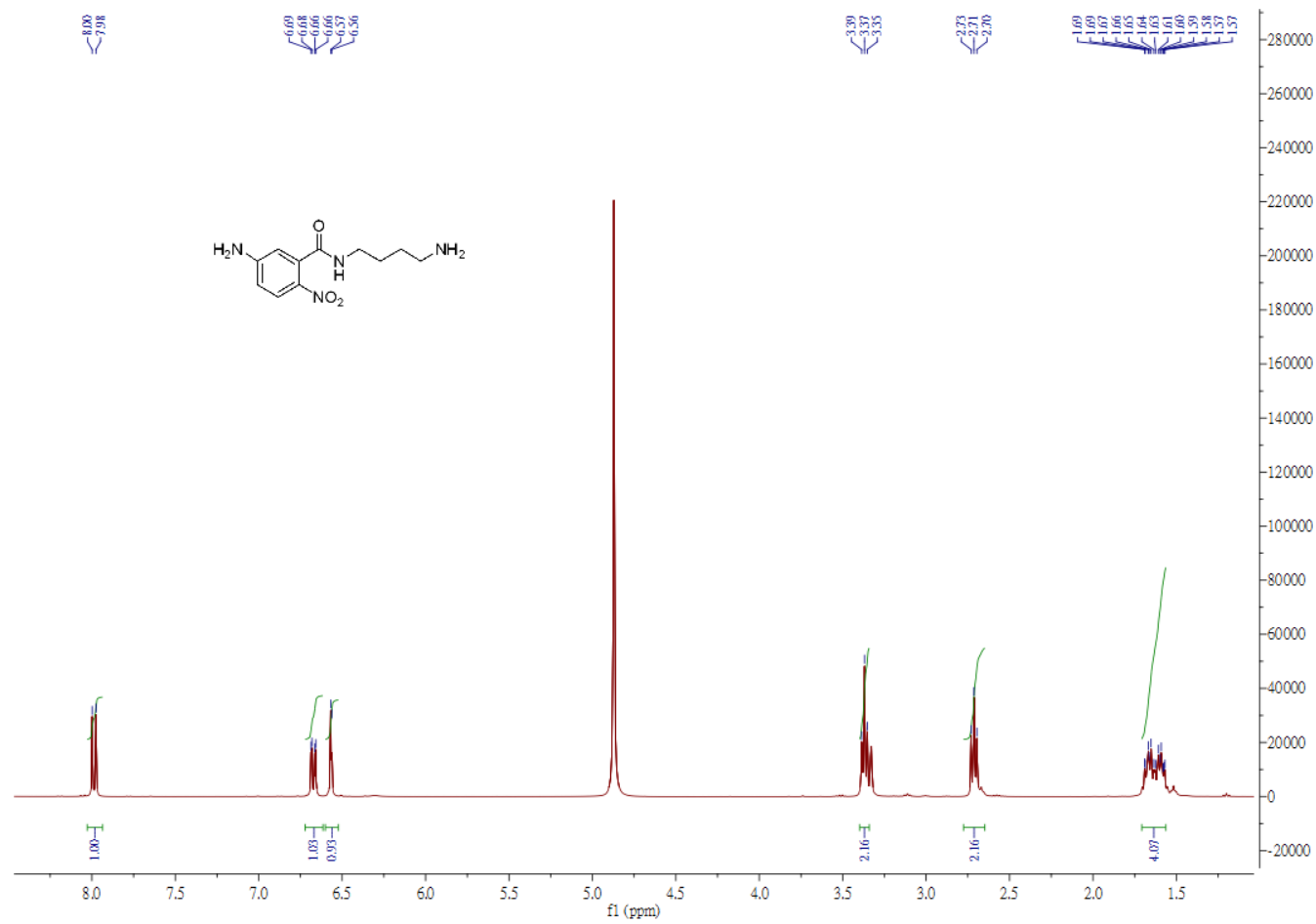


Fig. A8 ¹H NMR spectrum of **22**

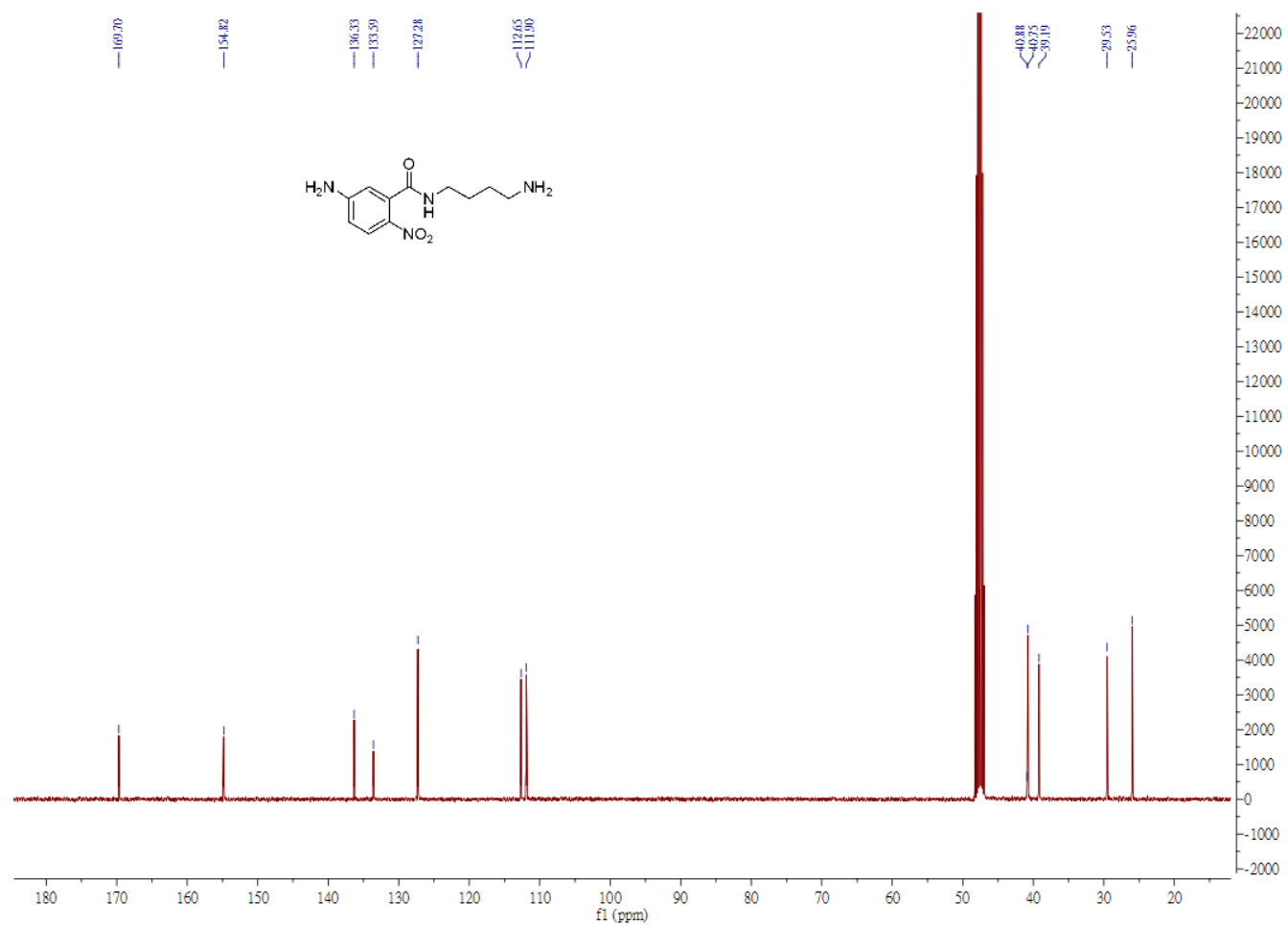


Fig. A9 ¹³C NMR spectrum of **22**

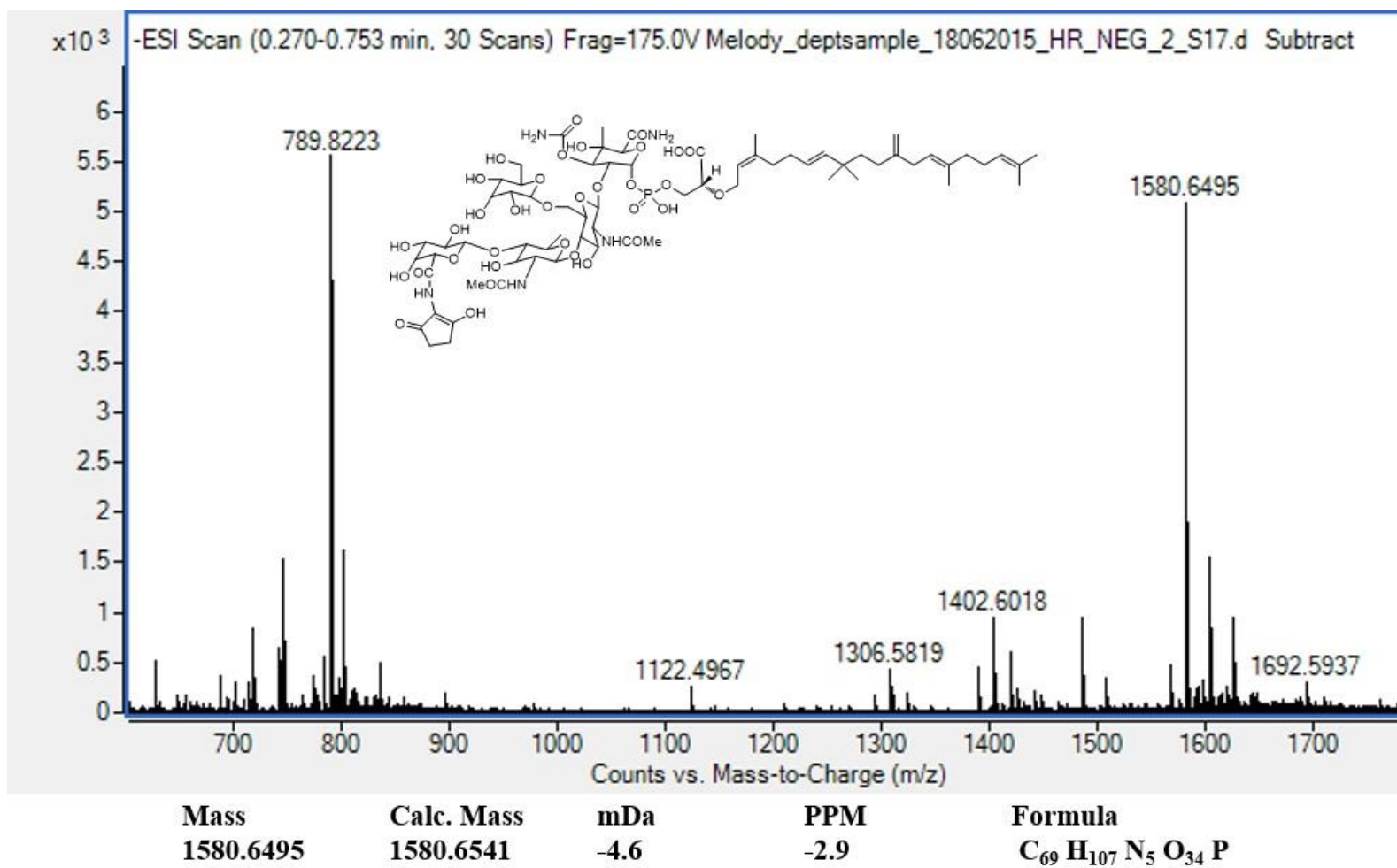


Fig. A10 HRMS spectrum of 1

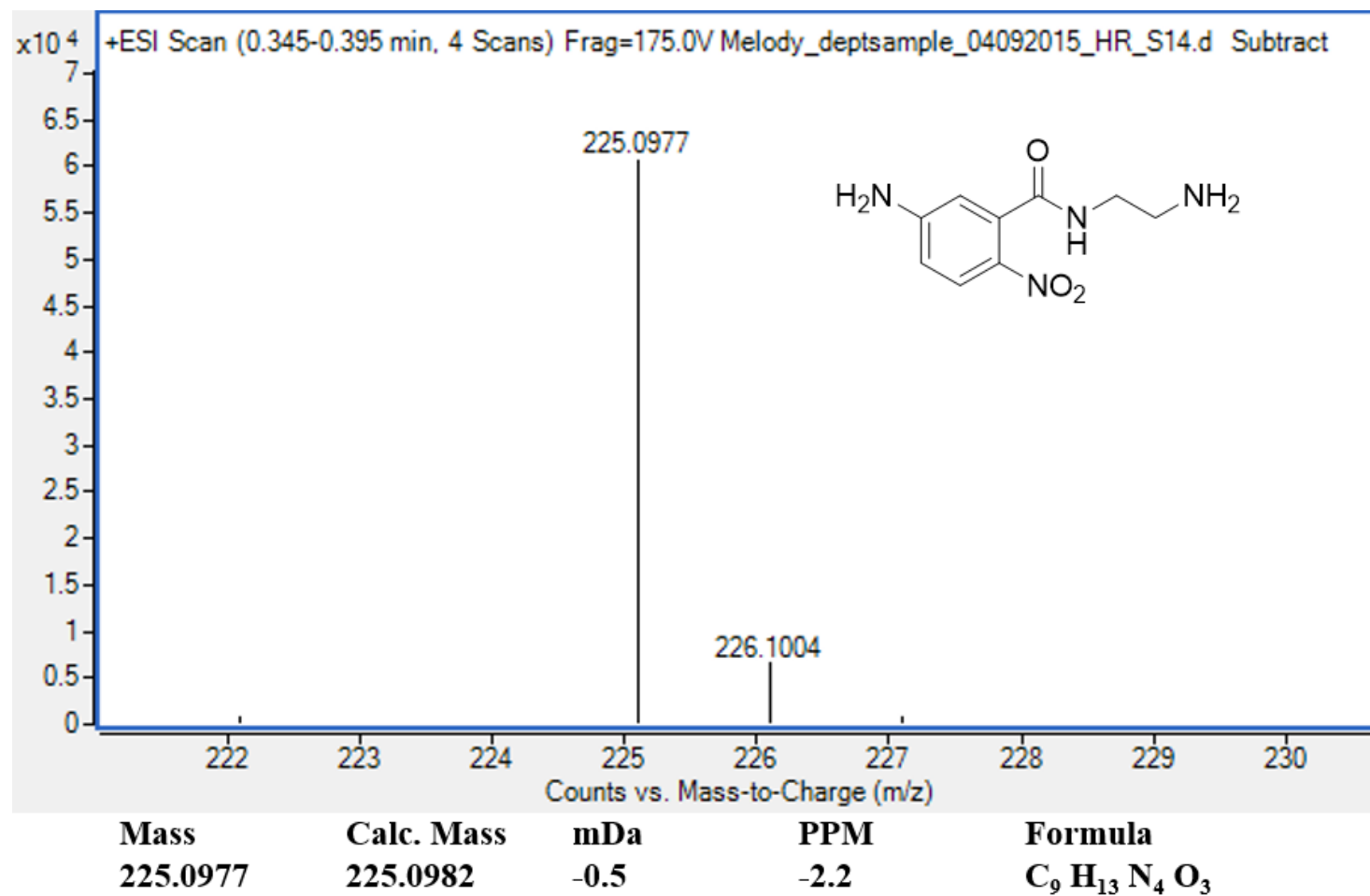


Fig. A11 HRMS spectrum of **20**

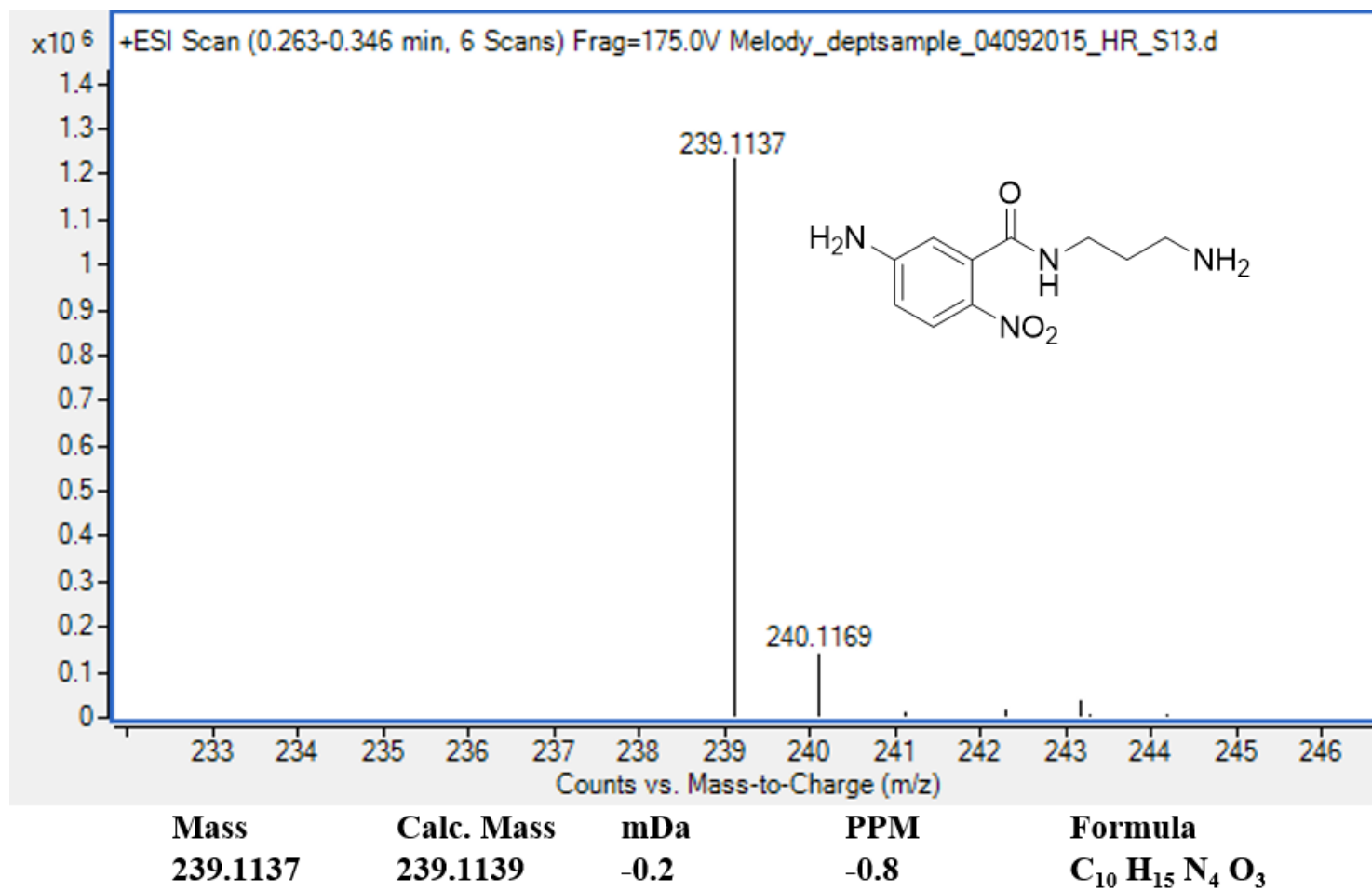


Fig. A12 HRMS spectrum of **21**

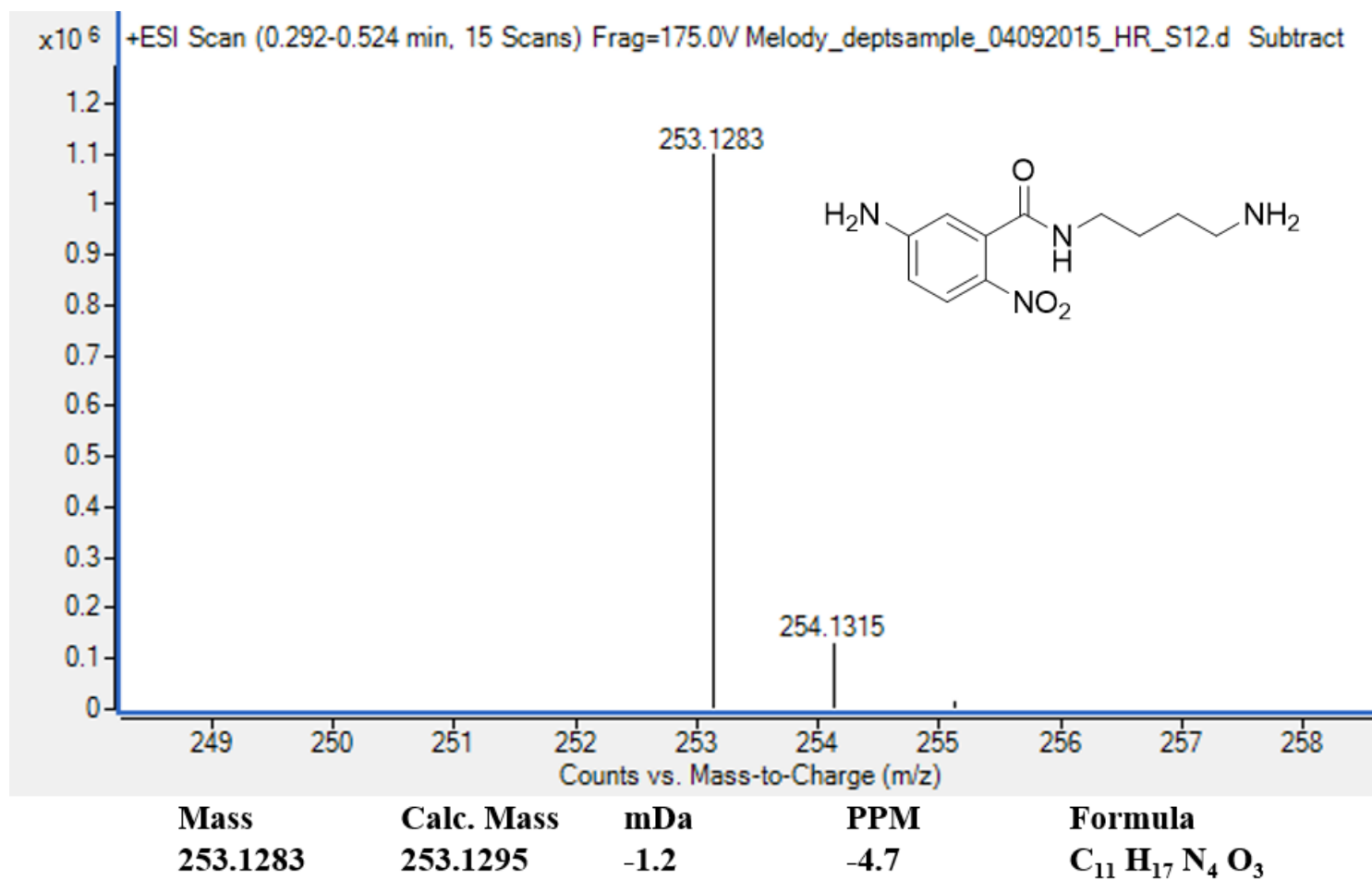


Fig. A13 HRMS spectrum of **22**

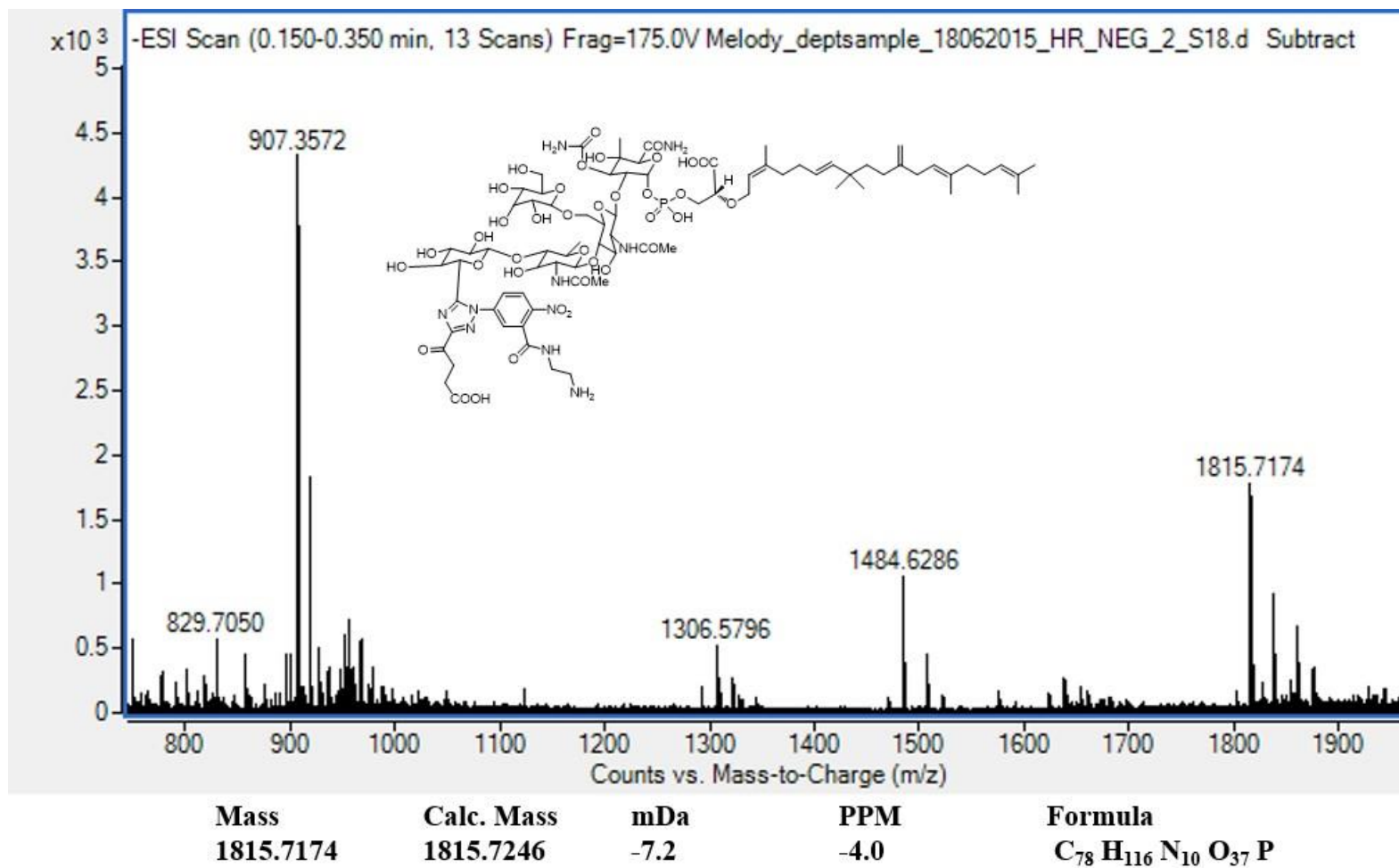


Fig. A14 HRMS spectrum of **23**

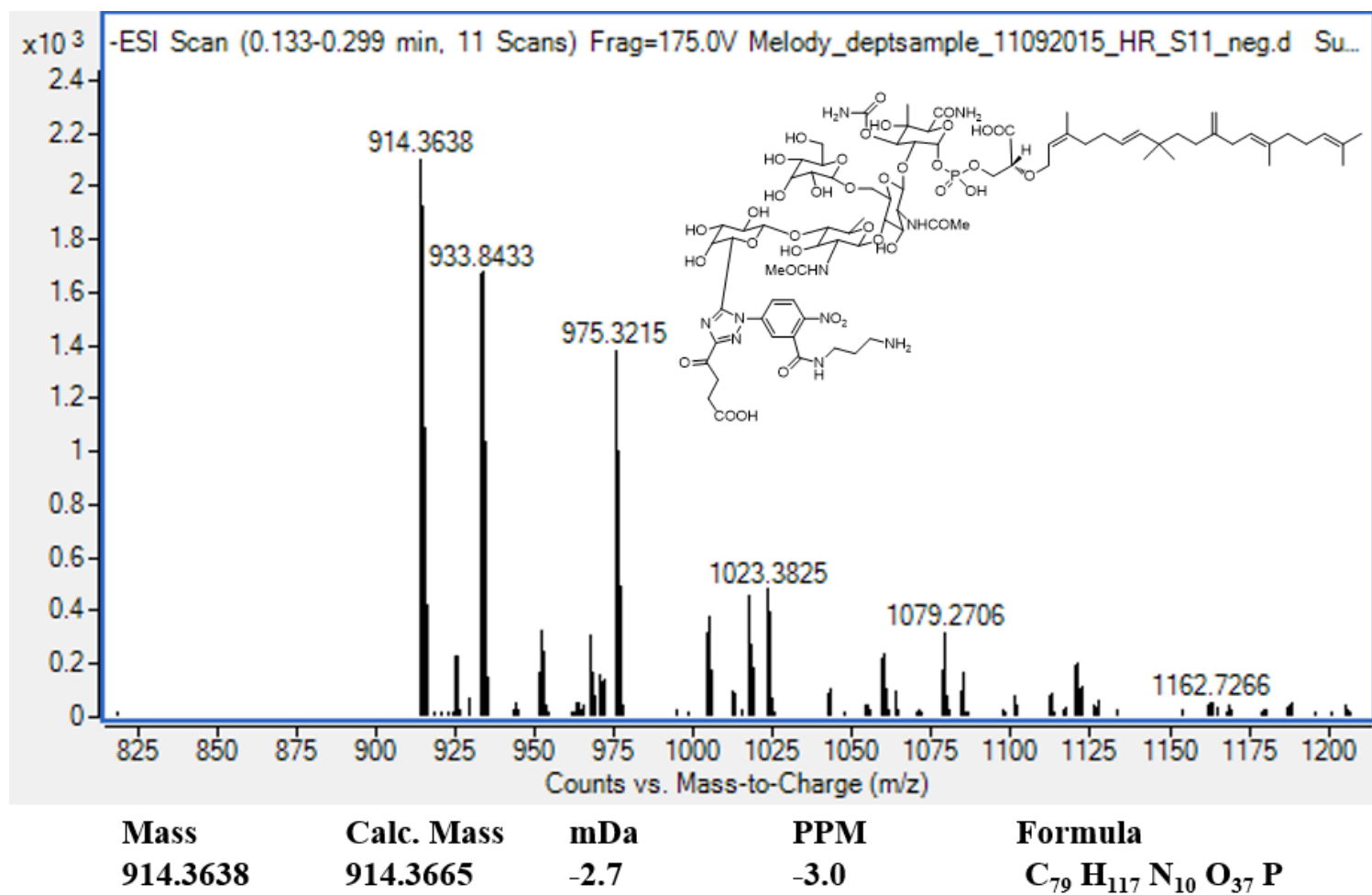


Fig. A15 HRMS spectrum of **24**

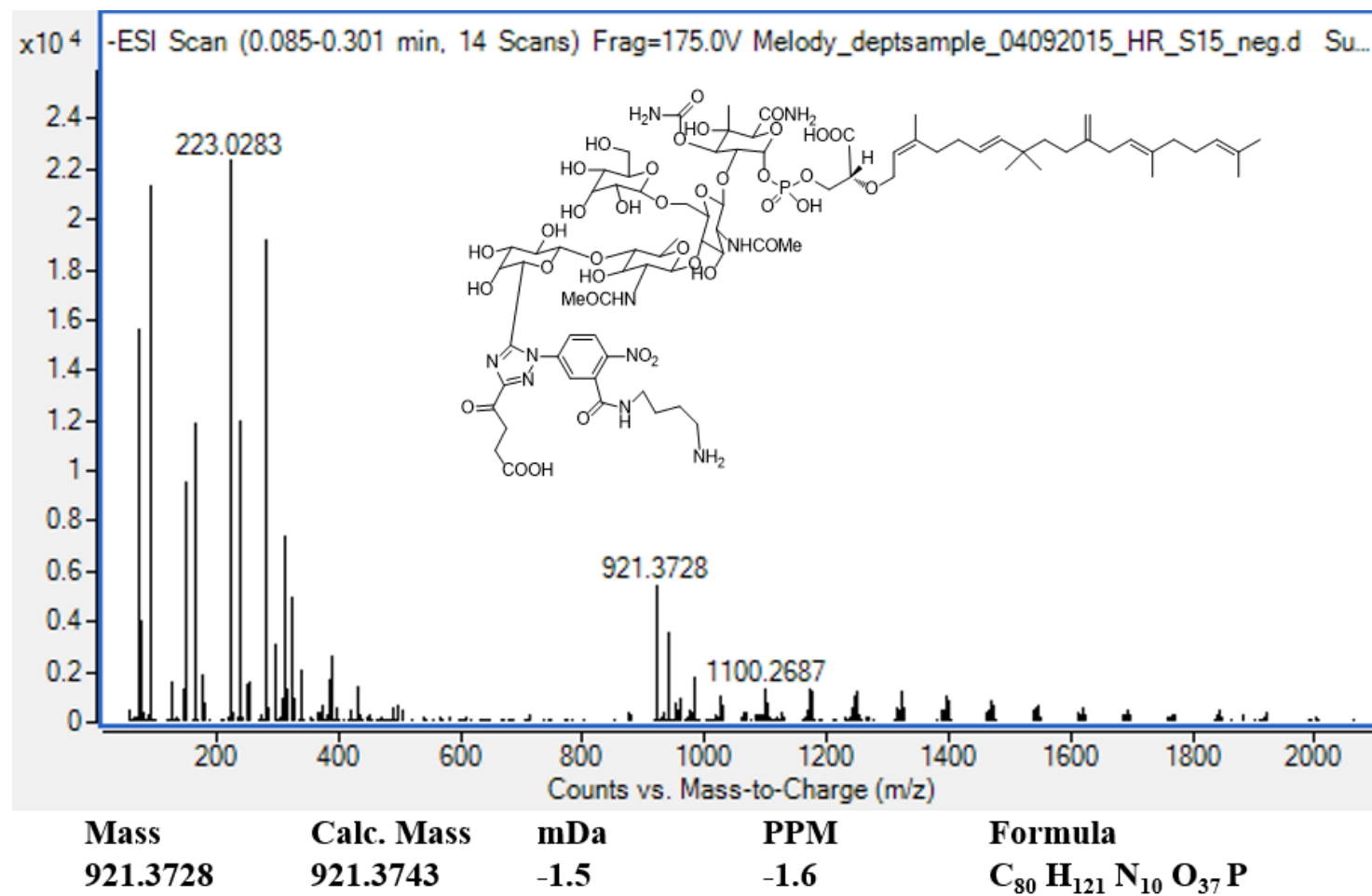


Fig. A16 HRMS spectrum of **25**

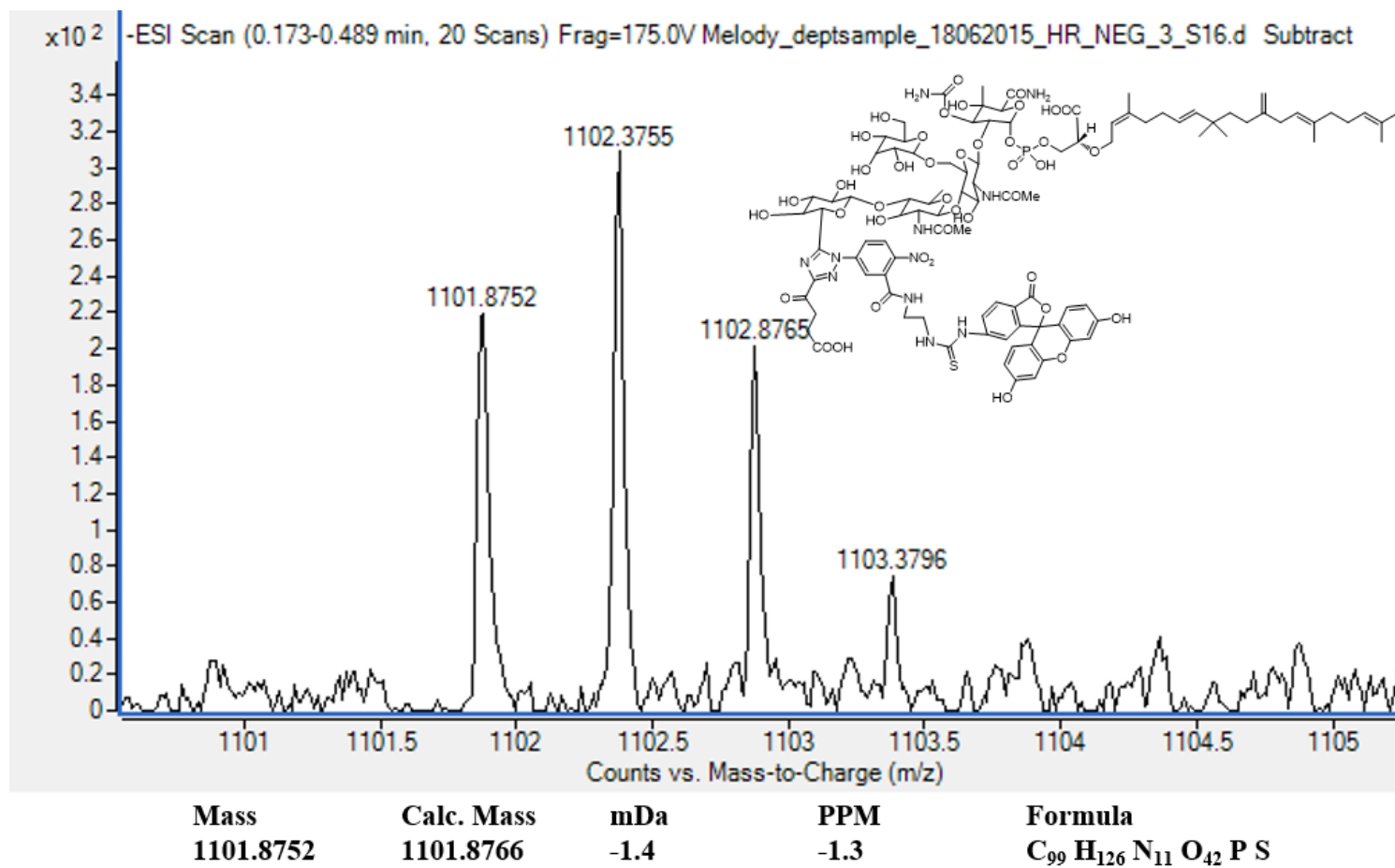


Fig. A17 HRMS spectrum of **F-2-Moe A (26)**

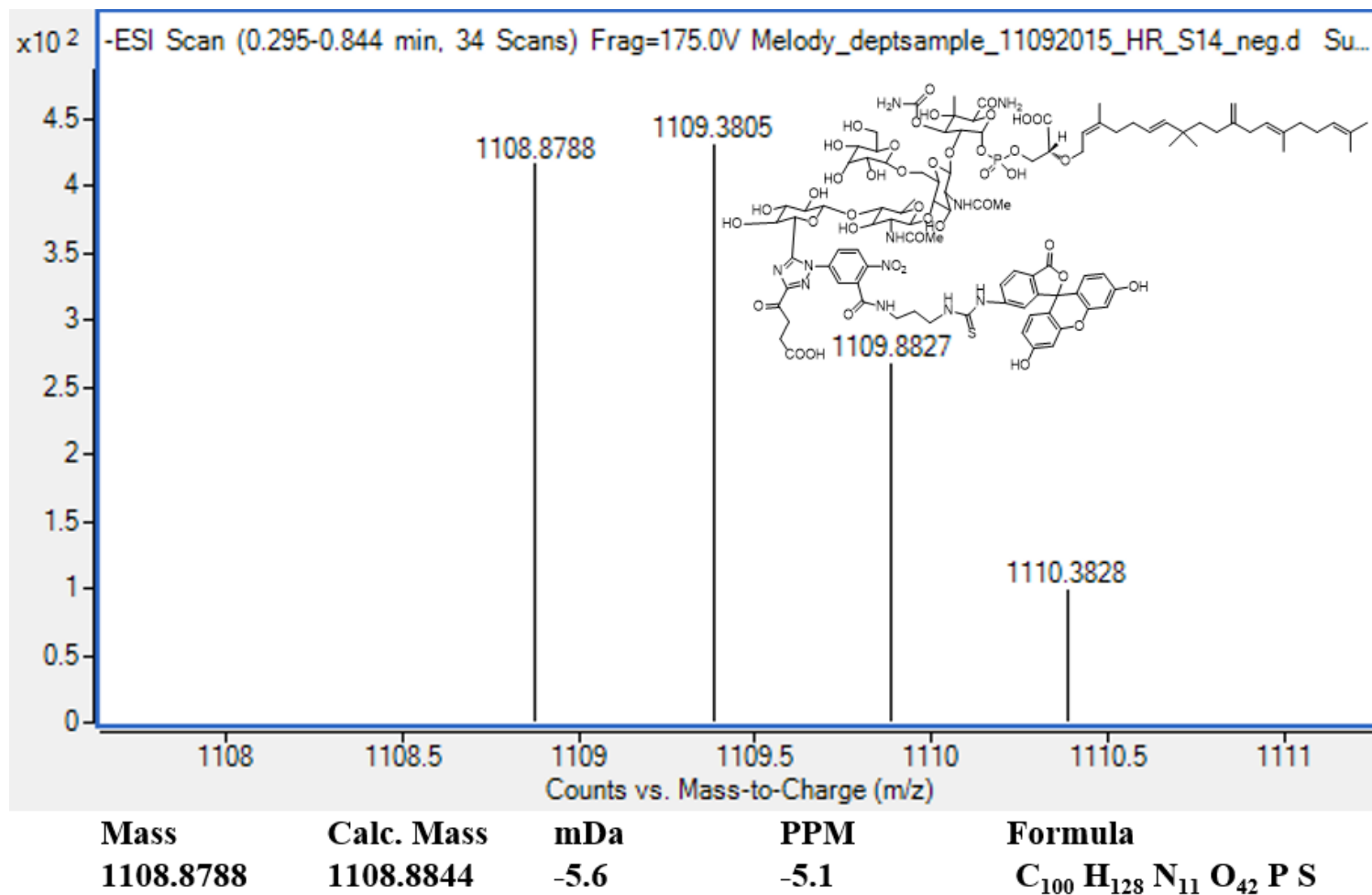
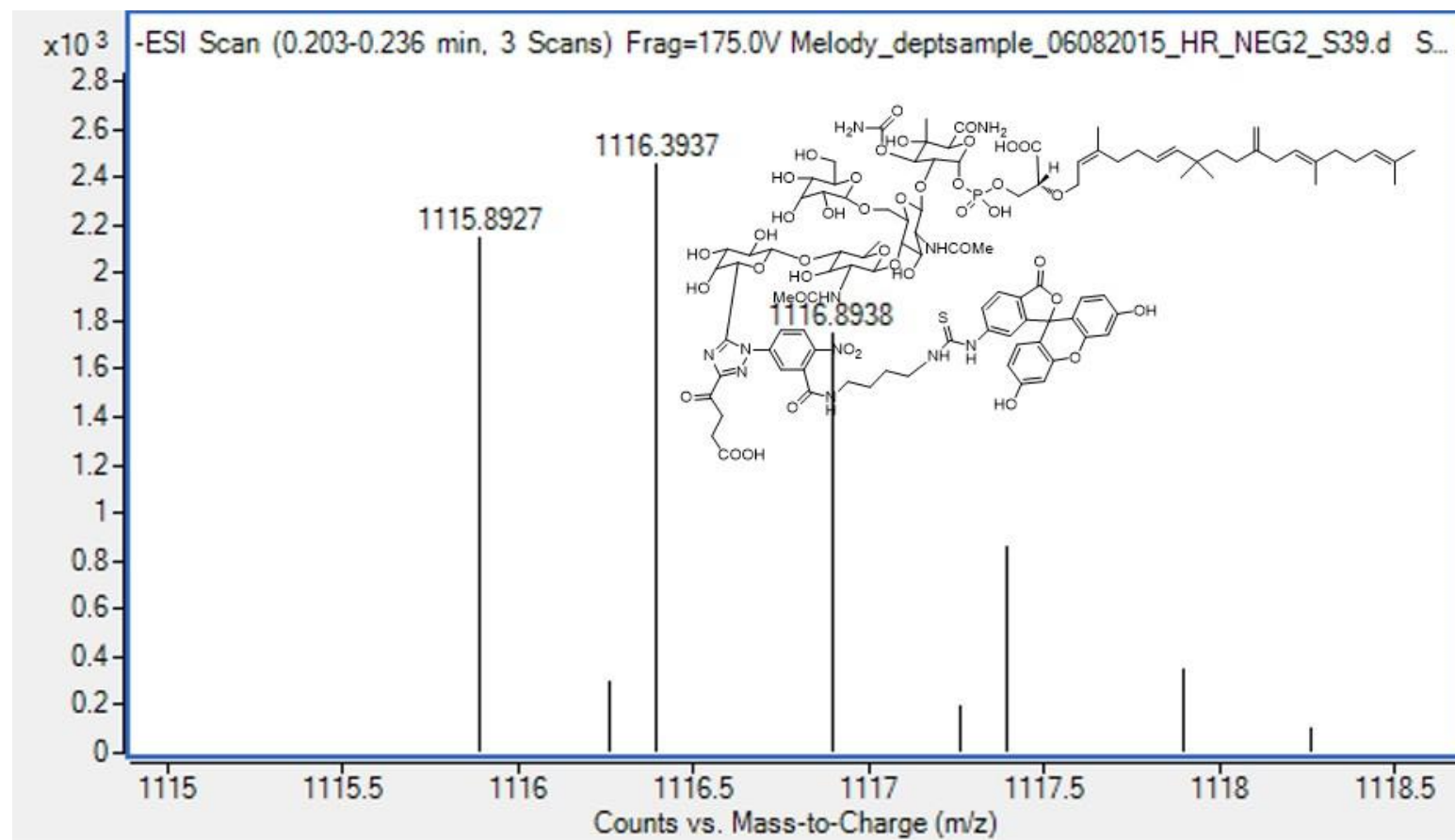


Fig. A18 HRMS spectrum of F-3-Moe A (27)



Mass	Calc. Mass	mDa	PPM	Formula
1115.8927	1115.8911	1.6	1.4	C ₁₀₁ H ₁₃₀ N ₁₁ O ₄₂ P S

Fig. A19 HRMS spectrum of **F-4-Moe A (28)**

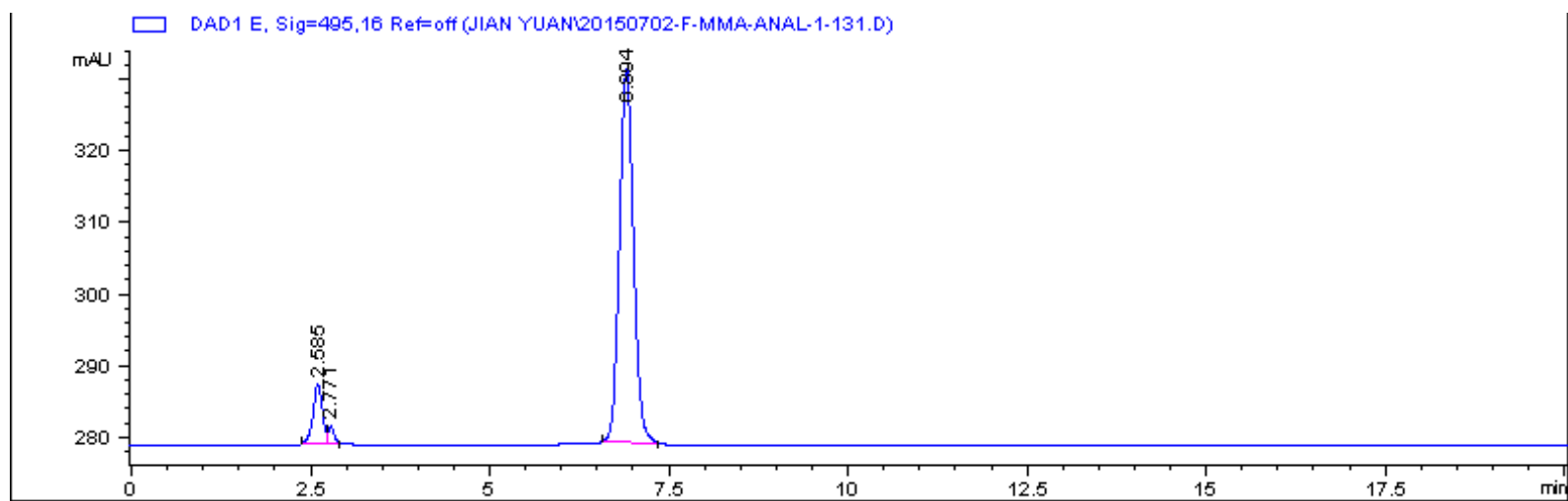


Fig. A20 HPLC spectrum of **F-2-Moe A (26)**

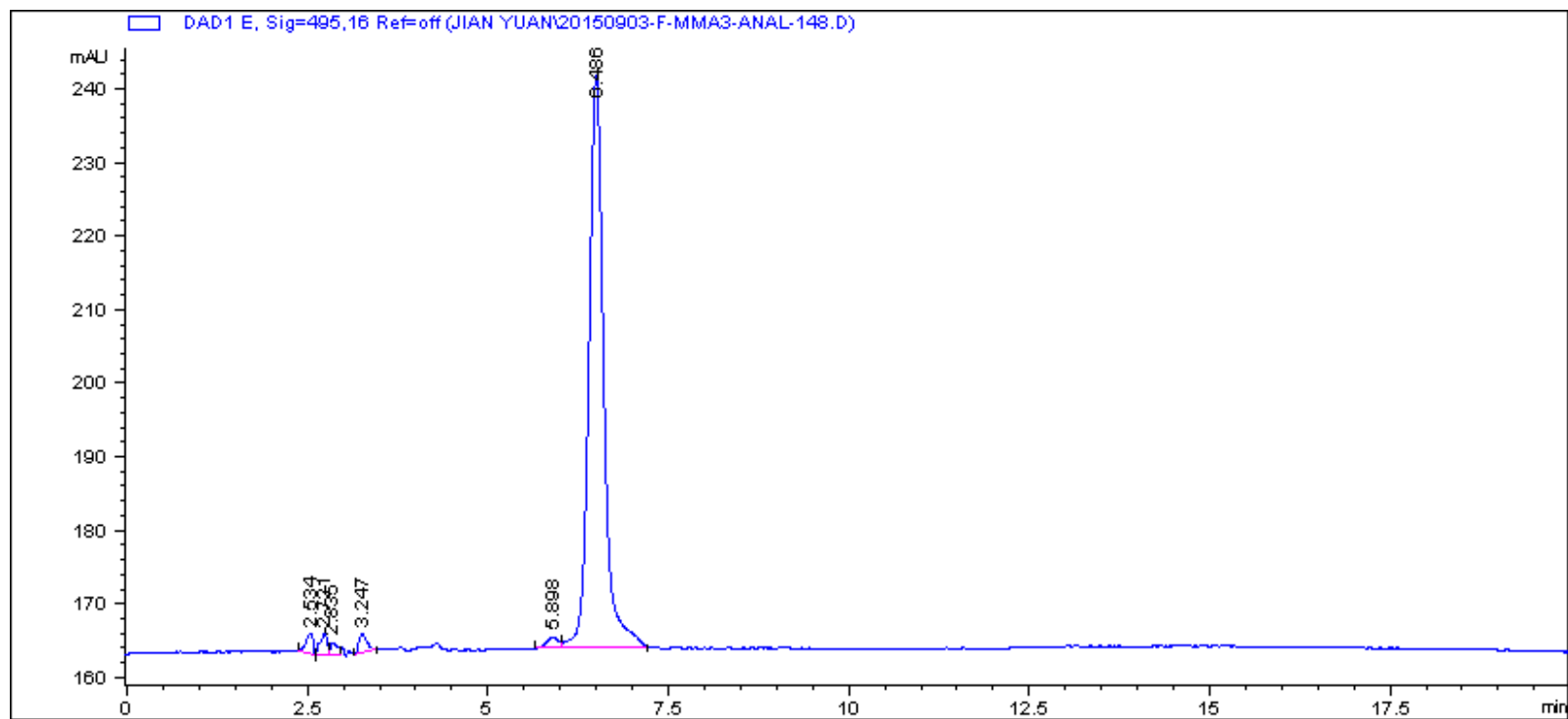


Fig. A21 HPLC spectrum of **F-3-Moe A (27)**

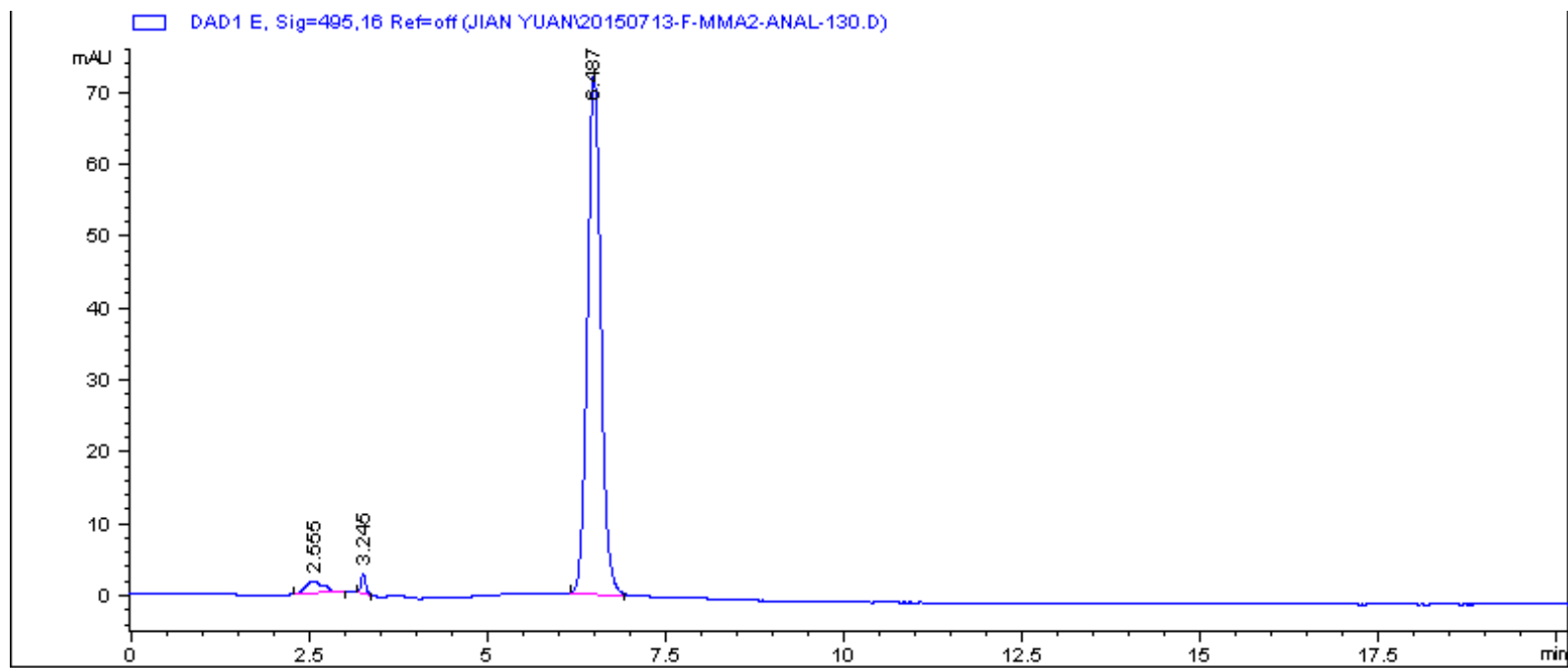


Fig. A22 HPLC spectrum of **F-4-Moe A (28)**

Appendix II

DNA sequencing results of PGT mutants including Q161W, H162W, D199W, Y210W and D241W

```

database          -----KIYDKNGELVKTLDNQQRHEHVNLDVDPKSMKDAVLATEDNRF  43
GT_pET24d_Q161W_5_T7PROM  MHHHHHHHKIYDKNGELVKTLDNQQRHEHVNLDVDPKSMKDAVLATEDNRF  50
                        *****

database          YEHGALDYKRLFGAIGKNLTGGFGSEGASTLTQQVVKDAFLSQHKSIGRK  93
GT_pET24d_Q161W_5_T7PROM  YEHGALDYKRLFGAIGKNLTGGFGSEGASTLTQQVVKDAFLSWHKSIGRK
100
                        *****

database          AQEAYLSYRLEQEYSKDDIFQVYLNKIYYSDGVTGIKAAAKYYFNKDLKD
143
GT_pET24d_Q161W_5_T7PROM  AQEAYLSYRLEQEYSKDDIFQVYLNKIYYSDGVTGIKAAAKYYFNKDLKD
150
                        *****

database          LNLAE EAYLAGLPQVPNNYNIYDHP  168
GT_pET24d_Q161W_5_T7PROM  LNLAE EAYLAGLPQVPNNYNIYDHP  175
                        *****

```

Fig. B1 Sequencing result of **Q161W**

```

database      -----KIYDKNGELVKTLDNQQRHEHVNLDVPSMKDAVLATEDNRF  43
GT_pET24d_H162W_5_T7PROM  MHHHHHHKIYDKNGELVKTLDNQQRHEHVNLDVPSMKDAVLATEDNRF  50
                        *****

database      YEHGALDYKRLFGAIGKNLTGGFGSEGASTLTQQVVKDAFLSQHKSIGRK  93
GT_pET24d_H162W_5_T7PROM  YEHGALDYKRLFGAIGKNLTGGFGSEGASTLTQQVVKDAFLSQWKSIGRK
100
                        *****

database      AQEAYLSYRLEQEYSKDDIFQVYLNKIYYSDGVTGIKAAAKYYFNKDLKD
143
GT_pET24d_H162W_5_T7PROM  AQEAYLSYRLEQEYSKDDIFQVYLNKIYYSDGVTGIKAAAKYYFNKDLKD
150
                        *****

database      LNLAEAYLAGLPQVPNNYNIYDHP  168
GT_pET24d_H162W_5_T7PROM  LNLAEAYLAGLPQVPNNYNIYDHP  175
                        *****

```

Fig. B2 Sequencing result of **H162W**

```

database      MHHHHHHKIIDKNGELVKTLDNQQRHEHVNLDVPSMKDAVLATEDNRFYEHGALDYKR 60
D199W_2      MHHHHHHKIIDKNGELVKTLDNQQRHEHVNLDVPSMKDAVLATEDNRFYEHGALDYKR 60
              *****

database      LFGAIGKNLTGGFGSEGASTLTQQVVKDAFLSQHKSIGRKAQEAYLSYRLEQEYSKDDIF 120
D199W_2      LFGAIGKNLTGGFGSEGASTLTQQVVKDAFLSQHKSIGRKAQEAYLSYRLEQEYSKDDIF 120
              *****

database      QVYLNKIYYSDGVTGIKAAAKYYFNKDLKDLNLAE EAYLAGLPQVPNNYNIYDHP 175
D199W_2      QVYLNKIYYSWGVTGIKAAAKYYFNKDLKDLNLAE EAYLAGLPQVPNNYNIYDHP 175
              *****

```

Fig. B3 Sequencing result of **D199W**


```

database      MHHHHHHKIIDKNGELVKTLDNQQRHEHVNLDVPSMKDAVLATEDNRFYEHGALDYKR  60.
Y210W_4      MHHHHHHKIIDKNGELVKTLDNQQRHEHVNLDVPSMKDAVLATEDNRFYEHGALDYKR  60.
              *****

database      LFGAIGKNLTGGFGSEGASTLTQQVVKDAFLSQHKSIGRKAQEAYLSYRLEQEYSKDDIF 120.
Y210W_4      LFGAIGKNLTGGFGSEGASTLTQQVVKDAFLSQHKSIGRKAQEAYLSYRLEQEYSKDDIF 120.
              *****

database      QVYLNKIYYSDGVTGIKAAAKYFYNKDLKDLNLAE EAYLAGLPQVPNNYNIYDHP  175.
Y210W_4      QVYLNKIYYSDGVTGIKAAAKWFYNKDLKDLNLAE EAYLAGLPQVPNNYNIYDHP  175.
              *****:*****

```

Fig. B4 Sequencing result of **Y210W**

```

database      MHHHHHHHKIYDKNGELVKTLDNGQRHEHVNLDVPSMKDAVLATEDNRFYEHGALDYKR 60
D241W_1      MHHH|HHHKIYDKNGELVKTLDNGQRHEHVNLDVPSMKDAVLATEDNRFYEHGALDYKR 60
              *****
↵
database      LFGAIGKNLTGGFGSEGASTLTQQVVKDAFLSQHKSIGRKAQEAYLSYRLEQEYSKDDIF 120
D241W_1      LFGAIGKNLTGGFGSEGASTLTQQVVKDAFLSQHKSIGRKAQEAYLSYRLEQEYSKDDIF 120
              *****
↵
database      QVYLNKIYYSDGVTGIKAAAKYYFNKDLKDLNLAEEAYLAGLPQVPNNYNIYDHP 175
D241W_1      QVYLNKIYYSDGVTGIKAAAKYYFNKDLKDLNLAEEAYLAGLPQVPNNYNIYWHP 175
              *****

```

Fig. B5 Sequencing result of **D241W**

Appendix III

FPLC chromatograms and SDS PAGE gel photo of GT mutants

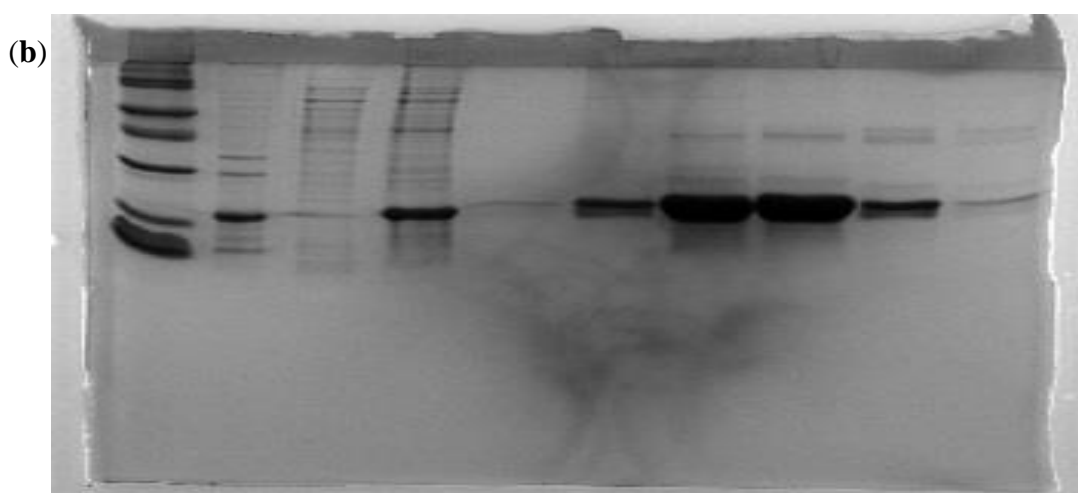
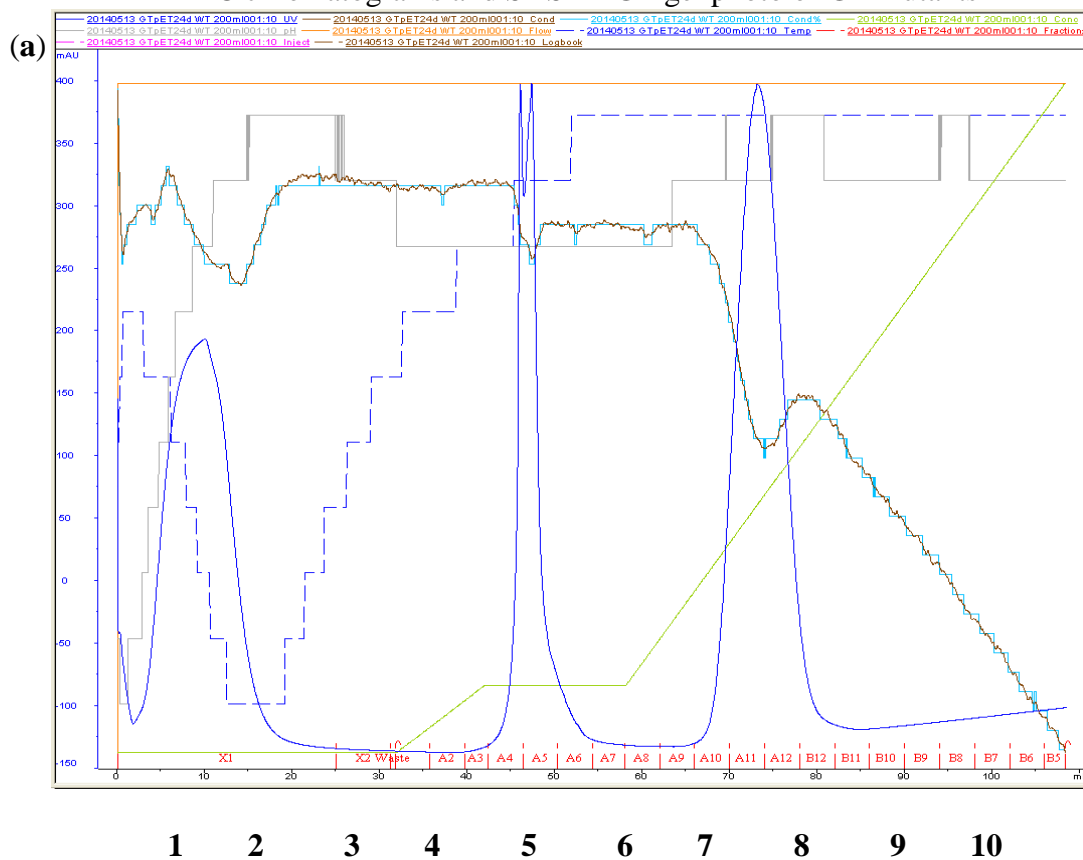


Fig. C1(a) FPLC chromatogram of GT-WT in plasmid PGT-pRSETk obtained from

200 ml culture and (b) SDS-PAGE gel photo of GT-WT in plasmid PGT-pRSETk

Note: lane 1: Low range molecular marker: Phosphorylase b (97.4 kDa), Serum albumin (66.2 kDa), Ovalbumin (45 kDa), Carbonic anhydrase (31 kDa), Trypsin inhibitor (21.5 kDa), Lysozyme (14.4 kDa); Lane 2: supernatant after adding fos-choline-14; Lane 3: supernatant before adding fos-choline-14; Lane 4: cell pellet after adding fos-choline-14; Lane 5-10: 15ul of fractions A9-B11.

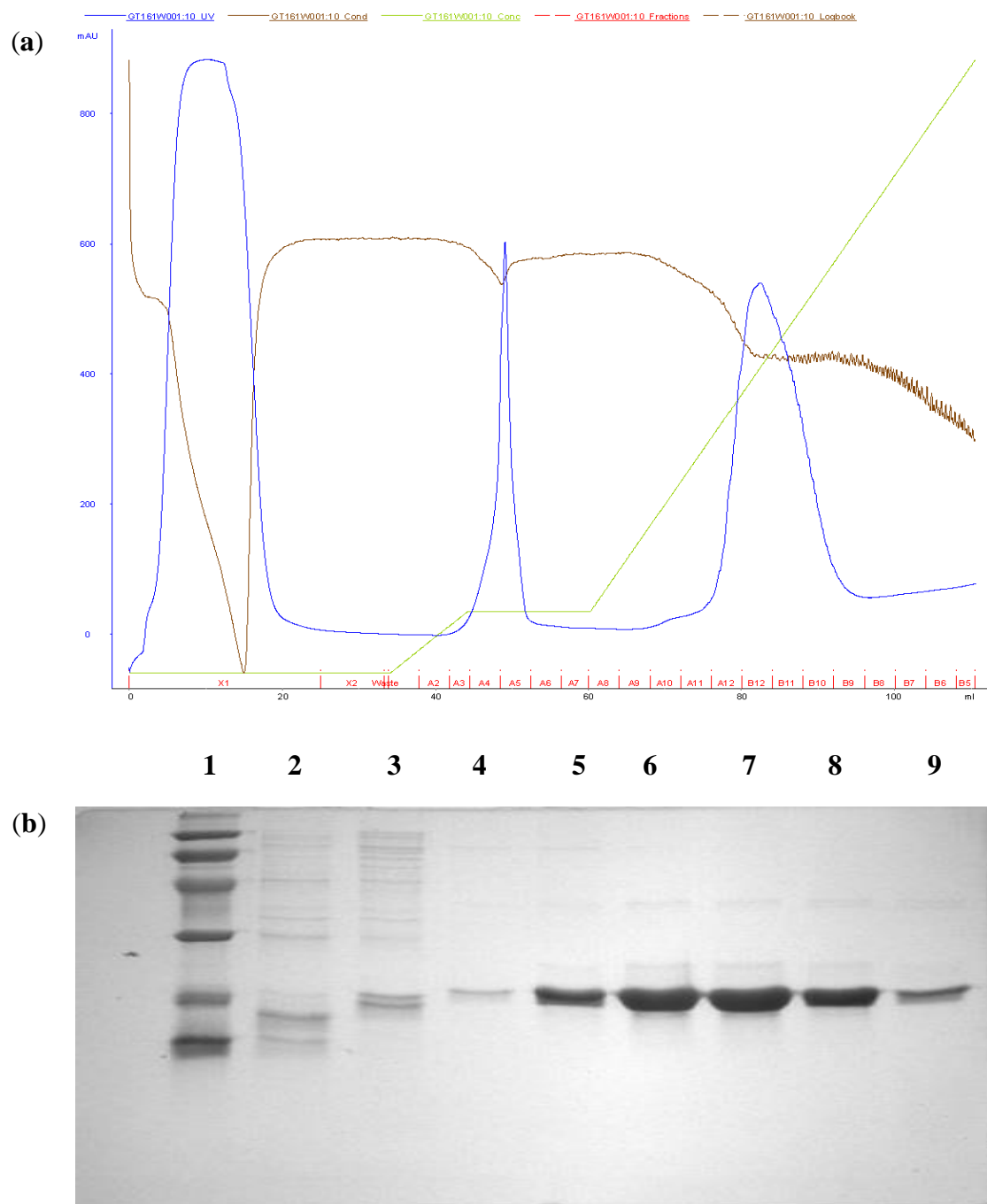


Fig. C2 **(a)** FPLC chromatogram of Q161W in plasmid PGT-pRSETk obtained from 200 ml culture and **(b)** SDS-PAGE gel photo of Q161W in plasmid PGT-pRSETk

Note: lane 1: Low range molecular marker: Phosphorylase b (97.4 kDa), Serum albumin (66.2 kDa), Ovalbumin (45 kDa), Carbonic anhydrase (31 kDa), Trypsin inhibitor (21.5 kDa), Lysozyme (14.4 kDa); Lane 2: X1; Lane 3: A4; Lane 4-9: 15ul of fractions A11-B9.

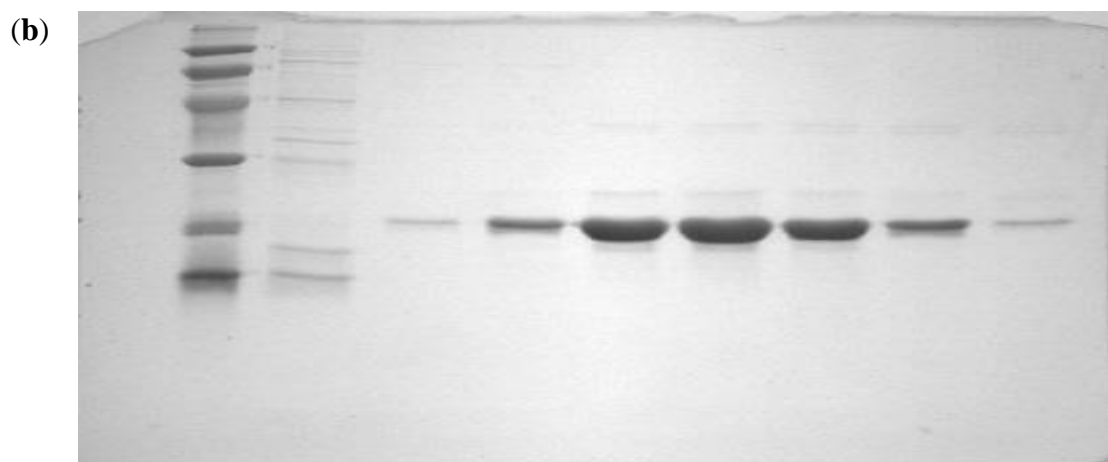
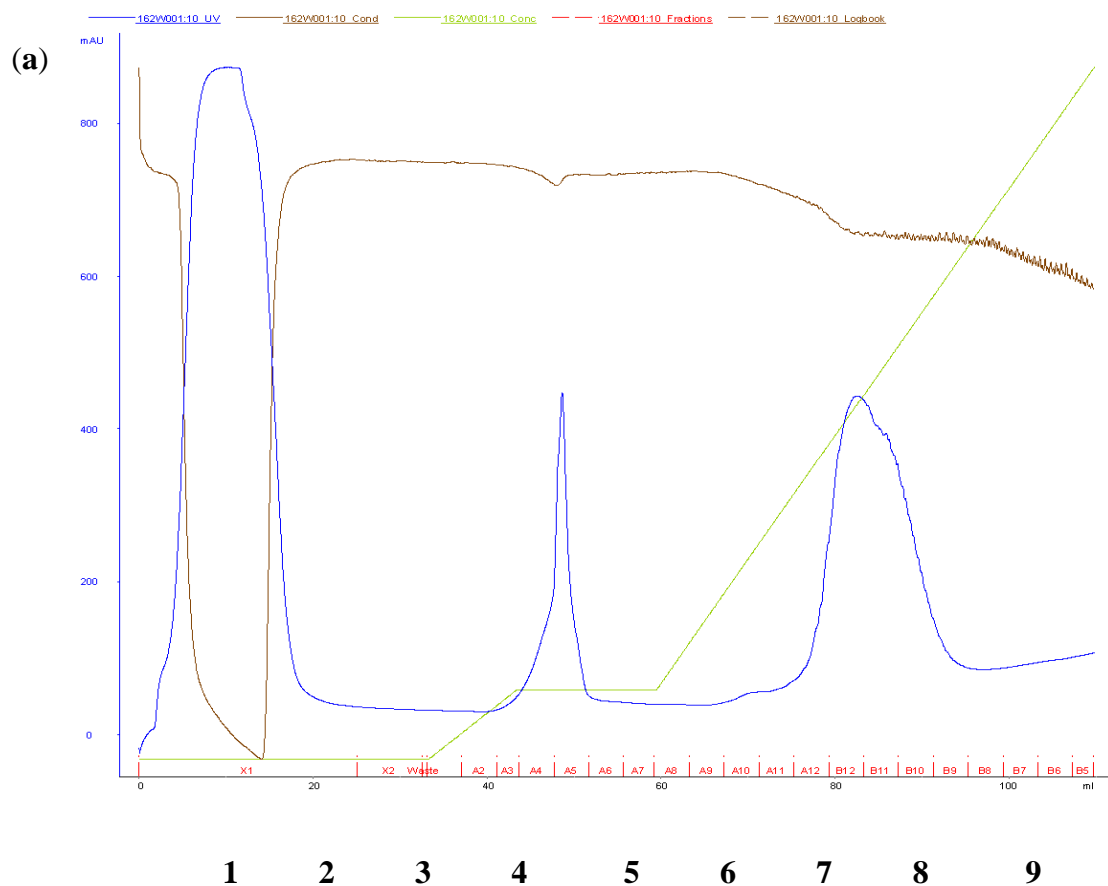


Fig. C3 **(a)** FPLC chromatogram of H162W in plasmid pET-24d obtained from 200 ml culture and **(b)** SDS-PAGE gel photo of H162W in plasmid PGT-pRSETk

Note: lane 1: Low range molecular marker: Phosphorylase b (97.4 kDa), Serum albumin (66.2 kDa), Ovalbumin (45 kDa), Carbonic anhydrase (31 kDa), Trypsin inhibitor (21.5 kDa), Lysozyme (14.4 kDa); Lane 2: X1; Lane 3-9: 15ul of fractions A11-B8.

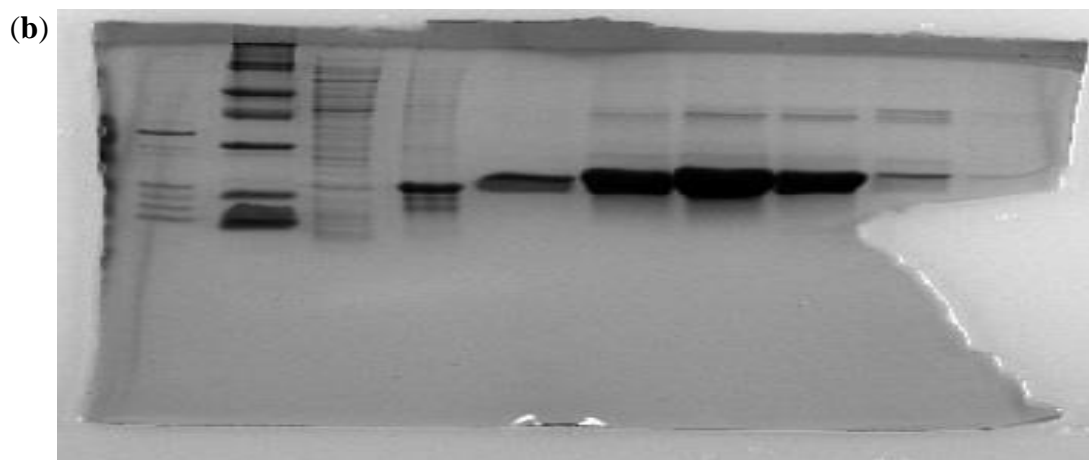
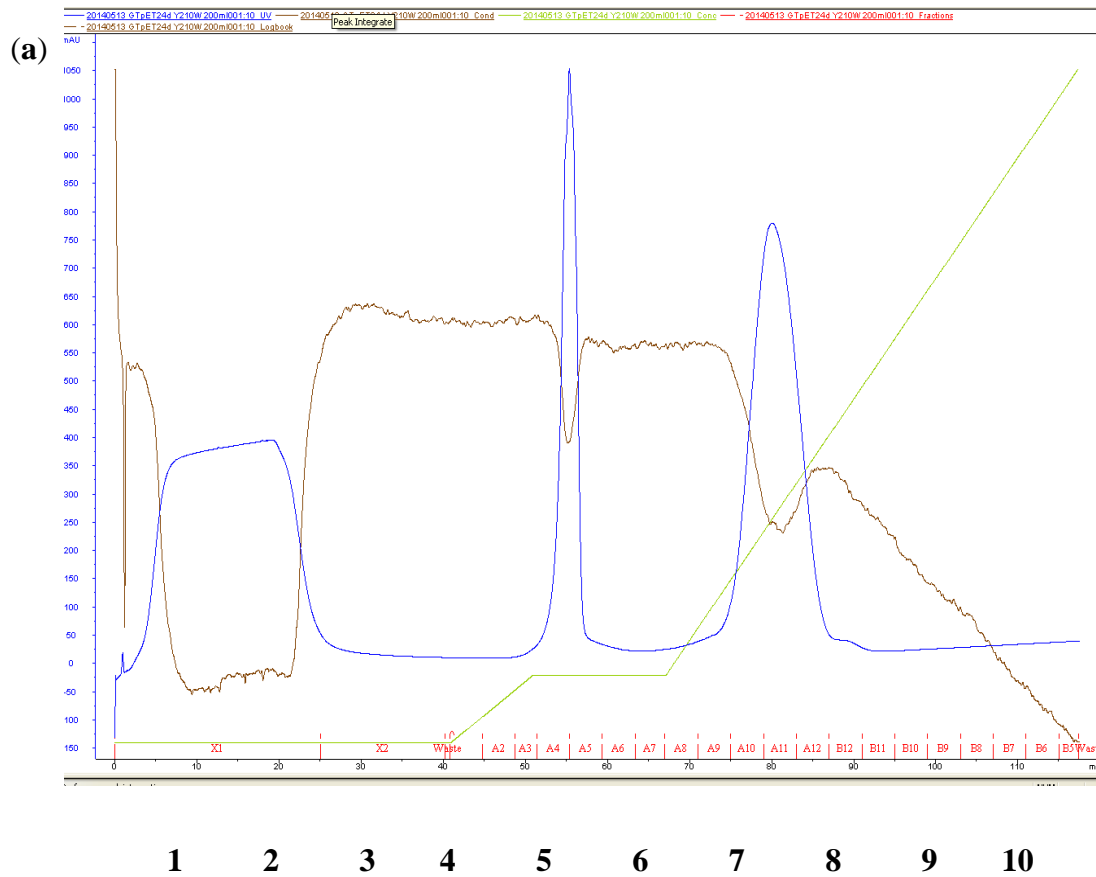


Fig. C5 (a) FPLC chromatogram of Y210W in plasmid pRSETK obtained from 200 ml culture and (b) SDS-PAGE gel photo of Y210W in plasmid PGT-pRSETk

Note: Lane 1: cell pellet after adding fos-choline-14; Lane 2: Low range molecular marker: Phosphorylase b (97.4 kDa), Serum albumin (66.2 kDa), Ovalbumin (45 kDa), Carbonic anhydrase (31 kDa), Trypsin inhibitor (21.5 kDa), Lysozyme (14.4 kDa); Lane 3: supernatant before adding fos-choline-14; Lane 4: supernatant after adding fos-choline-14; Lane 5-10: 15ul of fractions A9-B11.

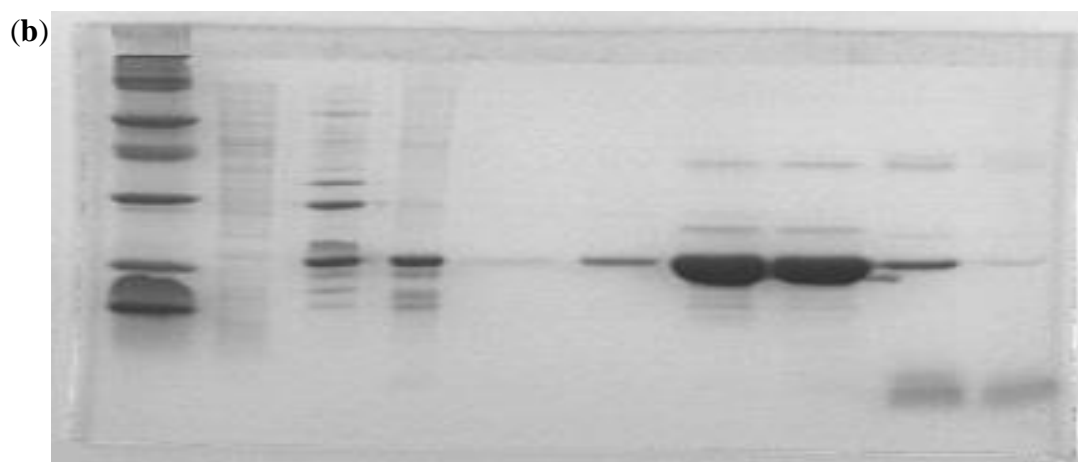
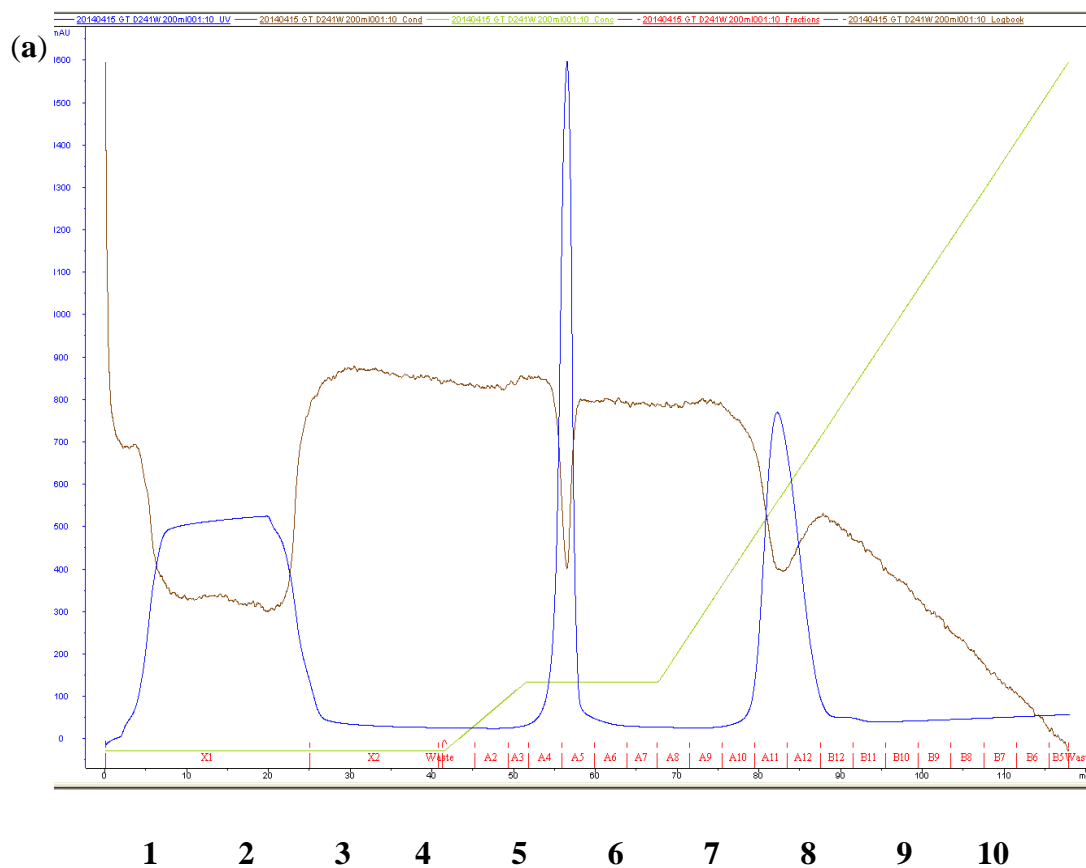


Fig. C6 (a) FPLC chromatogram of D241W in plasmid pRSETK obtained from 200 ml culture and (b) SDS-PAGE gel photo of D241W in plasmid PGT-pRSETk

Note: lane 1: Low range molecular marker: Phosphorylase b (97.4 kDa), Serum albumin (66.2 kDa), Ovalbumin (45 kDa), Carbonic anhydrase (31 kDa), Trypsin inhibitor (21.5 kDa), Lysozyme (14.4 kDa); Lane 2: supernatant before adding fos-choline-14; Lane 3: cell pellet after adding fos-choline-14; Lane 4: supernatant after adding fos-choline-14; Lane 5-10: 15ul of fractions A9-B11

Appendix IV
ESI-MS spectra of PGT proteins

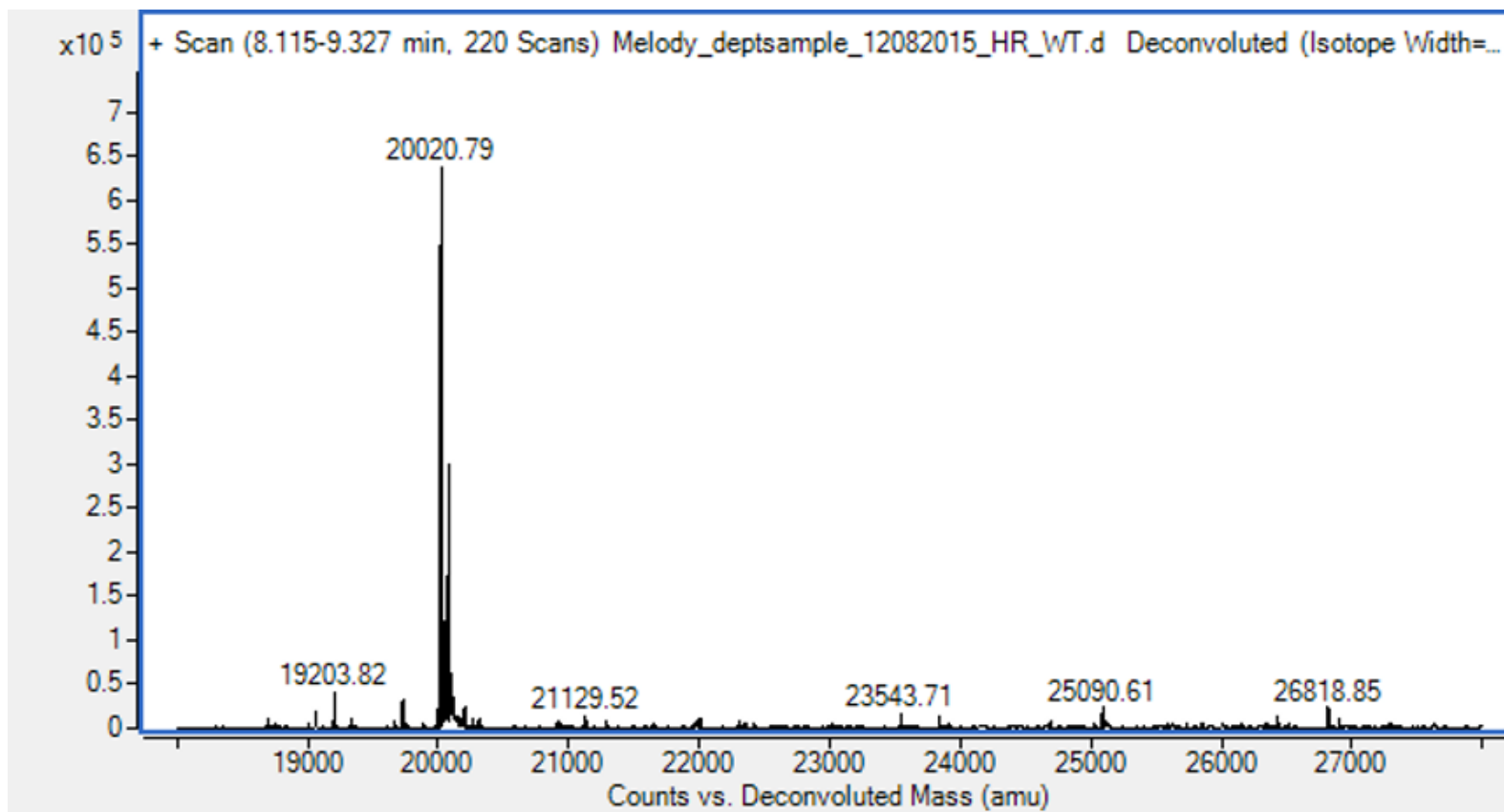


Fig. D1 ESI-MS spectrum of GT-WT

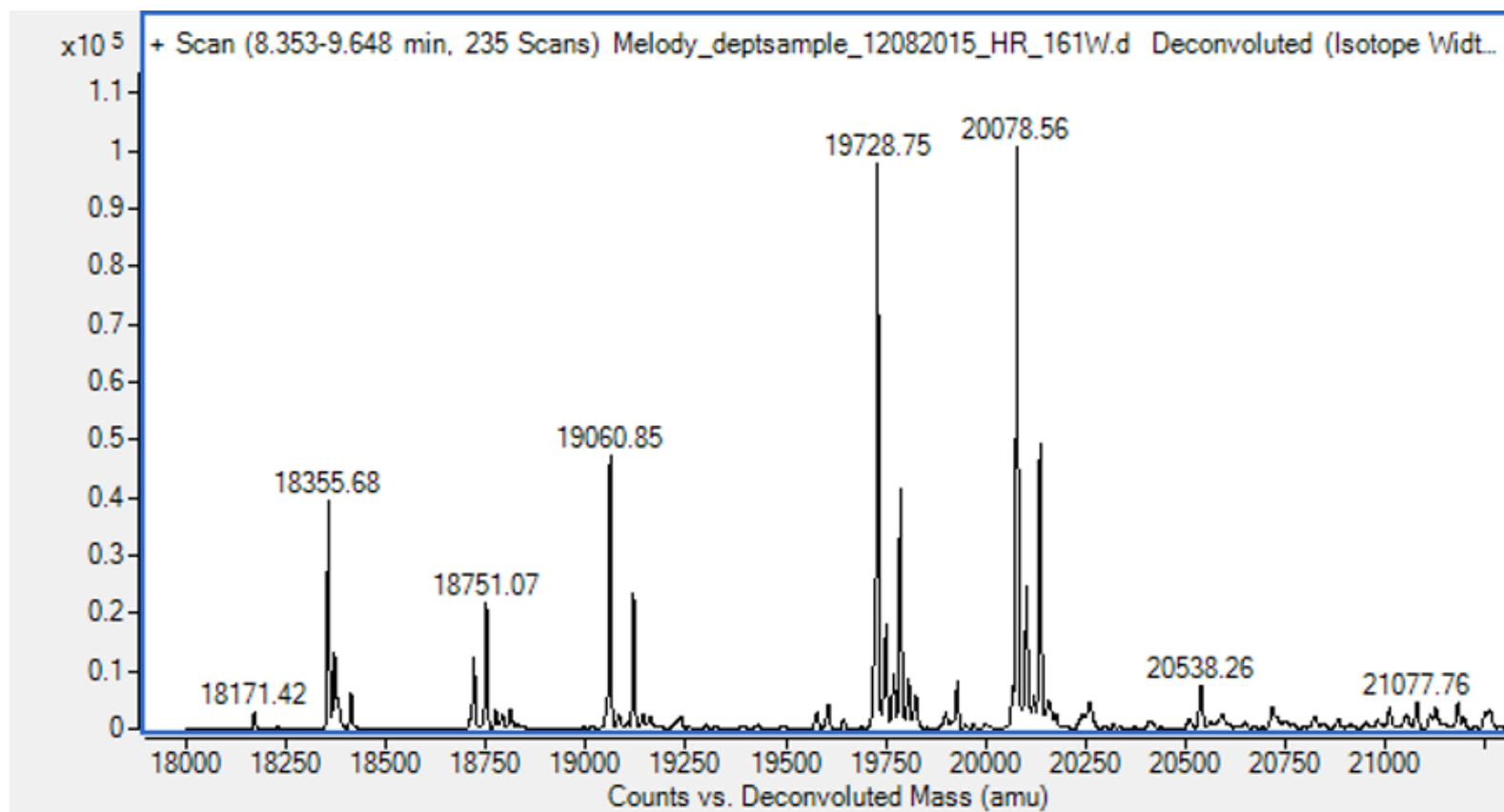


Fig. D2 ESI-MS spectrum of GT-Q161W

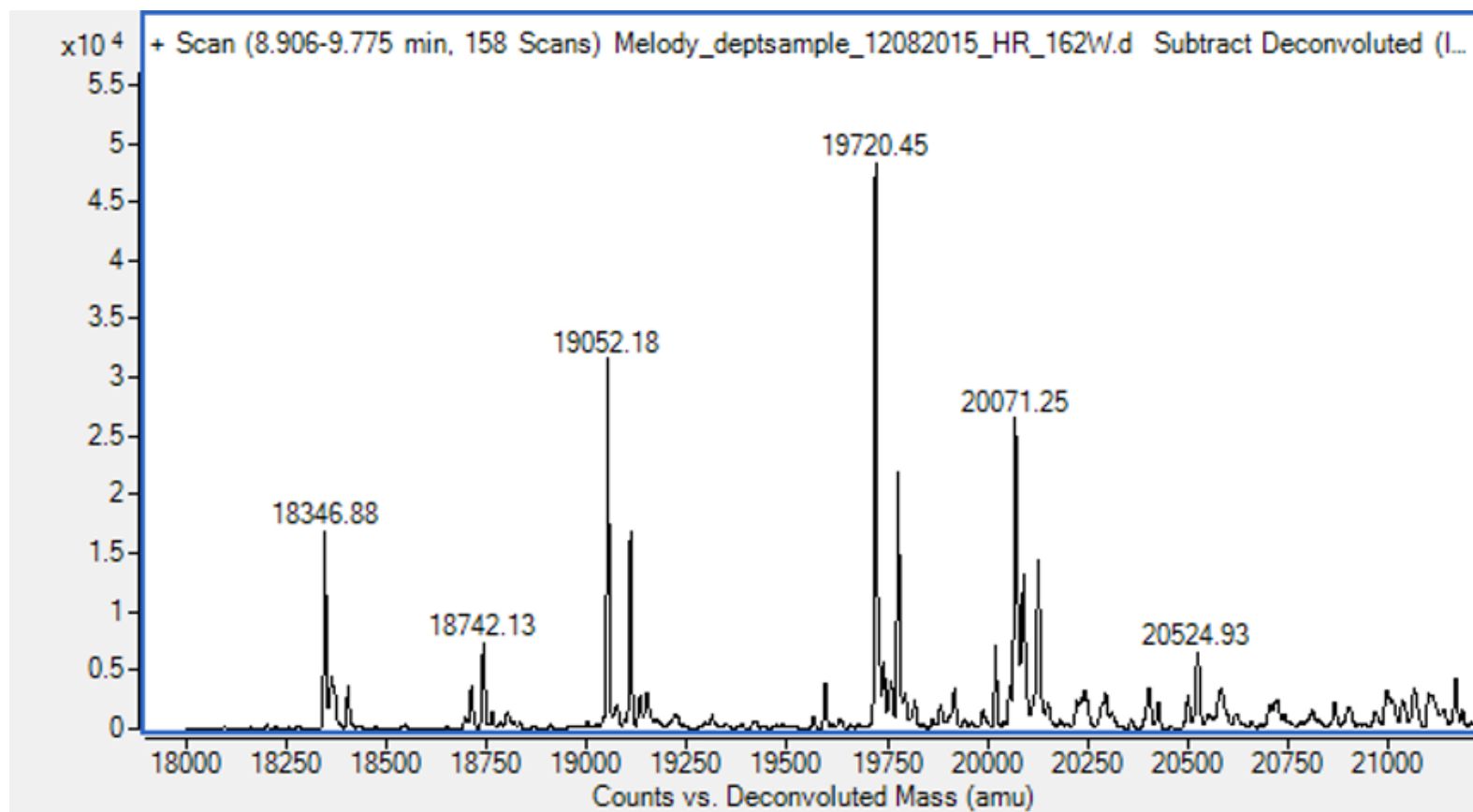


Fig. D3 ESI-MS spectrum of GT-H162W

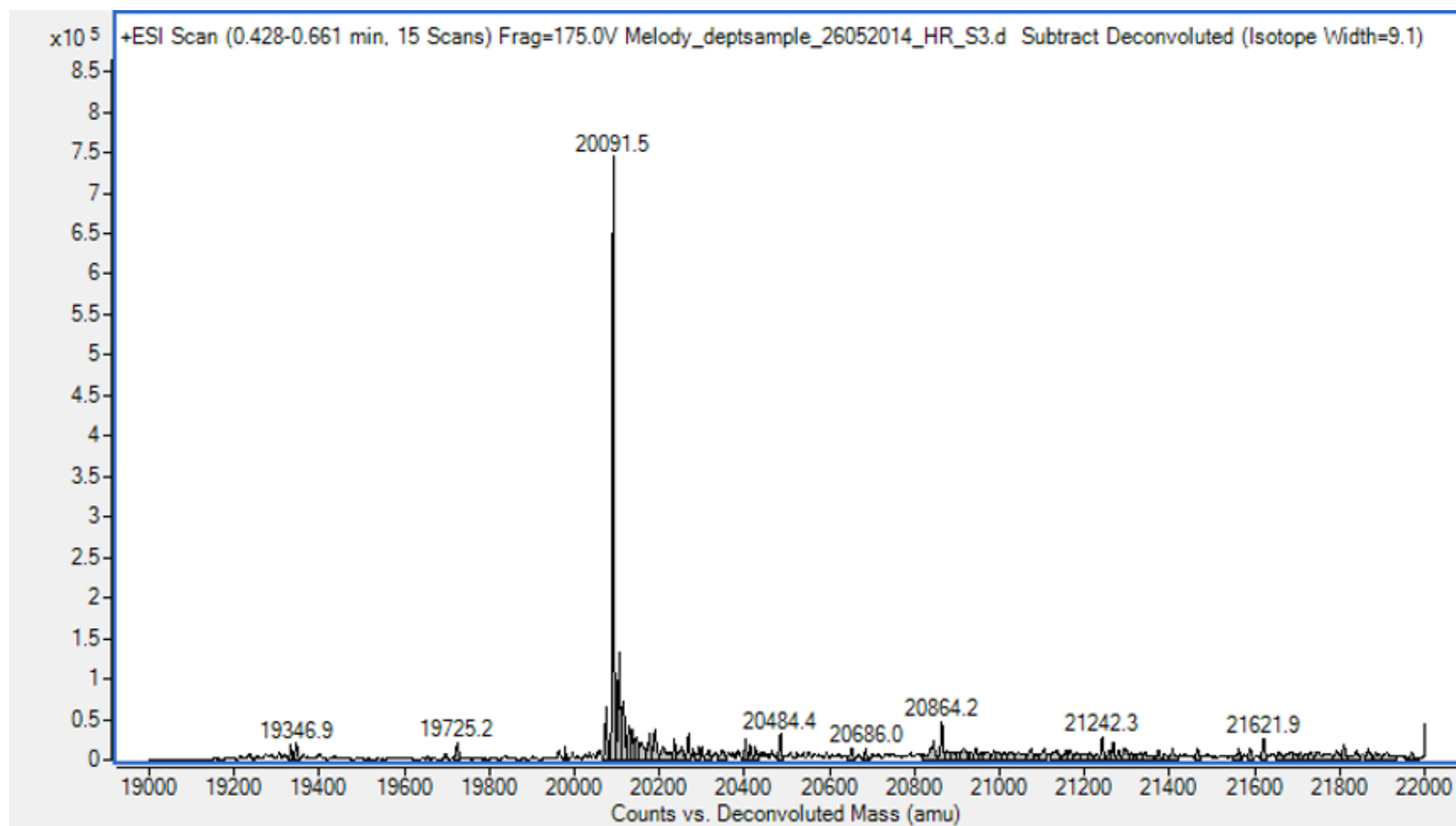


Fig. D4 ESI-MS spectrum of GT-199W

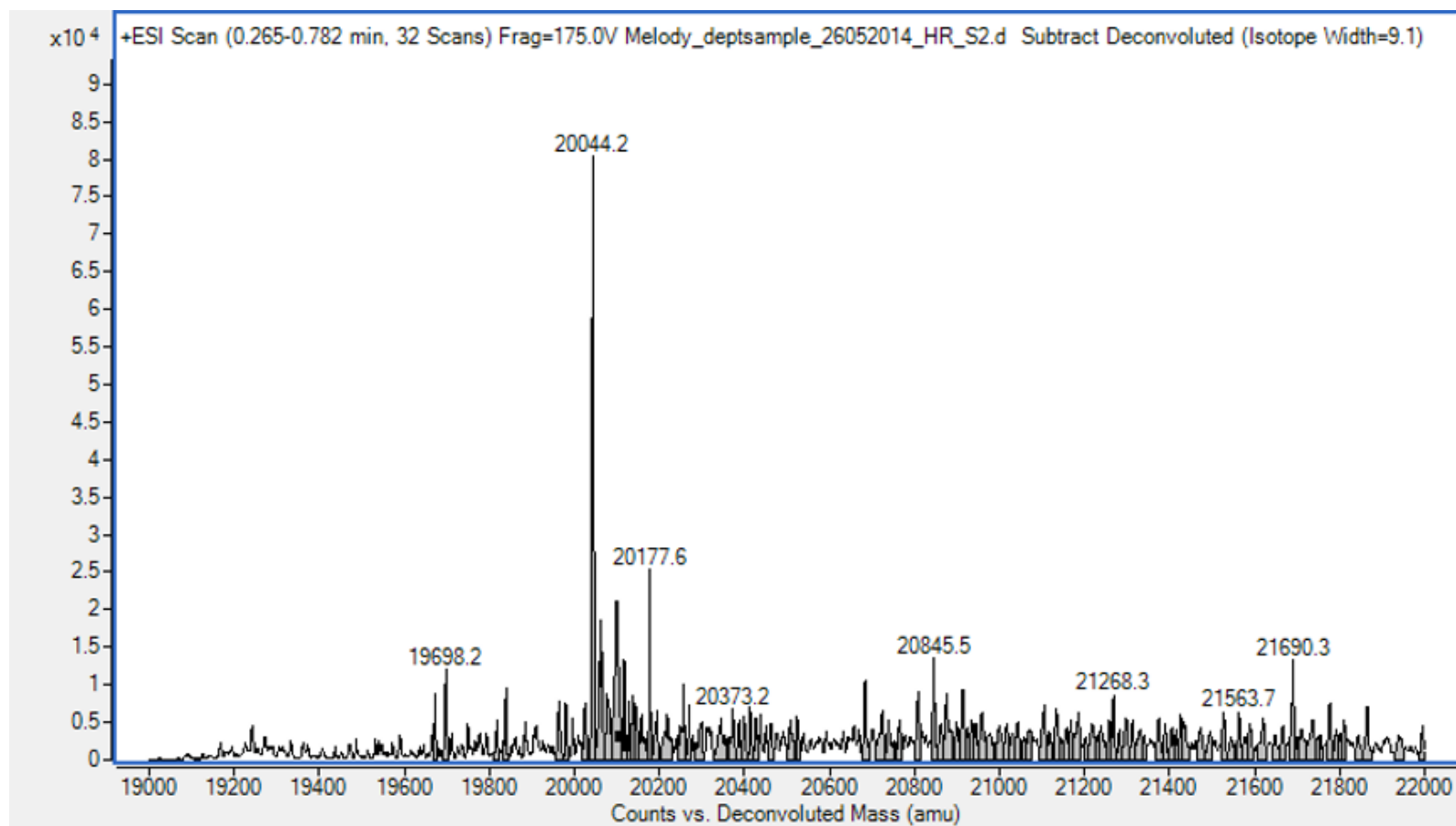


Fig. D5 ESI-MS spectrum of GT-Y210W

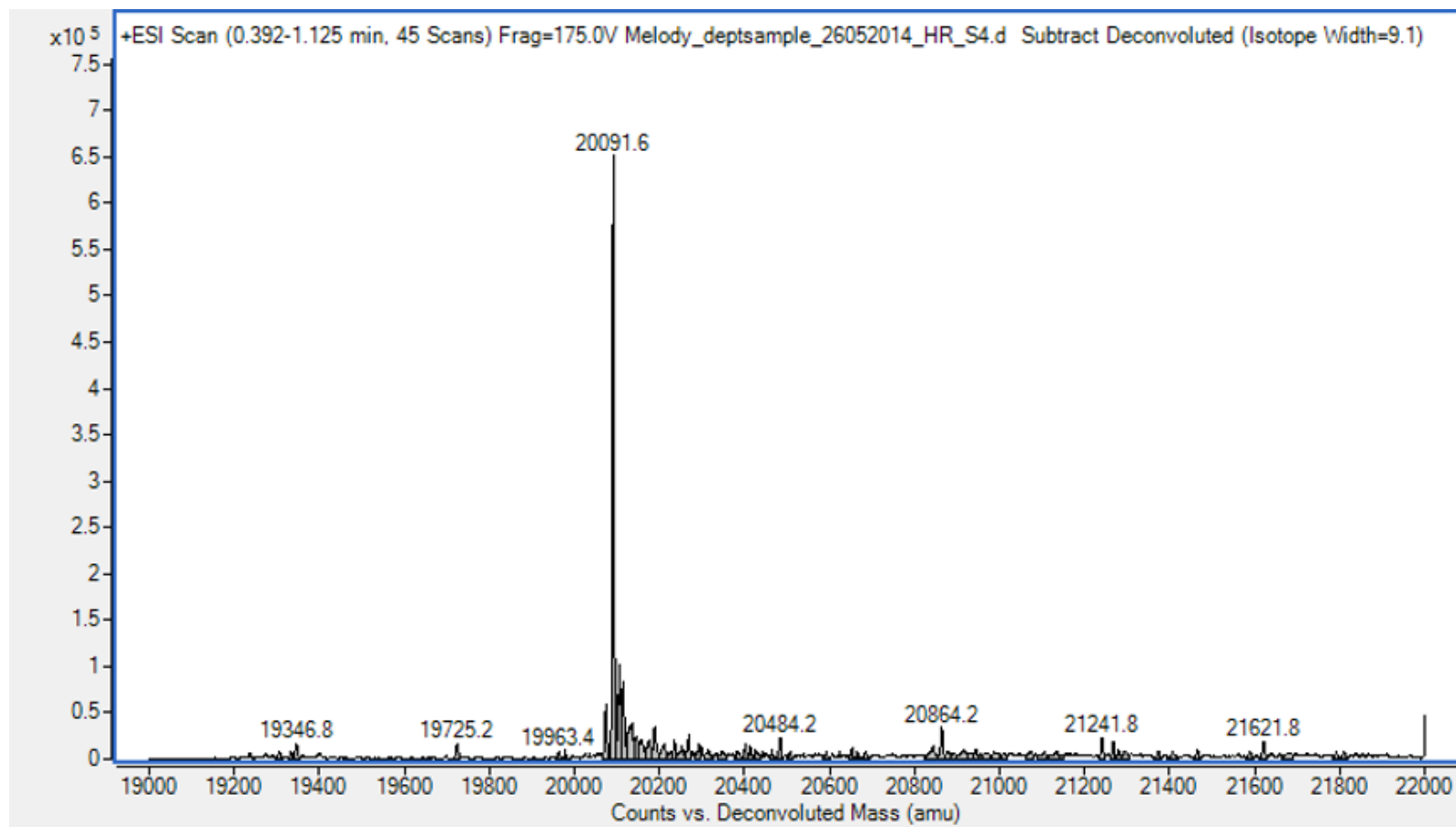


Fig. D6 ESI-MS spectrum of GT-D241W

References

- [1] Wainwright M. The mystery of the plate: Fleming's discovery and contribution to the early development of penicillin. *Journal of Medical Biography*. 1993;1:59-65.
- [2] Butler MS, Blaskovich MA, Cooper MA. Antibiotics in the clinical pipeline in 2013. *Journal of Antibiotics*. 2013;66:571-91.
- [3] Blair JM, Webber MA, Baylay AJ, Ogbolu DO, Piddock LJ. Molecular mechanisms of antibiotic resistance. *Nature Reviews Microbiology*. 2015;13:42-51.
- [4] Tamber S, Hancock R. On the mechanism of solute uptake in *Pseudomonas*. *Frontiers in Bioscience: a journal and virtual library*. 2003;8:s472-83.
- [5] Morita Y, Tomida J, Kawamura Y. MexXY multidrug efflux system of *Pseudomonas aeruginosa*. *Front Microbiol*. 2012;3:408.
- [6] Billal DS, Feng J, Leprohon P, Legare D, Ouellette M. Whole genome analysis of linezolid resistance in *Streptococcus pneumoniae* reveals resistance and compensatory mutations. *BMC Genomics*. 2011;12:512.
- [7] Kumar N, Radhakrishnan A, Wright CC, Chou TH, Lei HT, Bolla JR, et al. Crystal structure of the transcriptional regulator Rv1219c of *Mycobacterium tuberculosis*. *Protein Science*. 2014;23:423-32.
- [8] Livermore D. Defining an extended - spectrum β - lactamase. *Clinical Microbiology and Infection*. 2008;14:3-10.
- [9] Fuda C, Suvorov M, Vakulenko SB, Mobashery S. The basis for resistance to β -lactam antibiotics by penicillin-binding protein 2a of methicillin-resistant

Staphylococcus aureus. *Journal of Biological Chemistry*. 2004;279:40802-6.

[10] Lim D, Strynadka NC. Structural basis for the β lactam resistance of PBP2a from methicillin-resistant *Staphylococcus aureus*. *Nature Structural & Molecular Biology*. 2002;9:870-6.

[11] Laxminarayan R, Duse A, Wattal C, Zaidi AK, Wertheim HF, Sumpradit N, et al. Antibiotic resistance—the need for global solutions. *The Lancet Infectious Diseases*. 2013;13:1057-98.

[12] Holmes KK, Johnson DW, Floyd TM. Studies of Venereal Disease: I. Probenecid-Procaïne Penicillin G Combination and Tetracycline Hydrochloride in the Treatment of Penicillin-Resistant Gonorrhea in Men. *JAMA*. 1967;202:461-6.

[13] Rasnake MS, Conger NG, McAllister CK, Holmes KK, Tramont EC. History of US military contributions to the study of sexually transmitted diseases. *Military Medicine*. 2005;170:61-5.

[14] Global spread of carbapenemase-producing Enterobacteriaceae. CDC, 2011.

[15] Appelbaum PC. 2012 and beyond: potential for the start of a second pre-antibiotic era? *Journal of Antimicrobial Chemotherapy*. 2012:213.

[16] Health UDo, Services H. Antibiotic resistance threats in the United States, 2013. Centers for Disease Control and Prevention, 2013.

[17] Spellberg B, Guidos R, Gilbert D, Bradley J, Boucher HW, Scheld WM, et al. The epidemic of antibiotic-resistant infections: a call to action for the medical community from the Infectious Diseases Society of America. *Clinical Infectious Diseases*. 2008;46:155-64.

- [18] Spellberg B, Lipsky BA. Systemic antibiotic therapy for chronic osteomyelitis in adults. *Clinical Infectious Diseases*. 2011;842.
- [19] Fischbach MA, Walsh CT. Antibiotics for emerging pathogens. *Science*. 2009;325:1089-93.
- [20] Klevens RM, Morrison MA, Nadle J, Petit S, Gershman K, Ray S, et al. Invasive methicillin-resistant *Staphylococcus aureus* infections in the United States. *JAMA*. 2007;298:1763-71.
- [21] Talbot GH, Bradley J, Edwards JE, Gilbert D, Scheld M, Bartlett JG. Bad bugs need drugs: an update on the development pipeline from the Antimicrobial Availability Task Force of the Infectious Diseases Society of America. *Clinical Infectious Diseases*. 2006;42:657-68.
- [22] Chang S, Sievert DM, Hageman JC, Boulton ML, Tenover FC, Downes FP, et al. Infection with vancomycin-resistant *Staphylococcus aureus* containing the vanA resistance gene. *New England Journal of Medicine*. 2003;348:1342-7.
- [23] Fair RJ, Tor Y. Antibiotics and bacterial resistance in the 21st century. *Perspectives in Medicinal Chemistry*. 2014;6:25.
- [24] Antibiotic resistance threats in the United States, CDC, 2013.
- [25] Walsh C. Antibiotics; actions, origins, resistance. 2003.
- [26] Bugg T, Walsh C. Intracellular steps of bacterial cell wall peptidoglycan biosynthesis: enzymology, antibiotics, and antibiotic resistance. *Natural Product Reports*. 1992;9:199-215.
- [27] Foster SJ, Popham DL. Structure and synthesis of cell wall, spore cortex, teichoic

acids, S-layers, and capsules. *Bacillus subtilis* and its closest relatives: from genes to cells American Society for Microbiology. 2002:21-41.

[28] Rogers H, Perkins H, Ward J. Microbial Cell Walls and Membranes. *FEBS LETTERS*. 1981.

[29] Van Heijenoort J. Assembly of the monomer unit of bacterial peptidoglycan. *Cellular and Molecular Life Sciences CMLS*. 1998;54:300-4.

[30] Ghuysen J, Hakenbeck R. Biosynthesis of the bacterial peptidoglycan unit. *Bacterial Cell Wall*. 1994:39.

[31] Bugg TD, Braddick D, Dowson CG, Roper DI. Bacterial cell wall assembly: still an attractive antibacterial target. *Trends in Biotechnology*. 2011;29:167-73.

[32] Scheffers D-J, Pinho MG. Bacterial cell wall synthesis: new insights from localization studies. *Microbiology and Molecular Biology Reviews*. 2005;69:585-607.

[33] Ghuysen J-M. Serine beta-lactamases and penicillin-binding proteins. *Annual Reviews in Microbiology*. 1991;45:37-67.

[34] Höltje J-V. Growth of the stress-bearing and shape-maintaining murein sacculus of *Escherichia coli*. *Microbiology and Molecular Biology Reviews*. 1998;62:181-203.

[35] Den Blaauwen T, De Pedro MA, Nguyen-Distèche M, Ayala JA. Morphogenesis of rod-shaped sacculi. *FEMS Microbiology Reviews*. 2008;32:321-44.

[36] Zapun A, Vernet T, Pinho MG. The different shapes of cocci. *FEMS Microbiology Reviews*. 2008;32:345-60.

[37] Massova I, Mobashery S. Kinship and diversification of bacterial penicillin-binding proteins and β -lactamases. *Antimicrobial Agents and Chemotherapy*.

1998;42:1-17.

[38] Pereira S, Henriques A, Pinho M, De Lencastre H, Tomasz A. Role of PBP1 in cell division of *Staphylococcus aureus*. *Journal of Bacteriology*. 2007;189:3525-31.

[39] Pinho MG, de Lencastre H, Tomasz A. An acquired and a native penicillin-binding protein cooperate in building the cell wall of drug-resistant staphylococci. *Proceedings of the National Academy of Sciences*. 2001;98:10886-91.

[40] Navratna V, Nadig S, Sood V, Prasad K, Arakere G, Gopal B. Molecular basis for the role of *Staphylococcus aureus* penicillin binding protein 4 in antimicrobial resistance. *Journal of Bacteriology*. 2010;192:134-44.

[41] Suzuki H, Nishimura Y, Hirota Y. On the process of cellular division in *Escherichia coli*: a series of mutants of *E. coli* altered in the penicillin-binding proteins. *Proceedings of the National Academy of Sciences*. 1978;75:664-8.

[42] Denome SA, Elf PK, Henderson TA, Nelson DE, Young KD. *Escherichia coli* mutants lacking all possible combinations of eight penicillin binding proteins: viability, characteristics, and implications for peptidoglycan synthesis. *Journal of Bacteriology*. 1999;181:3981-93.

[43] Meberg BM, Sailer FC, Nelson DE, Young KD. Reconstruction of *Escherichia coli* *mrcA* (PBP 1a) mutants lacking multiple combinations of penicillin binding proteins. *Journal of Bacteriology*. 2001;183:6148-9.

[44] Wright GD. Biochemistry. A new target for antibiotic development. *Science*. 2007;315:1373.

[45] Halliday J, McKeveney D, Muldoon C, Rajaratnam P, Meutermans W. Targeting

- the forgotten transglycosylases. *Biochemical Pharmacology*. 2006;71:957-67.
- [46] Ostash B, Walker S. Bacterial transglycosylase inhibitors. *Current Opinion in Chemical Biology*. 2005;9:459-66.
- [47] Lovering AL, De Castro LH, Lim D, Strynadka NC. Structural insight into the transglycosylation step of bacterial cell-wall biosynthesis. *Science*. 2007;315:1402-5.
- [48] Yuan Y, Barrett D, Zhang Y, Kahne D, Sliz P, Walker S. Crystal structure of a peptidoglycan glycosyltransferase suggests a model for processive glycan chain synthesis. *Proceedings of the National Academy of Sciences*. 2007;104:5348-53.
- [49] Sung MT, Lai YT, Huang CY, Chou LY, Shih HW, Cheng WC, et al. Crystal structure of the membrane-bound bifunctional transglycosylase PBP1b from *Escherichia coli*. *Proceedings of the National Academy of Sciences of the United States of America*. 2009;106:8824-9.
- [50] Lovering AL, Gretes M, Strynadka NC. Structural details of the glycosyltransferase step of peptidoglycan assembly. *Current Opinion in Structural Biology*. 2008;18:534-43.
- [51] Huang CY, Shih HW, Lin LY, Tien YW, Cheng TJ, Cheng WC, et al. Crystal structure of *Staphylococcus aureus* transglycosylase in complex with a lipid II analog and elucidation of peptidoglycan synthesis mechanism. *Proceedings of the National Academy of Sciences of the United States of America*. 2012;109:6496-501.
- [52] Huber G, Nesemann G. Moenomycin, an inhibitor of cell wall synthesis. *Biochemical and Biophysical Research Communications*. 1968;30:7-13.
- [53] Huber G, Schacht U, Weidenmüller H, Schmidt-Thomé J, Duphorn J, Tschesche

- R. Meonomycin, a new antibiotic. II. Characterization and chemistry. *Antimicrobial Agents and Chemotherapy*. 1964;5:737-42.
- [54] Wallhausser K, Neemann G, Prave P, Steigler A. Moenomycin, a new antibiotic. I. Fermentation and isolation. *Antimicrobial Agents and Chemotherapy*. 1964;5:734-6.
- [55] Kahne D, Leimkuhler C, Lu W, Walsh C. Glycopeptide and lipoglycopeptide antibiotics. *Chemical Reviews*. 2005;105:425-48.
- [56] Butaye P, Devriese LA, Haesebrouck F. Antimicrobial growth promoters used in animal feed: effects of less well known antibiotics on gram-positive bacteria. *Clinical Microbiology Reviews*. 2003;16:175-88.
- [57] Rebets Y, Lupoli T, Qiao Y, Schirner K, Villet R, Hooper D, et al. Moenomycin resistance mutations in *Staphylococcus aureus* reduce peptidoglycan chain length and cause aberrant cell division. *ACS Chemical Biology*. 2013;9:459-67.
- [58] Huber G. Moenomycin and related phosphorus-containing antibiotics. *Mechanism of Action of Antibacterial Agents*. 1979:135-53.
- [59] Ostash B, Walker S. Moenomycin family antibiotics: chemical synthesis, biosynthesis, and biological activity. *Natural Product Reports*. 2010;27:1594-617.
- [60] Welzel P, Kunisch F, Kruggel F, Stein H, Scherkenbeck J, Hiltmann A, et al. Moenomycin A: minimum structural requirements for biological activity. *Tetrahedron*. 1987;43:585-98.
- [61] Adachi M, Zhang Y, Leimkuhler C, Sun B, LaTour JV, Kahne DE. Degradation and reconstruction of moenomycin A and derivatives: dissecting the function of the isoprenoid chain. *Journal of the American Chemical Society*. 2006;128:14012-3.

- [62] Garneau S, Qiao L, Chen L, Walker S, Vederas JC. Synthesis of mono- and disaccharide analogs of moenomycin and lipid II for inhibition of transglycosylase activity of penicillin-binding protein 1b. *Bioorganic & Medicinal Chemistry*. 2004;12:6473-94.
- [63] Sun B, Chen Z, Eggert US, Shaw SJ, LaTour JV, Kahne D. Hybrid glycopeptide antibiotics. *Journal of the American Chemical Society*. 2001;123:12722-3.
- [64] Lin CK, Chen KT, Hu CM, Yun WY, Cheng WC. Synthesis of 1-C-Glycoside-Linked Lipid II Analogues Toward Bacterial Transglycosylase Inhibition. *Chemistry a European Journal*. 2015;21:7511-9.
- [65] Zuegg J, Muldoon C, Adamson G, McKeveney D, Le Thanh G, Premraj R, et al. Carbohydrate scaffolds as glycosyltransferase inhibitors with in vivo antibacterial activity. *Nature Communications*. 2015;6.
- [66] Shih H-W, Chen K-T, Chen S-K, Huang C-Y, Cheng T-JR, Ma C, et al. Combinatorial approach toward synthesis of small molecule libraries as bacterial transglycosylase inhibitors. *Organic & Biomolecular Chemistry*. 2010;8:2586-93.
- [67] Gampe CM, Tsukamoto H, Doud EH, Walker S, Kahne D. Tuning the moenomycin pharmacophore to enable discovery of bacterial cell wall synthesis inhibitors. *Journal of the American Chemical Society*. 2013;135:3776-9.
- [68] Huang SH, Wu WS, Huang LY, Huang WF, Fu WC, Chen PT, et al. New Continuous Fluorometric Assay for Bacterial Transglycosylase Using Forster Resonance Energy Transfer. *Journal of the American Chemical Society*. 2013;135:17078-89.

- [69] Stembera K, Vogel S, Buchynskyy A, Ayala JA, Welzel P. A Surface Plasmon Resonance Analysis of the Interaction between the Antibiotic Moenomycin A and Penicillin - Binding Protein 1b. *ChemBioChem*. 2002;3:559-65.
- [70] Cheng T-JR, Sung M-T, Liao H-Y, Chang Y-F, Chen C-W, Huang C-Y, et al. Domain requirement of moenomycin binding to bifunctional transglycosylases and development of high-throughput discovery of antibiotics. *Proceedings of the National Academy of Sciences*. 2008;105:431-6.
- [71] Cheng TJ, Sung MT, Liao HY, Chang YF, Chen CW, Huang CY, et al. Domain requirement of moenomycin binding to bifunctional transglycosylases and development of high-throughput discovery of antibiotics. *Proceedings of the National Academy of Sciences of the United States of America*. 2008;105:431-6.
- [72] Cheng TJ, Wu YT, Yang ST, Lo KH, Chen SK, Chen YH, et al. High-throughput identification of antibacterials against methicillin-resistant *Staphylococcus aureus* (MRSA) and the transglycosylase. *Bioorganic & Medicinal Chemistry*. 2010;18:8512-29.
- [73] Bajorath J. Integration of virtual and high-throughput screening. *Nature Reviews Drug Discovery*. 2002;1:882-94.
- [74] Jorgensen WL. The many roles of computation in drug discovery. *Science*. 2004;303:1813-8.
- [75] Wang Y, Chan FY, Sun N, Lui HK, So PK, Yan SC, et al. Structure-based design, synthesis, and biological evaluation of isatin derivatives as potential glycosyltransferase inhibitors. *Chemical Biology & Drug Design*. 2014;84:685-96.

- [76] Sun N, Chan FY, Lu YJ, Neves MA, Lui HK, Wang Y, et al. Rational design of berberine-based FtsZ inhibitors with broad-spectrum antibacterial activity. *PloS One*. 2014;9:97514.
- [77] Chan PH, Liu HB, Chen YW, Chan KC, Tsang CW, Leung YC, et al. Rational design of a novel fluorescent biosensor for beta-lactam antibiotics from a class A beta-lactamase. *Journal of the American Chemical Society*. 2004;126:4074-5.
- [78] Chan PH, So PK, Ma DL, Zhao Y, Lai TS, Chung WH, et al. Fluorophore-labeled beta-lactamase as a biosensor for beta-lactam antibiotics: a study of the biosensing process. *Journal of the American Chemical Society*. 2008;130:6351-61.
- [79] Chow KY. Development of a biosensing system from chloramphenicol acetyltransferase: The Hong Kong Polytechnic University. 2012.
- [80] Gunnlaugsson T, Ali HDP, Glynn M, Kruger PE, Hussey GM, Pfeffer FM, et al. Fluorescent photoinduced electron transfer (PET) sensors for anions; from design to potential application. *Journal of Fluorescence*. 2005;15:287-99.
- [81] Yuan J, Guo W, Yang X, Wang E. Anticancer drug– DNA interactions measured using a photoinduced electron-transfer mechanism based on luminescent quantum dots. *Analytical Chemistry*. 2008;81:362-8.
- [82] Zhang L, Zhu J, Guo S, Li T, Li J, Wang E. Photoinduced electron transfer of DNA/Ag nanoclusters modulated by G-quadruplex/hemin complex for the construction of versatile biosensors. *Journal of the American Chemical Society*. 2013;135:2403-6.
- [83] Lakowicz JR. Principles of fluorescence spectroscopy: *Springer Science & Business Media*; 2013.

- [84] Marcus RA, Sutin N. Electron transfers in chemistry and biology. *Biochimica et Biophysica Acta (BBA)-Reviews on Bioenergetics*. 1985;811:265-322.
- [85] Barbara PF, Meyer TJ, Ratner MA. Contemporary issues in electron transfer research. *The Journal of Physical Chemistry*. 1996;100:13148-68.
- [86] Doose S, Neuweiler H, Sauer M. Fluorescence quenching by photoinduced electron transfer: a reporter for conformational dynamics of macromolecules. *ChemPhysChem*. 2009;10:1389-98.
- [87] Bixon M, Jortner J. Electron transfer—from isolated molecules to biomolecules: Wiley Online Library. 2007.
- [88] Adams DM, Brus L, Chidsey CE, Creager S, Creutz C, Kagan CR, et al. Charge transfer on the nanoscale: current status. *The Journal of Physical Chemistry B*. 2003;107:6668-97.
- [89] Chen H, Ahsan SS, Santiago-Berrios MEB, Abruña HD, Webb WW. Mechanisms of quenching of Alexa fluorophores by natural amino acids. *Journal of the American Chemical Society*. 2010;132:7244-5.
- [90] Lapidus LJ, Steinbach PJ, Eaton WA, Szabo A, Hofrichter J. Effects of chain stiffness on the dynamics of loop formation in polypeptides. Appendix: Testing a 1-dimensional diffusion model for peptide dynamics. *The Journal of Physical Chemistry B*. 2002;106:11628-40.
- [91] Marmé N, Knemeyer JP, Wolfrum J, Sauer M. Highly sensitive protease assay using fluorescence quenching of peptide probes based on photoinduced electron transfer. *Angewandte Chemie International Edition*. 2004;43:3798-801.

- [92] Zhang K, Wang K, Zhu X, Gao Y, Xie M. Rational design of signal-on biosensors by using photoinduced electron transfer between Ag nanoclusters and split G-quadruplex halves–hemin complexes. *Chemical Communications*. 2014;50:14221-4.
- [93] Bury D, Dahmane I, Derouaux A, Dumbre S, Herdewijn P, Matagne A, et al. Positive cooperativity between acceptor and donor sites of the peptidoglycan glycosyltransferase. *Biochemical Pharmacology*. 2015;93:141-50.
- [94] Buchynskyy A, Stembera K, Hennig L, Findeisen M, Giesa S, Welzel P. A Method for the Introduction of Reporter Groups into Moenomycin A, Based on Thiouronium Salt Chemistry. *European Journal of Organic Chemistry*. 2002;2002:1163-74.
- [95] Buchynskyy A, Kempin U, Vogel S, Hennig L, Findeisen M, Müller D, et al. Synthesis of Fluorescent Derivatives of the Antibiotic Moenomycin A. *European Journal of Organic Chemistry*. 2002;2002:1149-62.
- [96] Klonis N, Sawyer WH. Spectral properties of the prototropic forms of fluorescein in aqueous solution. *Journal of Fluorescence*. 1996;6:147-57.
- [97] Shi GH, Shang ZB, Wang Y, Jin WJ, Zhang TC. Fluorescence quenching of CdSe quantum dots by nitroaromatic explosives and their relative compounds. *Spectrochimica Acta Part A: Molecular and Biomolecular Spectroscopy*. 2008;70:247-52.
- [98] Beddard G, Carlin S, Harris L, Porter G, Tredwell C. Quenching of chlorophyll fluorescence by Nitrobenzene. *Photochemistry and Photobiology*. 1978;27:433-8.
- [99] Zhang XF, Zhang J, Liu L. Fluorescence properties of twenty fluorescein derivatives: lifetime, quantum yield, absorption and emission spectra. *J Fluoresc*.

2014;24:819-26.

[100] Lakey JH, Raggett EM. Measuring protein—protein interactions. *Current Opinion in Structural Biology*. 1998;8:119-23.

[101] Li Z, Wang Y, Wang J, Tang Z, Pounds JG, Lin Y. Rapid and sensitive detection of protein biomarker using a portable fluorescence biosensor based on quantum dots and a lateral flow test strip. *Analytical Chemistry*. 2010;82:7008-14.

[102] Keusgen M. Biosensors: new approaches in drug discovery. *Naturwissenschaften*. 2002;89:433-44.

[103] Morris MC. Fluorescent biosensors—probing protein kinase function in cancer and drug discovery. *Biochimica et Biophysica Acta (BBA)-Proteins and Proteomics*. 2013;1834:1387-95.

[104] Bradford MM. A rapid and sensitive method for the quantitation of microgram quantities of protein utilizing the principle of protein-dye binding. *Analytical Biochemistry*. 1976;72:248-54.

[105] Barrett D, Leimkuhler C, Chen L, Walker D, Kahne D, Walker S. Kinetic characterization of the glycosyltransferase module of *Staphylococcus aureus* PBP2. *Journal of Bacteriology*. 2005;187:2215-7.